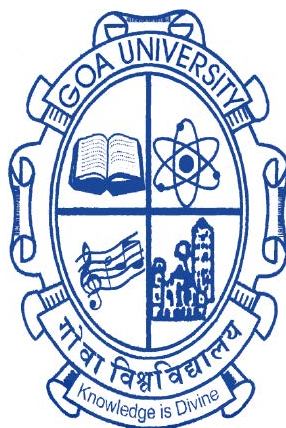


Trace elements and silicon stable isotopes in the Indian sector of Southern Ocean and Antarctic lakes

A THESIS SUBMITTED IN PARTIAL FULFILMENT FOR THE DEGREE OF

DOCTOR OF PHILOSOPHY

IN THE SCHOOL OF EARTH, OCEAN AND ATMOSPHERIC SCIENCES, GOA
UNIVERSITY



By

Mohammad Nuruzzama

School of Earth Ocean and Atmospheric Sciences,
Goa University,
Taleigao Plateau, Goa-403804, India

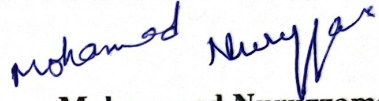
November 2022

DECLARATION

I, Mohammad Nuruzzama, hereby declare that this thesis represents work which has been carried out by me and that it has not been submitted, either in part or full, to any other University or Institution for the award of any research degree.

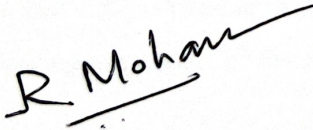
Place: Goa

Date: 22/11/2022


Mohammad Nuruzzama

CERTIFICATE

I hereby certify that the above Declaration of the candidate, Mohammad Nuruzzama is true and the work was carried out under my supervision.



Dr. Rahul Mohan

Scientist 'F', National Centre for
Polar and Ocean Research, Goa,
India

(Research guide)



Dr. Waliur Rahaman

Scientist 'E', National Centre for
Polar and Ocean Research, Goa,
India

(Research co-guide)

Acknowledgements

The work conducted in this thesis involves countless efforts and encouragement from my PhD supervisor Dr. Rahul Mohan. Thank you so much for providing me with constant support and guidance during this journey. I always found direction with your immense and rich experience in science and life advice during the hard hitting moments in the lab, as well as in my personal life. I remember his trust and confidence in me, which mostly figured out today who I am. His qualities as a supervisor cannot be stated in words, I can say that this thesis would not have been possible without his guidance and persistent support.

I am also grateful to my PhD co-supervisor, Dr. Waliur Rahaman, for constant support during the analysis of the isotopes, trace metals, paper writing and several scientific discussions. I sincerely thank him for allowing me to use the Isotrace lab and instrument facilities at NCPOR. I am highly grateful to Director NCPOR for his support throughout my research tenure at NCPOR.

I am very grateful for the suggestions and support of Departmental Research Committee members (Prof. C.U. Rivonkar and Dr. Sushant Naik). I sincerely thank all scientists in NCPOR's Cryosphere Division (Particularly Ms. Lathika N., Drs. Mahesh Badanal, Abhilash Nair, Sharmik Patil, and Mohammad Salim) whose suggestions during instrument operation and presentations helped me a lot. I want to thank my collaborator Dr. Gyana Ranjan Tripathy, who was instrumental for me and trained me in many ways for successful data acquisitions, verification, and scientific writing skills. I am also grateful to Prof MEA Mondal and Dr. Shaikh Abdul Rashid of AMU for the scientific training before admission to the PhD. Their role led me to land in NCPOR for this unique and exciting research opportunity. I sincerely thank Dr. Parijat Roy and Dr. P.V. Bhaskar for allowing me access to the XRF and spectrophotometer analytical facility at NCPOR.

Furthermore, I am highly thankful to my colleagues, Dr. Shramik Patil and Dr. Abhilash Nair for their help during the expedition to the Southern Ocean and Antarctica and for discussions during the manuscript preparation. Bunch of people (Tariq Ejaz, Tarique, Alok, Danish) always had my back, and they helped me during all the harsh moments of this wonderful PhD journey. I am also thankful to my research colleagues Priyesh, Rahul, Nibedita, Padma, Pallavi, Pooja, Kalpana, Harikrishnan, Gautami, Tejeshwar and Pranav. I will always be grateful to Anktia, Vinita, Valency, Akshaya for their help in the Isotrace lab and Geology lab. I also thank Ankita and Sweta for always helping me in various administrative assignments. I thank Midhun Mohan and Dr N.S

Magesh for the illustrative figure used in this thesis. I am thankful to the members of the Antarctic expeditions.

My family members deserve a huge thank for their unwavering support, wishes, and encouragement. They have always been there for me at difficult moments and have helped me finish my thesis. The University Grants Commission provided me with a PhD fellowship (Grant No. 2061520355), for which I am grateful. I gratefully accept the copyrights provided by the Hydrological Processes and Science of Total Environment Journals for allowing me to use the two published papers in the journal in my thesis. Finally, I would like to express my gratitude to all of those who helped me during this wonderful journey and the preparation of my PhD thesis.

Dedicated to
My loving family

Table of Contents

1	Introduction.....	1
1.1	Introduction	3
1.2	Objectives of this thesis	12
1.3	Outline of the thesis	12
2	Material and Methods	15
2.1	Study Area: Antarctic lakes	18
2.1.1	Geological settings of Larsemann Hills	18
2.1.2	Geohydrology and Climate	18
2.2	Sample collection from Antarctic lakes	19
2.3	Analysis of water samples from lakes	21
2.3.1	Alkalinity and major ions	21
2.3.2	Dissolved Sr	21
2.3.3	$^{87}\text{Sr}/^{86}\text{Sr}$ ratios	22
2.3.4	Trace metals	22
2.3.5	Biological parameters	23
2.4	Major oxides and Barium in bulk sediments from lakes	24
2.5	Sample collection from the Southern Ocean	24
2.6	Oceanographic Setting of the Indian sector of Southern Ocean	26
2.7	Analysis of nutrients, DOC and chlorophyll- <i>a</i>	27
2.8	Dissolved Barium (Ba_d) analysis in seawater	27
2.9	Silicon isotopes and its analytical methodology	28
2.9.1	Silicate fusion and silica purification steps	28
2.9.2	Mg-induced silica precipitation (MAGIC) from Seawater	29
2.9.3	Matrix removal through column chromatography	30
2.9.4	Silicon isotope measurement techniques	32
2.9.5	Working parameters of MC-ICP-MS	34
2.9.6	Mass Bias correction	37
2.9.7	Three isotope plot	38
2.9.8	Standard reproducibility	39

3	Dissolved major ions, Sr and $^{87}\text{Sr}/^{86}\text{Sr}$ of coastal lakes from Larsemann Hills, East Antarctica: Solute sources and chemical weathering in a polar environment	41
3.1	Introduction	43
3.2	Results	44
3.3	Discussion	50
3.3.1	Possible solute sources for major ions	51
3.3.2	Sources for dissolved Sr and $^{87}\text{Sr}/^{86}\text{Sr}$	54
3.3.3	Source-apportionment modelling	56
3.3.4	Silicate weathering rates and controlling factors	59
3.4	Conclusions	62
4	Sources, distribution and biogeochemical cycling of dissolved trace elements in the coastal lakes of Larsemann Hills, East Antarctica.....	63
4.1	Introduction	65
4.2	Results	66
4.2.1	Trace metals, nutrients, DOC and chlorophyll- <i>a</i> in water samples	66
4.2.2	Major oxides and trace elements abundances in sediments	68
4.3	Discussion	72
4.4	Data analysis using statistical methods	73
4.5	Sources of trace elements to the LH lakes	73
4.6	Identification of dominant factors	77
4.7	Biogeochemical processes	81
4.7.1	Productivity	82
4.7.2	Biological decompositions	84
4.8	Inorganic versus biological processes controlling Ba dynamics in the LH Lakes	85
4.8.1	Dissolved Ba	85
4.8.2	Particulate Ba	87
4.9	Conclusion	89
5	Biogeochemical cycling of Barium and Silica in the surface waters of the Indian sector of Southern Ocean	93
5.1	Introduction	95
5.2	Results	98
5.2.1	SST, SSS, and pH	98
5.2.2	Macronutrients (Silicate, phosphate, nitrate), DOC and Chlorophyll- <i>a</i>	99
5.2.3	Dissolved Barium (Ba_d)	101

5.2.4	Dissolved Silica (Si(OH) ₄) and δ ³⁰ Si in seawater samples from AASW	104
5.3	Discussion	105
5.3.1	Macronutrient stoichiometry, nutrient utilization, and biological decomposition	105
5.3.2	Dissolved Barium (Ba _d) distributions in Surface Ocean and controlling factors	108
5.3.3	Nutrient utilization, silica biogeochemical cycling, and Ba-Si(OH) ₄ in the Antarctic surface waters (AASW)	117
5.4	Summary and Conclusion	119
6	Conclusion and future perspectives	121
6.1.	Source identification, apportionment, estimation of silicate weathering and CO ₂ consumption rates using Sr isotopic approach:	123
6.2.	Trace metal biogeochemistry in the freshwater lakes of Antarctica:	124
6.3.	Barium, dissolved silica and silicon isotope study in the surface waters of the Indian sector of the Southern Ocean	125
6.4.	Future directions	126
7	Bibliography	129

Abstract

This thesis work was designed to assess the biogeochemical cycling of selected trace elements and isotope compositions ($^{87}\text{Sr}/^{86}\text{Sr}$ and $\delta^{30}\text{Si}$) in the Indian sector of the Southern Ocean and Antarctic lakes using the samples collected during the Antarctic field season in the austral summer of the 2017. The study in the Southern Ocean for Barium, nutrients and $\delta^{30}\text{Si}$ is focused on the dissolved phases i.e., water samples. In contrast, the study conducted in the Antarctic lakes focuses both on the dissolved and accumulated phases. These datasets were profoundly applied to assess the dominant influencing factors controlling the trace metals (particularly Barium) cycling in the Antarctic lakes, source apportionment, their corresponding chemical weathering rates and CO_2 consumption rates in the Antarctic lake catchments. The fate of these trace metals during biogeochemical processes such as the biological uptake and inorganic attenuation was also investigated. In the surface waters of the Indian sector of the Southern Ocean, these datasets were utilised to reveal the biogeochemical processes and their influence on Silica and Barium cycling.

Dissolved Strontium (Sr) in the lake waters shows a non-conservative behaviour along the salinity gradient in the Antarctic lakes. The close vicinity to seawater indicate a possible influence over the dissolved solute concentrations and Sr. $^{87}\text{Sr}/^{86}\text{Sr}$ compositions of lake waters range from 0.7110 to 0.7211, with an average of 0.7145, which is closer to the modern seawater value of 0.7092. Chemical and Sr isotopic data of lake waters suggest significant solute supply from chemical weathering of bedrocks and Ca-Mg rich salts formed during freezing of seawaters to these lakes, in addition to marine sources. Inverse model calculations employing these chemical datasets yield estimates of dissolved cations and Sr, which are primarily obtained from oceanic (seawater + snow) sources (cations 76%) and weathering sources (Sr 92%). The chemical weathering and corresponding CO_2 consumption rates (CCR) estimated from the major ions generated by silicate rock weathering suggest significant and comparable magnitude to the major river basins. These estimations infer the possible enhancement in the magnitude of the Silicate weathering rate (SWR) and CCR in induced melting scenarios that are likely to happen in the near geologic future.

During the austral summer, coastal lakes in Antarctica receive an enormous amount of solutes, including major ions and trace elements, some of which act as limiting nutrients for biological productivity in the lakes. The concentrations of selected dissolved trace metals (Ba, Mn, Cu, Co, Cd, Mo, and U) in the studied lakes of Larsemann Hills are sub-nanomolar, an order of magnitude lower than those found in global rivers. Among the dissolved nutrients and trace metals investigated, dissolved phosphate (PO_4) and Mo were shown to be limiting macro and micronutrients, respectively, supported by low chlorophyll-*a* concentrations (0.24–0.19 mg/m^3). Whereas, dissolved Cu plays a key role in bacterial-mediated organic decomposition. Inorganic and/or biologically produced Ba precipitation is typical in lake sediments and catchments. Ba-excess ($\text{Ba}_{\text{excess}}$), i.e., non-lithogenic source of Ba, was estimated to be between 26 and 63 percent in sediments from lakes and their catchments. The catchment sediments have a higher Ba-excess than the lake sediments, indicating that a considerable amount of the dissolved Ba is lost during the solute transport. These datasets provide a baseline character of pristine environments such as Antarctica and reveal the unique behaviour of a few trace metals such as Mo and Ba, which can be utilized to better interpret paleo-trace metal records.

The study carried out in the seawater samples were measured for macronutrients, dissolved Barium (Ba_d), $\delta^{30}\text{Si}$ and biological parameters (DOC and Chlorophyll-*a*) to better understand the Ba-Si(OH)₄ enigma and nutrient utilization in the surface waters of the Indian sector of Southern Ocean. Our findings imply that frontal mixing has the most influence on the Ba_d distribution, although the Ba-Si(OH)₄ correlation suggests that a wide range of biogeochemical processes are in play and indicate the nutrient intermediate character of Ba_d . The estimated Barite saturation index in surface waters indicates barite precipitation as a critical inorganic process/mechanism for removing dissolved Ba from surface waters. $\delta^{30}\text{Si}(\text{OH})_4$ in the transect samples vary between +1.80 to +2.97 ‰, indicating a variable nutrient utilization throughout the Southern Ocean. Higher nutrient utilization zones with heavier isotopic fractionation co-vary with depleted Ba_d . Thus, a common mechanism possibly drives the Ba-Si(OH)₄ relation in the surface waters of the Southern Ocean. These findings aid in explaining the role of nutrient utilization, physical mixing processes, and frontal variation

controlling dissolved silica and Ba and would be utilized to better interpret the past sedimentary records in the Indian sector of the Southern Ocean.

List of figures

Figure 1.1 Schematic photograph depicts the major physico- geochemical processes controlling metal cycling the polar lake of Larsemann Hills, Antarctica (Photo credit: Dr Mahesh, with permission).....	8
Figure 2.1 Classification chart for the sampling domain and parameters analysed for the thesis work.....	17
Figure 2.2 Location map of the ten coastal lakes near the Prydz Bay, East Antarctica. The regional geology of this region has also been shown (modified after Carson and Grew (2007)).....	20
Figure 2.3 Standard calibration plot for the dissolved trace metal (V, Mn, Co and Cd) measured in the water samples from Antarctic lakes.....	23
Figure 2.4 Sampling locations of the surface seawater collected from the Indian sector of Southern Ocean during the austral summer of the year 2017. T1, T2 and T3 with arrow represents the corresponding sampling transects and track of the expedition. The T1 commenced from South African waters to Prydz Bay East Antarctica during mid-austral summer (January 2017), T2 shows the track between the Prydz Bay and India Bay which was commenced during late summer (Feb, 2017) and T3 is return corresponding track to T1, between India Bay and South Africa where the sampling was done between the March and April, 2017.....	25
Figure 2.5 Calibration curve for the ^{137}Ba concentration measured in the seawater samples.....	28
Figure 2.6 Schematic representation of the silica separation and purification for the $\delta^{30}\text{Si}$ analysis in the seawater samples.....	30
Figure 2.7 Concentration of Si and cationic species in the aliquots obtained during column chromatographic steps for the sample elution and cleaning of cationic exchange resin.....	32
Figure 2.8 Isobaric interference observed for the Silicon isotopes in the medium resolution ($m/\Delta m=1000$).....	36
Figure 2.9 Three isotope plot constructed for the data obtained during analysis between $\delta^{29}\text{Si}$ and $\delta^{30}\text{Si}$ to assess the mass dependent fractionation of the silicon isotopes following Young et al., 2002.....	39
Figure 3.1 Ternary diagram for major cations and anions of the Antarctic lakes. For reference, average composition of possible major solute sources (seawater, Antarctica snow and silicate rocks) is also shown; See text for data source for the end-member compositions. The data distribution indicates dominancy of oceanic sources in regulating the lake water chemistry.....	46

Figure 3.2 Co-variation of dissolved Mg, HCO₃, Ca and SO₄ with chloride ion. The straight line represents the average seawater composition. Enriched Ca and Mg with respect to the seawater line indicate their supply also from other sources, such as chemical weathering of bed-rocks and/or Ca-Mg rich salts..... 52

Figure 3.3 Correlation plot between seawater-corrected alkalinity and (Ca+Mg) for the Antarctic lakes. The straight line represents the 2:1 line, a trend expected for chemical weathering of bed rocks..... 53

Figure 3.4 Mixing diagram between Sr/Ca (molar ratio) and ⁸⁷Sr/⁸⁶Sr ratios of the Antarctic lakes. Chemical compositions for major solute sources (*cf.* text for data source) are also shown here. The data fall closer to the seawater end-member, hinting at dominance of oceanic solute supply to the lake..... 55

Figure 3.5 Results from the inverse model on relative supply cations and strontium to the lakes from different sources..... 59

Figure 3.6 Results from the inverse model on relative supply cations and strontium to the lakes from different sources..... 61

Figure 4.1 Dissolved trace metal concentration in LH lakes are plotted with Cl⁻. The red dashed line represents the average seawater compositions. Any deviations from the seawater line indicate either supply from additional sources and removal/gain of these trace elements due to processes operating the water column..... 74

Figure 4.2 Results derived from PCA are plotted: (a) Biplot between two principle factors (PC1-PC2) of factor loadings obtained for variables (b) Biplot between two principle factors (PC1-PC2) for scores obtained for samples..... 77

Figure 4.3 Element concentration in lake water samples: (a) Samples and (b) Variables classification obtained by HCA..... 80

Figure 4.4 Micronutrient behaviour of dissolved Mo in 9 out of the total 10 lakes studied. (a) Correlation plot between *Chlorophyll-a* of water samples from lakes with dissolved Mo. (b) Correlation between dissolved Mo and Si suggesting common sources and identical behaviour in the lake water columns (c) Correlation between dissolved PO₄ and *Chlorophyll-a* in the lakes..... 83

Figure 4.5 Correlation plot for Cu vs dissolved organic carbon (DOC) and SO₄ in lake waters indicating for bacterial mediated organic decomposition in the lakes..... 85

Figure 4.6 SEM images of sediments obtained from lake bottom showing an exceptionally high concentration of Ba, Mn and Fe in their micro-precipitates..... 87

Figure 4.7 (a) Saturation index for minerals in the lake waters using PHREEQ (Mitchell and Brown, 2007; Parkhurst, 1995) (b) Bar plot for estimated Ba_{excess} in lake sediments and catchment sediments..... 89

Figure 4.8 Various processes/factors are highlighted in the schematic to explain how they control dissolved trace metal and major ions, their sources and sinks in the lakes of the Larasemann Hills, Antarctica.....	90
Figure 5.1 Variability of the insitu measured physical parameters (SST, SSS and pH) shows the clear frontal demarcations in the INSO.....	99
Figure 5.2 Dissolved macronutrients, and dissolved organic carbon (DOC) are spatially plotted to represent their latitudinal variability and differences in the three transects.....	100
Figure 5.3 (a) The nutrient utilization, N^* ($= NO_3^- - 16*PO_4^{3-}$) in the surface waters of the Indian sector of Southern Ocean (b) Insitu Chlorophyll- <i>a</i> distribution in the INSO.....	107
Figure 5.4 Distribution of the Ba_d in the sampling region of the Indian sector of the Southern Ocean representing the frontal (North of the 50°S) and non-frontal control (South of the 50°S).....	109
Figure 5.5 Inverse correlation observed between physical parameters (Salinity and SST) and dissolved Barium (Ba_d) indicates the control of the physical characteristics on Ba_d cycling in the INSO.....	110
Figure 5.6 The physical (temperature) and macronutrient parameters are plotted in the section defined. This represents an upwelling zone in the highlighted region (57-59°S) along the 10°E latitudinal extent.....	112
Figure 5.7 The SST shown with wind vectors represents the upwelling region in the sampling transect-3 near the 10°E in the Southern latitudes (b) The mesoscale sea-surface height of the region are shown along with the North and East wind vectors in the upwelling region.....	113
Figure 5.8 Correlation of the dissolved Barium with the dissolved silica showing the deviation from the linear regression (exponential correlation).....	115
Figure 5.9 Co-variation of the seawater Barium with the physicochemical parameters in the Southern Ocean surface water samples.....	116
Figure 5.10 Covariation between Si and $\delta^{30}Si$ in the Antarctic surface waters (AASW) indicating nutrient utilization in the region.....	118

List of tables

Table 1.1. Seawater compositions for key trace elements and parameters of interest.....	10
Table 2.1 Silica purification steps for seawater samples and standard solutions (George et al., 2006).....	31
Table 2.2 Polyatomic interferences associated with the mass of Si isotopes 28, 29, and 30.....	33
Table 2.3 Instrument operating parameters for the analysis of silicon isotopes using Neptune plus MC-ICP-MS coupled with Aridus-III desolvating nebulizer.....	35
Table 2.4 Standards for the silicon isotopes analysed during seawater sample measurements.....	40
Table 3.1 Chemical and Sr isotopic data for the coastal lakes from the East Antarctica.....	48
Table 3.2 <i>a-priori</i> values and associated uncertainties.....	50
Table 3.3 Percent contribution of cations and Sr in Antarctic lakes.....	58
Table 4.1 Trace metals and biological parameters analysed from coastal lake waters of Larsemann Hills, East Antarctica.....	69
Table 4.2 Major oxides, bulk Sr and Ba composition of lake sediments and catchment sediments from LH, East Antarctica.....	71
Table 4.3 Pearson correlation coefficient matrix (at 95% significance level) Bold numbers indicate significant correlations.....	76
Table 4.4 Factor loading after varimax rotation ($p < 0.05$).....	78
Table 5.1 Sampling details, physical parameters, dissolved nutrients, chlorophyll- <i>a</i> , and DOC of the samples collected during the austral summer of the year 2017 from the Indian sector of the Southern Ocean.....	102
Table 5.2 The measured silica concentration and stable silicon isotope ($\delta^{30}\text{Si}$) characteristics of the samples collected from Antarctic surface waters (AASW).....	104

List of publications

- 1) Nuruzzama, M., Rahaman, W., Tripathy, G.R., Mohan, R., Patil, S. Dissolved major ions, Sr and $^{87}\text{Sr}/^{86}\text{Sr}$ of coastal lakes from Larsemann hills, East Antarctica: Solute sources and chemical weathering in a polar environment. *Hydrological Processes*. 2020; 34: 2351– 2364. <https://doi.org/10.1002/hyp.13734>.

- 2) Nuruzzama, M., Rahaman, W., Mohan, R. Sources, distribution and biogeochemical cycling of dissolved trace elements in the coastal lakes of Larsemann Hills, East Antarctica. *Science of the Total Environment*. 2021; 764. doi: 10.1016/j.scitotenv.2020.142833.

Papers presented at conferences

1. Nuruzzama M., Rahaman W., Mohan R., Patil S., “Sr and $^{87}\text{Sr}/^{86}\text{Sr}$ in Antarctic Lakes: Chemical Weathering in Extreme Environment” at Polar-2018, Davos, Switzerland during 20-30 June, 2018 (Oral presentation)

2. Nuruzzama, M., Rahaman, W., Tripathy, G.R., Mohan, R., Patil, S., “Solute dynamics, source apportionment and glacial weathering in Antarctica” at National Conference for Polar Sciences (NCPS-2019), during 20-22nd August, 2019 (Poster presentation)

Chapter-1

Introduction

1.1 Introduction

Antarctica, the southern extreme of the globe is the storehouse for 70% of Earth's freshwater locked in the form of ice sheets which covers more than 98% of its area and acts as the modulator of the Earth's climate (Morlighem et al., 2019). The enhanced greenhouse effects in the past century due to industrial revolution pose threat to the Antarctic ice-sheets (Friedlingstein et al., 2019). In case of complete melting scenarios of these ice sheets, ~58m rise in global sea level would be observed (Fretwell et al., 2013). The vast areas of Antarctica and increasing meltwater supply induce surface and subsurface geochemical processes which generate significant amount of dissolved solutes (Lyons et al., 2017; Lyons et al., 2002; Nezat et al., 2001). The contribution of these dissolved solutes to the Southern Ocean (SO) and aquatic systems in Antarctica reveal its importance and role in the global geochemical cycling and ionic budget (Lyons et al., 2015; Wadham et al., 2010). Antarctic continent is surrounded by Southern Ocean which acts as a transition zone between Antarctica and tropical regions. The Southern Ocean enables global ocean circulation through Antarctic circumpolar currents which facilitates the interlinking of Pacific, Atlantic and Indian ocean basins (Murphy et al., 2021) and also significantly contribute to the ocean biological pump (Chisholm, 2000). The CO₂ sequestration through siliceous primary productivity requires dissolved nutrients and micronutrients which are mainly supplied by deep ocean currents and continental weathering in Antarctica. The interdependent relationship between the Southern Ocean and Antarctica and their relevance in controlling major earth's processes make them interesting to study. The understanding of biogeochemical processes help to assess the influence of natural and anthropogenic stress on these polar biogeochemical domains.

Dissolved trace metals in the global saline and freshwater reservoirs play an important role in biogeochemical cycling due to their bio-essential properties such as requirement in metabolic uptake of primary producers. The trace elements and their isotopes (TEIs) serve as important proxies to assess the nutrient utilization, redox changes, water circulation, and primary productivity in the present as well as in the past for paleo-reconstructions (Castrillejo et al., 2013; De La Rocha, 2006; De La Rocha et al., 2011; Dehairs et al., 1980; Dymond et al., 1992; Ganeshram et

al., 2003; Paytan et al., 1996; Rubin et al., 2003; Wu et al., 2014). The balance between sources (continental inflow, atmospheric deposition, hydrothermal activity, and sea-floor alteration) and sinks (authigenic and biogenic mineral formations) governs the distribution of TEIs in the modern ocean (Murray, 1987; Sunda and Huntsman, 1998).

Inventory of trace metals in the polar reservoirs such as the Southern Ocean and Antarctic lakes are complex and revolve around the geochemical generation and biological utilization. One of the largest polar reservoirs, i.e., the Southern Ocean is established as globally significant carbon sink and account for ~50% of global carbon sequestration (Chisholm, 2000; Hauck et al., 2015). The SO biological carbon production (BCP), in particular, contributes to biogeochemical carbon cycle and export 3 Pg C yr⁻¹ from a total of 10 Pg C yr⁻¹ global export production from surface waters (Arteaga et al., 2019). On glacial-interglacial periods, the effectiveness of the BCP is linked to the export and preservation of surface particulate matter and is directly tied to atmospheric CO₂ levels (Honjo et al., 2014; Sigman and Boyle, 2000). The biological pump mechanisms are mainly linked to the pathway of inorganic carbon consumption and release by phytoplanktons through photosynthetic processes and respiration (Basu and Mackey, 2018). These biological activities rely on macronutrients and micronutrients (Fe, Zn, Cd, Mn, etc.) in the upper surface ocean and significantly contribute to carbon uptake down the route. Among these trace metals, dissolved Barium (Ba_d) possesses nutrient-intermediate characteristics (Hendry et al., 2018). Barium accumulated in ocean sediments over geological time has been used extensively to reconstruct the paleo-productivity (Dehairs et al., 1980; Eagle et al., 2003; Gonneea and Paytan, 2006; Griffith and Paytan, 2012; Martinez-Ruiz et al., 2018; Paytan et al., 1996). The elemental Barium/Calcium ratio of foraminifera shells is used as a proxy for paleo circulation during glacial-interglacial intervals (Lea and Boyle, 1989; Lea, 1993). However, behaviour of dissolved Barium (Ba_d) and its role in the biological processes are not yet well understood in the modern ocean. Ba_d is recognised as a nutrient-intermediate element due to its nutrient type profile in the water column, which is inferred from its removal from the surface oceanic layers and deep regeneration (Hendry et al., 2018; Pyle et al., 2018) and their strong correlation with silicic acid/dissolved silica (Si(OH)₄) (Jacquet et al.,

2005; Jacquet et al., 2007). Unlike Si(OH)_4 , which has a direct role in diatom productivity of the Southern Ocean, the role of the Ba_d during metabolic processes of marine photo-synthesizers is not much revealed (Sternberg et al., 2005). The Ba_d in the sub-surface waters is influenced by barite saturation and precipitation, their re-dissolution, and remineralization which are often reflected in the surface waters (Griffith and Paytan, 2012; Jacquet et al., 2005). The global distribution of the Ba_d in the open ocean varies between 35-140 nmol kg^{-1} (Rubin et al., 2003; van Horsten et al., 2022), which increases towards the higher latitudes, especially in the Southern Ocean (Pyle et al., 2018). The dominating process for the Ba_d variation in the Southern Ocean is frontal variations along its latitudinal extent (Jacquet et al., 2005; Pyle et al., 2018). However, strong linear correlation of Ba_d with Si(OH)_4 in the subsurface waters (>300 m) of the Southern ocean (Jacquet et al., 2007) also indicates a significant role of biological processes in the water column.

The coupled Ba-Si(OH)₄ relation in the global seawaters is a major enigma of modern ocean biogeochemistry (Hendry et al., 2018; Pyle et al., 2018). The Ba-Si(OH)₄ biogeochemistry becomes more important in the Southern Ocean since a major portion of the SO primary productivity is siliceous. The Southern Ocean, due to its high consumption of silicate nutrients, favorable physicochemical conditions, and micronutrient availability, makes it most suitable for the siliceous primary production, known as the opal belt of the world ocean. Silicifying marine organisms such as diatoms, silicoflagellates, radiolarians, and sponges discriminates against heavier isotopes (²⁹Si and ³⁰Si) and preferential uptake of lighter isotopes of silicon (²⁸Si) during frustule formations results in relatively enriched silicon isotopic signature ($\delta^{30}\text{Si}$) of residual seawaters (Milligan et al., 2004; Sutton et al., 2013). Among these siliceous organisms, diatoms are dominantly responsible for silica cycling within ocean through silica uptake and export due to their anomalously varying nature of populations and life span (Sutton et al., 2016). Diatoms account for ~40% of primary productivity and are responsible for largest silica fluxes in global ocean (Baines et al., 2010; Treguer and De La Rocha, 2013). These regions are mainly located in the upwelling regions of tropical coasts and polar open oceans and significantly contribute to the ocean biological pump (Buesseler, 1998). Seawater $\delta^{30}\text{Si(OH)}_4$ variations are primarily resulted due to the fractionation by diatom uptake in the euphotic zone of the ocean, where these photosynthesizers

grow (Hendry et al., 2014; Leng et al., 2009). However, the role of other siliceous organisms such as siliceous sponges and radiolarians are dominant in a restricted environmental regime where diatoms rarely thrive due to micronutrient unavailability and/or other physicochemical conditions (Maldonado et al., 2011). Thus the marine silica and carbon cycle are complexly interlinked, and diatoms play a crucial role in the ocean carbon biogeochemical budget (Ragueneau et al., 2000; Smetacek et al., 2012). The silica biogeochemical cycling and their role in biological productivity evidently indicate their possible relation with the dissolved Barium. Thus a thorough isotopic investigation of dissolved silica in the top oceanic layer could explain the enigma behind the observed Ba-Si(OH)₄ correlation throughout the global ocean and in particular, the Southern Ocean. The biogeochemical cycling of silica, barium and other trace metals show unique characteristics and associations in the Antarctic surface environments. Largely, solutes including macronutrients and trace metals in the Antarctic terrestrial environments are generated from rock weathering followed by its biological uptake and inorganic attenuation, as potential sink. The residual solutes are ultimately delivered to the coastal oceans via terrestrial aquatic bodies, majorly lakes.

Chemical weathering of silicate rocks plays a vital role in global geochemical cycles, soil formations, and nutrient supply to ecosystems (Conley, 2002; Livingstone, 1963). Formation of weak carbonic acid (H₂CO₃) in the tropical river basins and its action on the rocks induce silica removal and storage of CO₂ in the sediments resulting atmospheric CO₂ removal on geologic time scale (Brennan et al., 2014; Moon et al., 2014; Moon et al., 2007; Walker et al., 1981). Chemical weathering of the continental rocks contributes dissolved solutes such as nutrients and trace metals to the coastal oceanic regimes (Moon et al., 2007; Oliva et al., 2003; Wu et al., 2005). Though, the cold polar environments are less susceptible to weathering pertaining to restricted water availability (Lyons et al., 2021; Shevnina and Kourzeneva, 2017; Zelano et al., 2017), meltwater supply due to localized melting during austral summers induces chemical weathering (Li et al., 2022). However, the extent and intensity of these surface processes are unknown. Ignoring the role of surface and subglacial processes in Antarctica can introduce errors in the global cation and trace metal budget and could lead to erroneous paleo-reconstructions.

To model the global carbon cycling and atmospheric CO₂ variations in geological past, we need to understand ongoing silicate weathering processes and quantify its rates in different geomorphic/tectonic/geologic settings and climatic regimes. Though Antarctica is mostly covered with ice, with no known perennial river system, a few studies have been carried out e.g., the polar desert of Taylor Valley (Nezat et al., 2001), Onyx River (the longest river, 32 km) in the Wright Valley in the Southern Victoria Land (Green et al., 2005) of West Antarctica. These studies clearly indicate that the rate of chemical weathering per unit area could be significant compared to the temperate regions (Anderson et al., 1997; Lyons et al., 2021; Nezat et al., 2001). Glacier-induced mechanical breakdown and erosion provide a larger surface area for the chemical weathering and thereby increase the rate of chemical weathering (Herman et al., 2013; Torres et al., 2017). Considering vast area of Antarctica (approximately 14 million square km), which is larger than the size of the continental U.S.A (9.36 million square km), chemical weathering processes and corresponding CO₂ consumption could be significant. However, it is not accounted for the global ionic budgets. Antarctica has less than 2% permanent ice-free area (28000 km²) during summer, which is prone to glacial-induced chemical weathering, particularly in the ice sheet margin. The ice-free area in the geologic past went through large changes due to the waxing and waning of the Antarctic ice sheet associated with climatic fluctuations (Hodgson et al., 2012). A recent study suggests that ice-free region in Antarctica could increase by 25% by the end of the century due to the recent warming (Siegert et al., 2019). Another important aspect is to understand the relative role of controlling factors of chemical weathering. The frost/glacial action is considered one of the strong agent for the mechanical breakdown of rocks and subsequently act as a good substrate for chemical weathering (Anderson et al., 1997). To understand relative role of glacial mediated chemical weathering, most of the studies have been carried out in the tropical and temperate mountains where precipitation is also known to play an important role. Therefore, study of chemical weathering in Antarctica would be ideal for assessing the role of glacial mediated chemical weathering. In absence of perennial rivers in East Antarctica, lakes remain as the only suitable archive to understand surface geochemical processes. These lakes possess the signatures of ongoing surface processes in their catchments and are ideal reservoirs to study the modern biogeochemical cycling in the pristine Antarctic environments. The

biogeochemical characterization of lake waters, their sources, and information about their trace metal cycling would reveal the behaviour of these geochemical components in the unique polar environments. This information would help to further assess the geochemical budget and to compare their significance in the global ionic balance in the natural reservoirs.

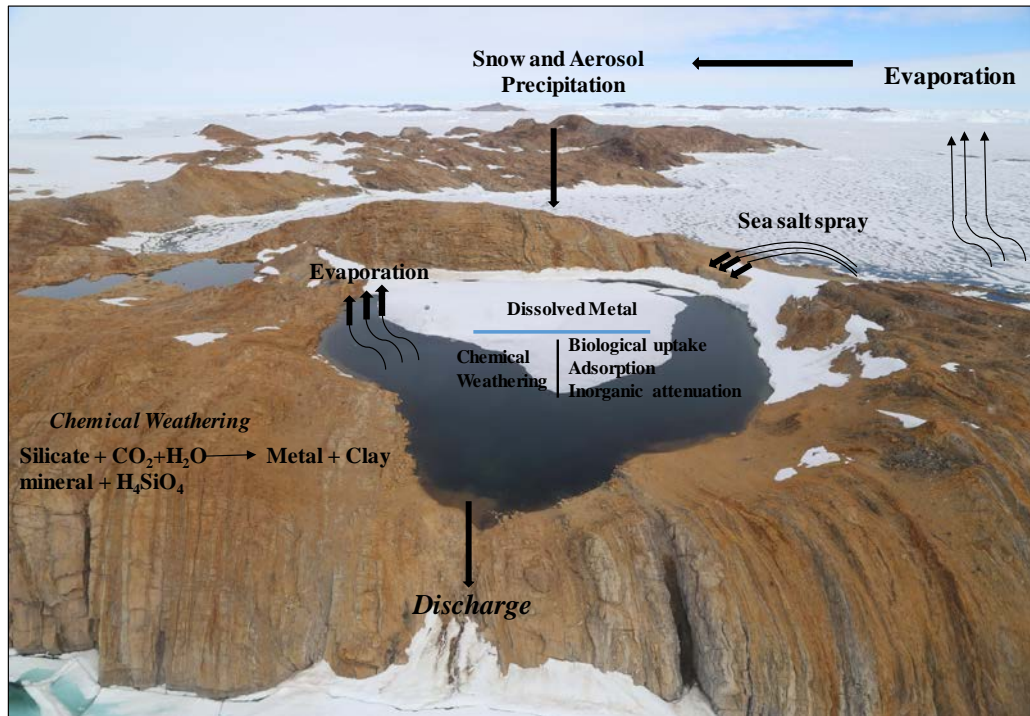


Figure 1.1. Schematic photograph depicts the major physico- geochemical processes controlling metal cycling the polar lake of Larsemann Hills, Antarctica (Photo credit: Dr Mahesh, with permission).

Continental weathering of a specific rock types produces its unique solute composition, which possesses its signature metal and isotopic compositions (Lyons et al., 2003; Rahaman and Singh, 2012; Tripathy et al., 2012). A major portion of these solutes are altered through several geochemical and biological processes during transportation. Various geochemical and biological processes such as ion exchanges, adsorption-desorption, attenuation, precipitation, biological uptake and dissolution alter their chemical signatures. However, dissolved Sr and their isotopic ratios ($^{87}\text{Sr}/^{86}\text{Sr}$) in the dissolved solutes remain unaffected by the biological uptake or dissolution (Drever, 1997; Krishnaswami et al., 1992; Shand et al., 2009). Dissolved Sr and its isotope ratio ($^{87}\text{Sr}/^{86}\text{Sr}$) are unique proxies for the source characterization and chemical weathering studies as they show negligible fractionation and are unaffected by the biological processes during their transport

from source to reservoirs. The Sr isotopes are widely used to trace chemical weathering rates as they pose unique ratios ($^{87}\text{Sr}/^{86}\text{Sr}$) in various end members (rock types, reservoirs), uniform ratios for the global ocean due to sufficiently large residence time and consistent record through the geological time (Tripathy and Singh, 2010). Consequently, estimation of chemical weathering using major ions/trace metal without their source characterization and apportionment contribute to imprecise estimation and existing lacustrine ionic imbalances, which in turn limits their application to paleoclimate reconstructions in Antarctica.

Antarctic lakes in the Larsemann Hill regions are primarily freshwater and oligotrophic in nature (Gasparon et al., 2002; Sabbe et al., 2004; Sabbe et al., 2003). Most of the biological activities take place on the lake bottom due to their pristine character and clear waters, which allows the formation of thick (upto 2m) algal benthic mats (Sabbe et al., 2003). The uniqueness of these lacustrine settings provides an opportunity to study the behavior of redox-sensitive and nutrient-limiting trace metals. The nutrient-limiting behaviour of trace metals often depends on their scarcity in the system (Blain et al., 2007; Takano et al., 2014). The bioavailability of these trace metals essentially controls the carbon cycling by limiting the primary productivity in the photic zone of global oceanic and freshwater reservoirs (Cid et al., 2011; Lyons et al., 2015). However, the utilization pattern, limiting characteristic, and influence of unique climatic settings in Antarctic lakes are not well understood for these trace metals. Assessment of trace metals in polar environments is also influenced by diurnal temperature fluctuations and biological induced attenuation during the transportation from source to reservoirs (Saelens et al., 2018) which drive inaccuracy to the polar ionic budget. Assessment of this elemental cycling is complex and challenging due to their alteration during transportation as well as within the lacustrine systems and non-point nature. Consequently, imprecise estimation of these polar processes further extends the enigma behind the biogeochemical cycling of several elements, which derive the limitation and inaccurate interpretations of the paleoclimate reconstructions in these environments.

Table 1.1. Seawater compositions for key trace elements and parameters of interest.

Element	Major functions	Upper continental crust (UCC)	Mean seawater	Residence time	References
Sr	Incorporation and stabilization in Aragonite shells	320 $\mu\text{g g}^{-1}$	87.4 $\mu\text{mol/kg}$	~4 Myr	[1-5]
$^{87}\text{Sr}/^{86}\text{Sr}$			0.70916		
Ba	Functions similar to Sr with lesser extent	624 $\mu\text{g g}^{-1}$	110 nmol/kg	10 kyr	[6, 13]
Mo	Nitrate reductase, Nitrogenase	1.1 $\mu\text{g g}^{-1}$	105 nmol/kg	~760 kyr	[7-8]
Cd	Functions as alternative carbonic anhydrase in <i>Thalassiosira weissflogi</i> (diatom). Toxic for other organisms.	0.09 $\mu\text{g g}^{-1}$	600 pmol/kg	130 kyr	[9]
Mn	Important in various biological functions mainly in the electron/hydrogen transfer, Protein and DNA/RNA synthesis	0.1 wt% (as MnO_2)	0.3 nmol kg^{-1}	60 yr	[10-11]
V	Functions as alternate nitrogenase	97 $\mu\text{g g}^{-1}$	30-36 nmol kg^{-1}	50 kyr	[12]
Cu	Important in transport of O_2 and various oxidation/reduction in cell	28 $\mu\text{g g}^{-1}$	3 nmol Kg^{-1}	5 kyr	[13-14]
Co	Important component in B12 (Vitamin), acts as methylation nutrient for various algae species	17.3 $\mu\text{g g}^{-1}$	20 pmol kg^{-1}	340 yr	[16]
Cr	Acts as glucose tolerance factor	92 $\mu\text{g g}^{-1}$	4 nmol kg^{-1}	8kyr-45kyr	[17-18]
$\delta^{30}\text{Si}$	Silicate rocks, diatoms	66.62 wt% (as SiO_2)	0-200 $\mu\text{mol kg}^{-1}$ (0.5 to -3.0 ‰)	20 kyr	19]

(¹Rudnick and Gao, 2003; ²Richter et al., 1992; ³Peucker-Ehrenbrink et al., 2010; ⁴Tripathy et al., 2012; ⁵Jacobson and Blum, 2000; ⁶Hsieh and Henderson, 2017; ⁷Glass et al., 2012; ⁸Emerson and Husted; 1991 ⁹de Souza et al., 2022; ¹⁰van Hulst et al., 2017; ¹¹Hansel, 2017; ¹²Jeandel et al., 1987; ¹³Campbell et al., 2014; ¹⁴Takano et al., 2014; ¹⁵Turner et al., 1981; ¹⁶Quinby-Hunt and Turehian, 1983; ¹⁷Rickli et al., 2019; ¹⁸Bonnand et al., 2016; ¹⁹Sutton et al., 2018)

This thesis attempts to study the geochemical characterization (major ions, Sr, and $^{87}\text{Sr}/^{86}\text{Sr}$) and biogeochemical cycling of trace metals in Antarctic lakes of Larsemann Hills (LH) and to assess the source apportionment, chemical weathering rates (CWR), and CO_2 consumption rates (CCR) in the LH, Antarctica. Also, the

thesis documents the silica and barium cycling in the surface waters of the Indian sector of the Southern Ocean. The strategy behind selecting these elements (Si and Ba) in the southern polar domain is to provide a holistic view of the surface biogeochemical processes controlling silica and trace metals. The compilation of the key parameters, including selected trace metals concentrations with typical seawater concentrations, is summarized in Table 1.1. Existing studies on the trace metals and isotopes ($^{87}\text{Sr}/^{86}\text{Sr}$) pose diverging views on the significance of chemical weathering in Antarctica compared to low latitude surface weathering in major river basins. For instance, few studies (Diaz et al., 2020; Nezat et al., 2001 ; Wadham et al., 2010) indicate a significant role of the local factors such as salt dissolution and dust inputs to the increased supply of the solutes during the austral summers. Although, limited water-rock interaction due to freezing in austral winters restricts the magnitude of the flux generated from the surface processes in Antarctica.

Unlike major ions and Sr, few of the other trace metals such as Mo, Ba, Cu, Mn, Cd and Co pose a different character and supposed to be influenced by the various biological and inorganic processes. Particularly, the dissolved Ba in Antarctica shows its removal during the transport in the Antarctic surface environments, although the deciding factor of the Ba control is yet to be explored (Saelens et al., 2018). Few of the other elements (Cd, Mo, Cu) take part in the biological uptake by the phytoplankton in the freshwater oligotrophic limnic environments. For example, dissolved Mo does not show its limiting characteristics in the seawater. In case of concentration below the seawater threshold, it shows active nitrogenase character and participates in the primary productivity in global lacustrine coastal reservoirs (Glass et al., 2012). Apart from the direct biological uptake, it also varies with fluctuations in the oxidation concentration in the water column of global reservoirs (Castrillejo et al., 2013; Ho et al., 2010). Few of the elements, such as Cu and Mn, also reflect these fluctuations and show the adsorption and/or desorption onto the clay surfaces in the lake sediments (Cuozzo et al., 2020). The combined assessment of these trace metals with the biological parameters such as chlorophyll-*a* and dissolved organic carbon (DOC) in the East Antarctic lakes would reveal behaviour of these individual elements in the cold Antarctic environments.

The other aspect of interest in this thesis is to understand the Ba and Si biogeochemical cycling in the surface waters of the Indian sector of the Southern Ocean. There is an established global relation between the Si(OH)_4 -Ba in the seawaters (Pyle et al., 2018). However the reason for their covariation is enigmatic (Sternberg et al., 2005) and provides a significant research gap to better understand the global phenomenon controlling barium and silica biogeochemical cycling. The enigma of the Ba-Si(OH)₄ relation in the surface waters of the global ocean could be linked to the biological uptake processes majorly and to the physical circulation derived chemical changes to a lesser extent (Pyle et al., 2018). Diatoms, which comprise ~50% of the world ocean primary productivity during the silica uptake, prefer the lighter isotopes (²⁸Si) and discriminate against the heavier isotope of silica (³⁰Si). This results in more positive $\delta^{30}\text{Si}$ signature of the seawaters in the high productivity zones (De La Rocha et al., 2011; De La Rocha et al., 2000). Investigating $\delta^{30}\text{Si}$ in the Southern Ocean waters with the dissolved Barium could reveals the common connection between the two and possibly reveal their controlling factors. The Ba-Si(OH)₄ covariation in the global seawater could be possibly linked to the silica fractionation during uptake/dissolution is yet to be explored.

1.2 Objectives of this thesis

The major objectives identified for this thesis work are listed below:

- Understanding the behaviour of trace elements in the water column of the Indian Sector of the Southern Ocean and Antarctic lakes
- To establish chemical extraction procedures and measurement techniques for the measurements of Si isotope in water samples using MC-ICPMS
- Understanding the biogeochemical cycle of Si and its isotopes (³⁰Si) in the Indian Sector of Southern Ocean, Antarctic and its link to carbon and nitrogen cycles.

1.3 Outline of the thesis

Chapter 1 introduces the literature review on existing chemical weathering studies and biogeochemical cycling of the trace metals (particularly Barium) in Antarctica

and the Southern Ocean. An overview of the silica cycling in the surface waters of Southern ocean is also provided.

Chapter 2 provides the details about the sample collection during the research expedition to Antarctica and the Southern Ocean. Further, the analytical details of the trace metals and $\delta^{30}\text{Si}$ measurements in the dissolved seawater have been discussed thoroughly.

Chapter 3 focuses on the source apportionment and chemical weathering studies in the Antarctic environments using dissolved major ions, Sr and $^{87}\text{Sr}/^{86}\text{Sr}$, in the lake waters of the Larsemann Hills, East Antarctica.

Chapter 4 discusses the role of biological as well as inorganic processes on the biogeochemical cycling of the dissolved trace metals in the Antarctic lakes of the Larsemann Hills. For this, we have investigated the spatial and water column distribution of the dissolved trace metals in the lake waters along with the biotic parameters such as chlorophyll-*a* and dissolved organic carbon. Accumulated barium and Sr, along with major oxides, are also assessed in the lake and catchment sediment to further deduce the fate of the Barium in the polar environment.

Chapter 5 presents the distribution of the dissolved Ba and $\delta^{30}\text{Si}(\text{OH})_4$ in the surface seawater samples of the Indian sector of the Southern Ocean. These data are used to evaluate the Barium and silica cycling in surface southern ocean and attempt to explain the enigma of Ba-Si(OH)₄ relation.

Chapter 6 summarizes the major conclusion drawn out from this thesis work. This chapter also highlights the future directions for the research on biogeochemical cycling of trace metals and silica in the Southern Ocean and Antarctic environments.

Chapter-2

Material and Methods

The major objectives proposed for the thesis work, as mentioned in the introduction chapter, focuses on the polar domain i.e., Antarctica (lakes) and the Southern Ocean. For Antarctic lakes, the primary objective was to identify and evaluate the extent of physicochemical factors controlling the trace metal cycling in Antarctic lakes. While in the surface waters of the Southern Ocean, the major objective was to understand trace metal cycling (mainly Ba) and enigma of $\text{Si}(\text{OH})_4$ - Ba relationship in the seawater. To achieve these objectives, geochemical (trace metals, major ions), biological and isotopic ($\delta^{30}\text{Si}$, $^{87}\text{Sr}/^{86}\text{Sr}$) analyses were carried out in water and sediment samples collected during the austral summers of the year 2017. Details about the geological settings, hydrological and oceanographic conditions that help to further interpret these datasets are provided in the following sections. Although the sampling protocols and other details are already reported in several previous literature, a brief presentation has been attempted for the sampling and analytical strategy. The summary of the analyses performed is shown in figure 2.1.

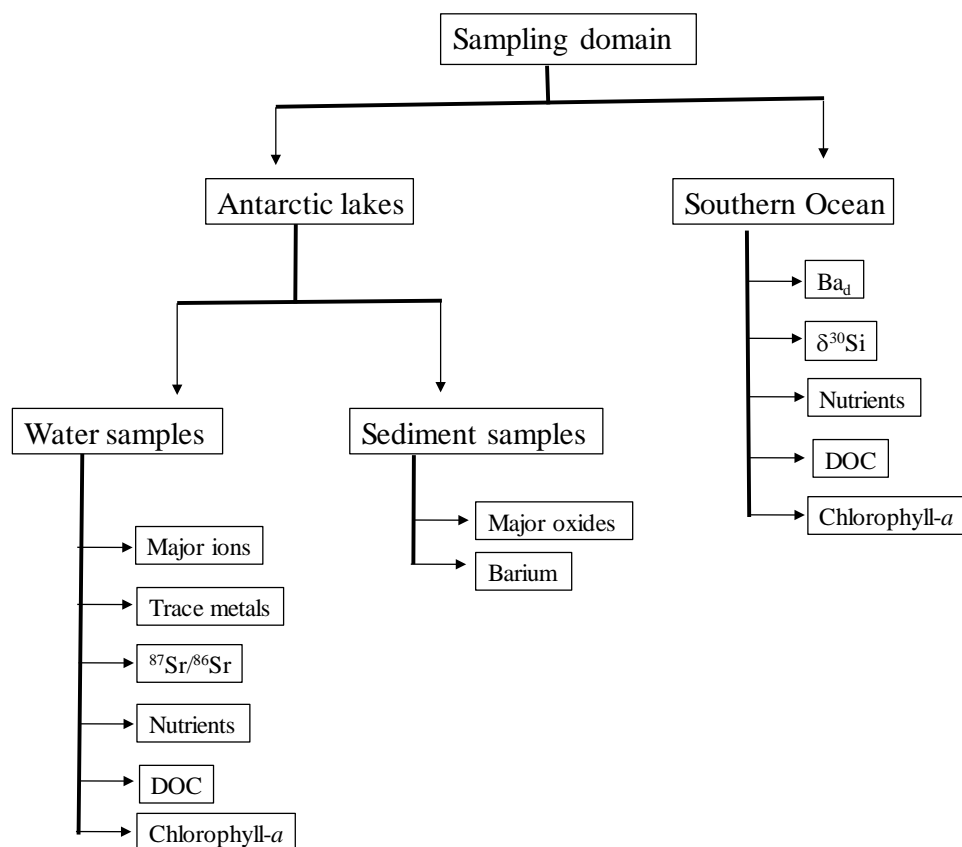


Figure 2.1. Classification chart for the sampling domain and parameters analysed for the thesis work.

2.1 Study Area: Antarctic lakes

2.1.1 Geological settings of Larsemann Hills

Samples for the study were collected from 10 lakes (Figure 2.2) from the coastal region of the Prydz Bay (69°20'S-69°34'S,66°E-79°E), East Antarctica, near the Princes Elizabeth Land. The Prydz Bay water discharge accounts for almost 16% of the meltwater from the East Antarctic Ice sheet (Hodgson et al., 2016). The major source of this meltwater is the Amery ice shelf and neighboring glaciers (Hodgson et al., 2016). There are ~120 major and minor ice-free islands, which comprise ~100 km² areas and constitute three distinct regions such as Larsemann Hills (LH), Vestfold Hills and Rauer Group. The Larsemann Hills are comprised of two major and four minor peninsulas (Figure 2.2). The basement rock of Larsemann Hills is of Meso- to Neo-Proterozoic age, which consists of a layered complex of iron rich gneiss and heterogeneous garnet bearing migmatitic paragneiss. Metapelites lenses are also found as an intrusion in the basement rocks composed of sillimanite, spinel, cordierite, garnet, K-feldspar, and biotite (Carson et al., 1995; Stüwe et al., 1989). A thin layer of permafrost develops at a depth of 0.3-0.9 m (Kaup and Burgess, 2002; Shevnina and Kourzeneva, 2017). The previous study based on the metal in topsoil suggests the soil in the Larsemann Hills is compositionally immature, indicating that the region could possibly fall in an active but slow weathering zone (Shi et al., 2018).

2.1.2 Geohydrology and Climate

More than 150 freshwater lakes ranging from small ponds to deep glacial water bodies are present in Larsemann Hills (Liu et al., 2007). The origin of these lakes is not yet known, however, based on current knowledge, multiple advancement and retreat of glaciers resulted isostatic readjustment and mechanical weathering to form the lakes in Larsemann Hills (Burton, 1981; Hodgson D A. et al., 2005). These lakes are fed by meltwater supplies during the austral summer through small streams and channels. The daily mean discharge varies from 0.02 to 1.6 m³/s in different lakes (Shevnina and Kourzeneva, 2017). During austral winters, the melting of ice/snow is limited; therefore, the amount of water available in the stream is meagre, which comes from the melting of snow at the bottom and flows

through the micro seepages. These lakes are generally considered oligotrophic in nature due to low nutrient availability and low biological productivity (Sabbe et al., 2003). Earlier studies suggest that these lakes are pristine and unaffected by any anthropogenic activities in the area (Gasparon and Matschullat, 2006a, b; Kaup and Burgess, 2002). The monthly mean temperature during austral summers (December, January, and February) is close to 0 °C, the maximum temperature goes up to 8 °C and varies between -15 °C to -18 °C during winters (Gillieson et al., 1990). In addition to the cold and dry climate, strong katabatic westerlies leave imprints of wind erosion (e.g., honeycomb structures) onto the North-South facing hillocks (Spate et al., 1995). The strong winds cause internal mixing in ice-free lakes, whereas perennially ice-covered lakes are less affected. Physical and chemical stratification are found in these ice-covered lakes. The ideal location of these lakes, i.e., proximity to the sea, nourishing biological environment, and significant input of meltwater, makes them an ideal natural system to understand the ongoing surficial processes in their catchments.

2.2 Sample collection from Antarctic lakes

Samples were collected for dissolved trace metals, nutrients and biological parameters from 10 different lakes of Larsemann Hills during the 36th Indian Scientific expedition to Antarctica during the austral summer (Jan-March) of the year 2017 (Figure 2.2). A total of twenty-eight surface and benthic water samples were collected. Pre-cleaned and rinsed Niskin bottles were used for sample collection. A coring platform attached to the inflatable rubber ponton was used to collect the samples from the deepest point of the lakes. Physical parameters (pH and temperature) of the samples were measured using an on-site portable sensor. A total of six litre of water samples were collected using Niskin bottles from a coring platform attached to a metal-free rubber pontoon and preserved in cleaned bottles in two separate aliquots. The depths corresponding to benthic samples were measured manually using a graduated rope. The samples were collected in pre-cleaned HDPE bottles after rinsing it a few times with the ambient water. We filtered these samples using 0.45 µm cellulose acetate filters within 24 hrs of their collection. The filtered samples were split into two aliquots, and one of these aliquots was acidified with ultra-pure HNO₃ acid to pH~2. The first aliquot for trace

metals and dissolved nutrients were filtered with 0.45 μm cellulose acetate filters, and the part of the sample (~500 ml) was acidified with Merck® ultrapure nitric acid to pH-2, Whereas the non-acidified aliquot of the samples for nutrient (SiO_4 , PO_4^{2-} , NO_3^-) analysis was immediately preserved at -20°C . A small unfiltered aliquot of these samples was preserved in clean bottles left un-acidified for the major ions. Samples were handled carefully to avoid any contamination during sample processing in the laboratory.



Figure 2.2. Location map of the ten coastal lakes near the Prydz Bay, East Antarctica. The regional geology of this region has also been shown (modified after Carson and Grew (2007)).

A separate aliquot of four litres of lake water was filtered with GF/F filters at low pressure for the measurement of *Chlorophyll-a*. The filter paper obtained for *Chlorophyll-a* analysis was immediately preserved at -80°C temperature in a deep-freeze facility. To assess the dissolved organic carbon (DOC) in lake waters, filtered samples were immediately preserved in glass ampoules and preserved at -20°C temperature.

Lake bed sediments and surface sediments (n=11; Figure 2.2) were also collected from nearby catchment areas using a cleaned plastic scoop and preserved at -5°C

in a pre-cleaned zip lock bag. Samples were analysed for major oxides (SiO_2 , Na_2O , Fe_2O_3^* (total), K_2O , MgO and CaO), Ba, and Sr concentrations. SEM-EDS analysis was carried out in these lake sediments to identify micro-precipitates and determine their chemical composition, phases, and distributions. This analysis would enable us to investigate the role of biological and/or inorganic processes and mechanisms for the precipitations and environmental conditions during their precipitation in the lakes.

2.3 Analysis of water samples from lakes

2.3.1 Alkalinity and major ions

The alkalinity of the samples was measured in their unacidified aliquots using the Gran-titration method following Tripathy et al. (2019). Selected nutrients (silicates and nitrates) were measured in unacidified aliquots (stored at -20°C until analyses) using an automated spectrophotometer. Major cations (Na^+ , K^+ , Ca^{2+} , Mg^{2+}) and anions (Cl^- and SO_4^{2-}) in the unacidified aliquots were measured using an Ion chromatography (Dionex) instrument. The water samples were passed through the IonPac CS17 column to separate the cations and the IonPac AS11-HC column to separate anions. The individual cation and anion peaks were quantified following a standard calibration approach to estimate the ionic concentrations. Reference standard solutions were measured repeatedly at certain intervals to check the accuracy of measurements, whereas several replicates were analysed to constrain the analytical precision. The accuracy and precision of the measurements were better than 5%.

2.3.2 Dissolved Sr

Dissolved Sr concentrations were measured in acidified aliquots using a Quadrupole ICPMS (Agilent 7700x) instrument. Towards this, the signal of the ^{88}Sr isotope of the sample was quantified by a standard calibration approach. Freshwater reference standard SLRS-6 was analysed several times during the course of analysis. The average Sr concentration of the SLRS-6 measured during the course of analysis (39.5 ng/g, $n=5$) was found to be consistent with its reported value of 40.7 ± 0.3 ng/g. Replicate analyses of samples ($n=3$) yielded a precision better than 3% for the Sr concentration measurements.

2.3.3 $^{87}\text{Sr}/^{86}\text{Sr}$ ratios

Sr isotopes were analysed in the filtered and acidified water samples using the multi-collector-ICPMS (Neptune Plus, Thermo[®] Scientific) facility at NCPOR, India. These analyses were performed following the analytical approach adopted by Rahaman and Singh (2012). Briefly, about 10 ml of water samples were passed through Eichrom Sr specific resin 50–100 μm to extract pure Sr from the samples and analysed for Sr isotopes. The measured Sr isotopic composition was corrected for instrumental mass bias by normalizing natural ratio of $^{86}\text{Sr}/^{88}\text{Sr}$ 0.1194. The isotopic signal at mass 85 amu was observed constantly to monitor any ^{87}Rb interference. A standard solution of NIST NBS-987 with comparable sample Sr concentrations was measured at regular intervals during the course of sample measurements. The Sr isotopic data are reported hereafter sample-standard bracketing normalization following the approach of Weis et al. (2006). The average $^{87}\text{Sr}/^{86}\text{Sr}$ value of NBS 987 during the period of this study yielded a value of 0.710280 ± 0.000011 (2σ , $n = 5$) which is well within its recommended value of NBS-987 (0.710250 ± 0.00040 (2σ)). A few replicate samples were also investigated, yielding a measurement precision of ~ 5 ppm. The average total procedural blank for Sr isotopic measurement was found to be ~ 150 pg which is less than 0.02% of total Sr analysed in samples, and therefore, blank correction was not done.

2.3.4 Trace metals

Dissolved trace metals (Cu, Cd, Co, Mn, Ba, Pb, Cr, As, U and Mo) were measured in acidified aliquot using Q-ICP-MS (model Agilent 7700x) at the National Centre for Polar and Ocean Research (NCPOR), Goa. Samples were directly measured without any preconcentration or dilution. Since dissolved metals in the lakes are in the sub-nM level, blanks were measured at regular intervals during the analysis to monitor any kind of contamination. The sample introduction system (tubing and nebuliser) was cleaned repeatedly with a 2% HNO_3 matrix between measurements to minimize memory effects. Reference standards SLRS-6 and NIST-1640e were also measured at regular intervals during the analysis. Accuracy of the measurements to the reference standard was found within 10% of uncertainty ($n=5$) for all the reported trace elements analysed except for Mo and U (11.5%). Precision

and accuracy were better than 3% determined based on several replicate analyses of standard SLRS-6 (n=5) and samples (n=3). External calibration performed for the trace metals measurement in the lake waters are shown in the figure 2.3.

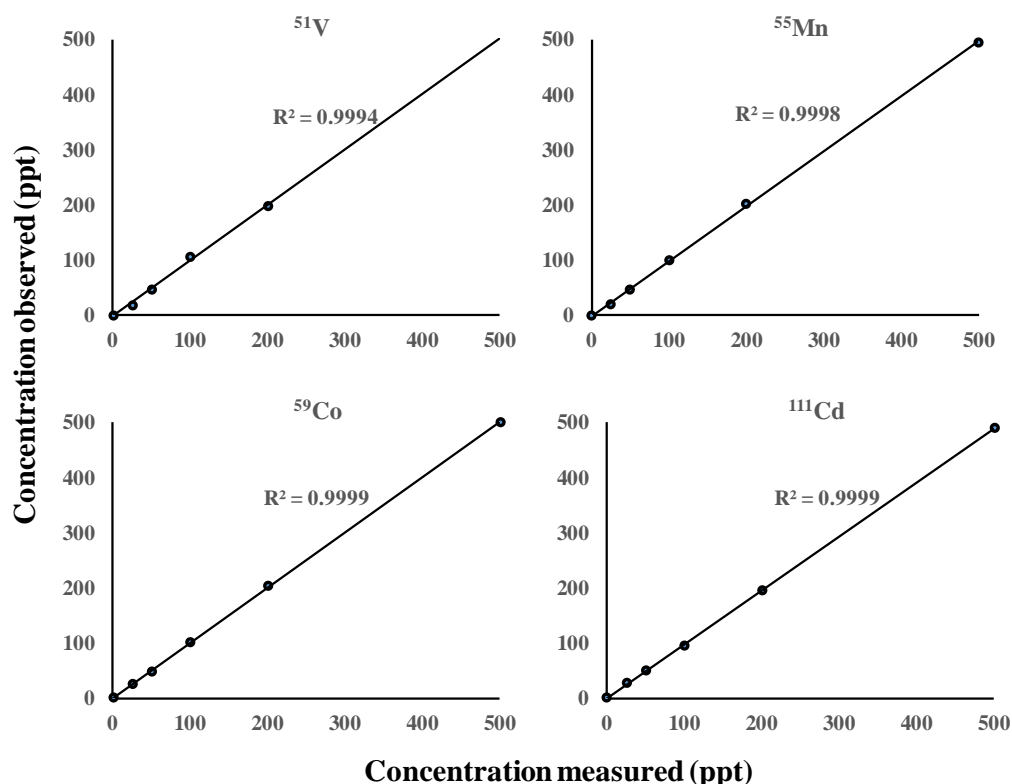


Figure 2.3. Standard calibration plot for the dissolved trace metal (V, Mn, Co and Cd) measured in the water samples from Antarctic lakes.

2.3.5 Biological parameters

We have also analysed *Chlorophyll-a* in preserved filters following the method of (Sinha et al., 2019). Filters were first poured in ultrapure acetone to extract the pigments, followed by the measurement of fluorescence with a Triology®-7200 fluorometer. The Dissolved Organic Carbon (DOC) in the syringe filtered samples was determined using a TOC analyzer (TOC-VCSH, Shimadzu, Japan). An aliquot of the treated water sample (50 μl) was injected onto a combustion column. Non-purgeable organic carbon compounds are combusted and converted to CO_2 , which is then detected by a non-dispersive Infrared sensor (NDIR). Reference seawater and blanks were regularly measured. Based on

standard and sample analysis, accuracy was better than 5% whereas obtained measurement precision were better than 3%.

2.4 Major oxides and Barium in bulk sediments from lakes

Sediment samples were freeze-dried and powdered for the analysis of major oxides and trace element (Ba and Sr) abundances using a wavelength-dispersive X-Ray fluorescence spectrometer (WD-XRF; Model: PANalytical Axios Max) equipped with an automatic sample changer and software Super Q V5 Wavelength dispersive at NCPOR, Goa. An international reference standard, JLK-1 was measured at regular intervals during the analysis of sediment samples. The accuracy of the measurements for the major oxides was better than 3%, with an exception for Fe_2O_3^* (8.9%) and precision based on replicate (n=3) analysis was better than 4% except for SiO_2 (6.8 %) and Fe_2O_3^* (7.5%). For bulk Ba and Sr concentration measurement in sediment standard (JLK-1), the accuracy and precision were better than 3%.

Micro-precipitates in the lake bottom sediments were also analysed using SEM-EDS at NCPOR, Goa. A small amount (~2 gm) of the samples was freeze-dried and platinum-coated for a thickness of ~2 nm and analysed with JEOL JSM –6360LV SEM with a voltage range between 25-50 kV. The semi-quantitative major element analysis (area average) was carried out using Energy dispersive spectroscopy (OXFORD INCA 200), equipped with JEOL 6360 LV SEM.

2.5 Sample collection from the Southern Ocean

The seawater sample collection for the analysis of the macronutrients and biological parameters was done onboard MV/Ivan-papnin as part of the Indian Scientific Expedition to Antarctica during the austral summer in 2017. A total of 67 surface water samples were collected during three transects of the expedition (Figure 2.4). The first transect (T1) represents the track between Capetown and Prydz Bay and the early phase of the austral summer. The third transect (T3) is the track representing the corresponding samples along 9-15°E between the India Bay (Antarctica) to Capetown and the late phase of the austral summers (Figure 2.4).

The second transect (T2) represents the track covering the longitudinal variations along coastal Antarctica during the peak austral summer of 2017 (Figure 2.4).

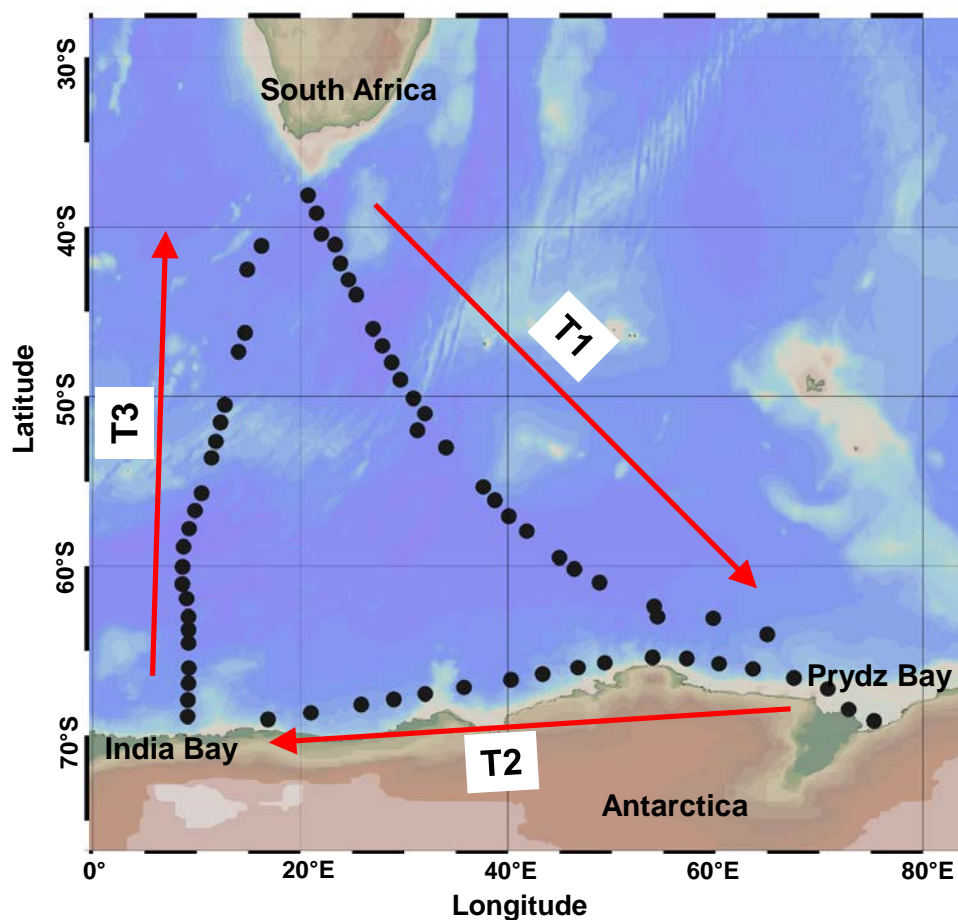


Figure 2.4. Sampling locations of the surface seawater collected from the Indian sector of Southern Ocean during the austral summer of the year 2017. T1, T2 and T3 with arrow represents the corresponding sampling transects and track of the expedition. The T1 commenced from South African waters to Prydz Bay East Antarctica during mid-austral summer (January 2017), T2 shows the track between the Prydz Bay and India Bay which was commenced during late summer (Feb, 2017) and T3 is return corresponding track to T1, between India Bay and South Africa where the sampling was done between the March and April, 2017.

The sample collection was done during the 36th Indian Scientific expedition to Antarctica (ISEA) during the austral summer from December 2016 to March 2017. Surface seawater samples were collected using a 15-liter pre-cleaned plastic container attached to a pre-cleaned graduated plastic rope. The samples were filtered onboard using a cellulose acetate filter of 0.45 μM size in a cleaned environment. The sample aliquots for the dissolved Barium and silicon isotope ($\delta^{30}\text{Si}$) analysis were acidified below pH \sim 2 using the suprapure nitric acid (HNO_3)

(Merck Millipore®) following the standard protocols for trace elements and their isotopes (TEIs) in seawater (Singh et al., 2015). Blanks for the sampling container and ambient environment were also collected.

The sample aliquots for the macronutrients were immediately frozen and preserved at -20°C in a controlled environment. This temperature was maintained till the sample analysis in the laboratory at National Centre for Polar and Ocean Research (NCPOR), Goa. An aliquot of the ~50 ml filtered sample preserved in the pre-cleaned glass ampoules for dissolved organic carbon (DOC) analysis. Ampoules were fused immediately after the sample collection, using the gas-supported flame, which restricted sample exposure to the ambient air, and preserved at the -20°C till the analysis at the laboratory. The samples for chlorophyll-*a* were collected using GF/F filters. Approximately 4 liters of seawater were filtered onboard for chlorophyll-*a* measurement in each sample. The filters were kept in the cleaned petri-dishes and preserved at -80°C till analysis is done in the laboratory at NCPOR, Goa.

2.6 Oceanographic Setting of the Indian sector of Southern Ocean

The oceanic circulation in the Indian sector of Southern Ocean (INSO) is dominated by the Antarctic circumpolar currents (ACC) and contains several fronts characterising the water masses with marked changes in physicochemical properties (Orsi et al., 1995). Three important fronts are clearly visible in the INSO; the Agulhas retroflection front (ARF), Sub tropical front (STF), and Sub Antarctic Front (SAF) (Sokolov and Rintoul, 2007). The ARF is characterised by 15.7-21 °C SST and shows the link between the South Atlantic and Southern Ocean currents and is also responsible for the exchange of water masses between the Southern Indian and Atlantic Ocean (Lutjeharms, 2006). Further south (~42°S), the STF marks the interface between the subtropical and sub-Antarctic waters with characteristics SST of 10-14°C (Whitworth III and Nowlin Jr., 1987). Further south, the major fronts follow as sub-Antarctic Front and Polar front at 45° and 50°S approximately and the temperature gradient becomes less for the Polar front.

2.7 Analysis of nutrients, DOC and chlorophyll-*a*

Dissolved macronutrients (Si(OH)_4 , NO_x , PO_4^{3-}) in the seawater samples were analysed using SKALAR auto-analyser following the molybdate blue colorimetric method (Strickland and Parsons, 1972). The samples were melted before analysis at room temperature. The standards were analysed at regular intervals to ascertain precision ($\pm 3\%$) and accuracy ($\pm 6\%$) of in-house laboratory standard during analysis. Chlorophyll-*a* obtained from filters (GF/F) were analysed using a fluorometer (Triology®-7200) (Sinha et al., 2019). The filters containing chlorophyll-*a* were extracted from pigments using ultrapure acetone. The pigment fluorescence was normalized to the total amount of the filtered seawater. The chlorophyll-*a* data is reported in the mg m^{-3} unit.

Syringe-filtered samples were used for the Dissolved Organic Carbon (DOC) analyses using a TOC analyser (TOC-VCSH, Shimadzu, Japan) (Sanyal et al., 2020). Approximately 50 μl of melted water samples were introduced into the combustion column, where non-purgeable organic carbon compounds get converted into CO_2 and detected by the non-dispersive Infrared sensor (NDIR). To check the accuracy and precision of the analysis samples, known seawater standards were measured at a regular interval during the analysis. The precision and accuracy ascertained for the analysis were better than $\pm 3\%$ and $\pm 5\%$, respectively.

2.8 Dissolved Barium (Ba_d) analysis in seawater

The Ba_d was analysed using the ICP-MS (Agilent 77000x) facility at Isotrace laboratory NCPOR, Goa. Measurements of trace elements in seawater are tricky due to the high matrix. Therefore, the strategy of barium measurements in seawater samples was performed by diluting the matrix at the optimum level so that matrices effect was minimum at the same time signal was sufficient to measure in the samples (Singh et al., 2013). In the case of dissolved Ba analysis using a direct measurement technique, the seawater samples were diluted by 35 times (salinity ~ 35). The analysis was performed for the two isotopes (^{135}Ba and ^{137}Ba) using the ICP-MS (Quadrupole), which are free from the isobaric interferences (Singh et al., 2013). However, the concentration of the Ba_d in the samples was calculated based on the signal (counts) of the higher abundance isotope, i.e., ^{137}Ba .

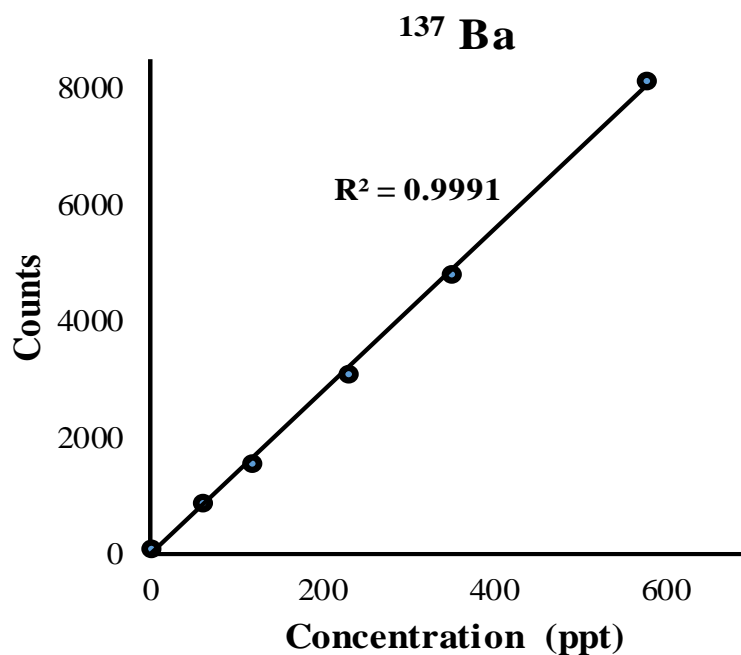


Figure 2.5. Calibration curve for the ^{137}Ba concentration measured in the seawater samples.

To monitor the recovery of the signals, samples were spiked with Rhodium (Rh) and ^{103}Rh isotope signal throughout the analysis. The Ba concentrations in the samples are mainly conducted through the external calibration method (Figure 2.5). Total of three international reference standards (NASS-6 and CASS-6 for seawater, SLEW-3 for estuary water) were measured to check the accuracy of the analysis. The accuracy-based measurements of these standards several times were found well within $\pm 5\%$ of the reported values. The precision of the dissolved Ba analysis determined based on the repeat measurements of the standards and samples ($n=9$) was $\pm 3\%$ (2σ). The long term reproducibility of Ba analysis of the NASS-6 produce the average concentration of 48 nM which agrees well with the reported values i.e., 48.6 nM (Hendry et al., 2018).

2.9 Silicon isotopes and its analytical methodology

2.9.1 Silicate fusion and silica purification steps

The setup of the Thermo Neptune MC-ICP-MS at the National Centre for Polar and Ocean Research consists of two sample introduction systems, i.e., wet plasma and dry plasma systems (Aridus III). Before introduction, solid samples need to be

digested, and silica purification steps should be performed to avoid matrix introduction into the systems. Solid standards such as NBS-28, IRMM-18a, Diatomite, and Big-Batch were measured during the analysis, where the NBS-28 is used as the bracketing standard. Approximately ~15 mg of pulverized, homogenized sediment samples are digested for 15 min at 750°C in a muffle furnace by NaOH fusion (400 mg NaOH pellets, Merck, p.a. grade) in Ag-crucibles (customised as the quality of requirement). This forms a fusion cake of the targeted samples which easily dissolve in the weak acidic solutions. After the dissolution of the fusion cake in Milli-Q water (>18 MΩ) and 1.5M HCl (pH 1.5), the sample solution is diluted to <30 ppm SiO₂ and acidified to pH 1.5 with HCl. These solutions were kept for 24 hrs and observed for visible particles if any were left. If so, the solutions were kept at 60°C until the solution became clearly visible. These standard silica solutions were stored in the ultraclean teflon containers in a dark and cool place in the laboratory and were utilized throughout the year. The reproducibility of data obtained for δ³⁰Si was regularly monitored for these aliquots.

2.9.2 Mg-induced silica precipitation (MAGIC) from Seawater

Silica pre-concentration is applied to the seawater sample for efficient column chromatography and high silica recovery (Figure 2.6). A total of ~3.6 μg of Si(OH)₄ from seawater was processed for each analysis. Seawater possesses a high amount of matrix as dissolved ions, the direct introduction of these samples matrix would exceed the column capacity and pose matrix interference issues to the analysis in the mass spectrometer. The Brucite co-precipitation method involves the induced precipitation of the Si-Mg-oxyhydroxides (MgO(OH)₂) out of seawater using NH₃ or Na(OH) solution (Karl and Tien, 1992; Zhang et al., 2014). An increase in the pH of seawaters using a strong base induces the silica precipitation out of the seawater and preconcentration by a magnitude of 2-5 times. In the case of samples having lower Si(OH)₄ concentration, a two-step silica precipitation was applied (Reynolds et al., 2006). Approximately 90% of the total silica from the sample was separated out in the first step of brucite precipitation. During this, sample was superannuated out of the precipitating centrifuge and the base (NaOH) was introduced twice to ensure the complete recovery of the silica. After each step of precipitation, the sample was centrifuged to avoid any silica loss from the sample.

To ensure the complete silica yield, the silica concentrations were measured using the spectrophotometric method (Strickland and Parsons, 1972). Following pre-concentration, the silica precipitate was dissolved in the minimum amount of 6M HCl and further diluted to 2 ml using deionised water to the final concentration of the 1.8 ppm with cationic matrix at approximate pH 2.

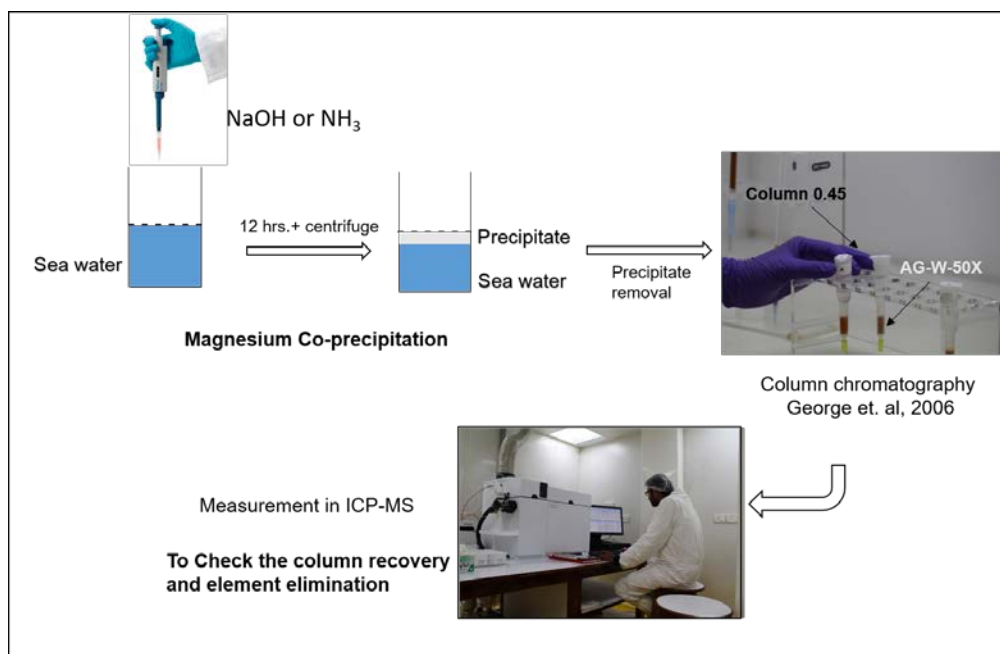


Figure 2.6. Schematic representation of the silica separation and purification for the $\delta^{30}\text{Si}$ analysis in the seawater samples.

2.9.3 Matrix removal through column chromatography

Silica purification steps were adopted and calibrated following George et al., 2006. Aliquots of $\sim 3.6 \mu\text{g}$ Si of this solution are loaded onto cation exchange columns (DOWEX AG 50W-X8, 200–400 mesh) from which silicon is eluted with 4 ml Milli-Q water. The steps followed for the matrix removal, and silica purification is given in the Table 2.1.

There are two established methods to separate silica from ionic matrix i.e., anion and cation exchange chromatography. For anionic resin chromatography, conversion of silica to H_2SiF_6 is required, which involves the use of HF and poses the risk of fractionation during processing (Engström et al., 2006). This method, however, produces a satisfactory silica recovery of $\sim 97\%$. The major inadequacy of this method is that it does not meet the requirement of HF-free solutions hence the cationic resin exchange column chromatography was used to purify silica for

silicon isotope analysis in this thesis (Georg et al., 2006). Cation exchange resin functions as a non-retaining agent for both nonionic silicic acid and anionic species ($\text{H}_3\text{Si}(\text{OH})_4^-$) between pH 2 to 8, which majorly prevail in the natural waters.

Table 2.1. Silica purification steps for seawater samples and standard solutions (Georg et al., 2006).

Rinsing	
Deionised MQ	6ml
Sample Load	
Collection	
Acidified sample	2ml
MQ-e	2ml+4ml
Cleaning	
3M HCl	3 ml
6M HCl	3 ml
7M HNO ₃	3 ml
10M HCl	3 ml
6M HCl	3 ml
3M HCl	3 ml
MQ-e	6ml+6ml

The $\text{Si}(\text{OH})_4$ purification was achieved by passing samples through a 1.8 ml resin bed of DOWEX 50W-X12 (200–400 mesh) in H^+ form. This resin allows the processing of a relatively small amount of samples ($\sim 3.6 \mu\text{g}$) than utilised in the anionic species-based resin (Engström et al., 2006). Before sample loading, process for the precleaning of the resin using double Teflon distilled HCl, HNO₃, and MQ-e water in several steps was performed described in Table 2.1. Before sample loading, MQ-e was passed through the resin to ensure a neutral pH. Silica elution occurs in both the sample loading and elution steps (MQ-e 2 ml) since resin retains all the cationic species. The final solution was made for 0.6 ppm diluted in the final volume of 6ml. The column chromatography steps complete in ~ 3 hrs for the one cycle of the resin cleaning and Si purification. Sample aliquots for each step were analyzed by ICP-MS before isotope analyses to check for column recovery and for purity of the Si sample solution (Figure 2.7). For the mass spectrometric analysis, the final dilution of standards and samples were diluted using 0.1 M HCl to < 0.5 ppm Si. After column chromatography, the Mg (Alfa Aesar Specpure 14430) was added to match Si concentrations. Cationic resin does not bind the anionic species such as Cl^- and SO_4^{2-} present mainly in the seawater, which could possibly interfere with the analysis. However, these deviations were not observed during the course

of the analysis. Another challenge posed by the samples with high DOC, which were also left unseparated from the cationic chromatography, were treated with the UV lamp to eliminate the excess carbon present in the sample (Oelze et al., 2016).

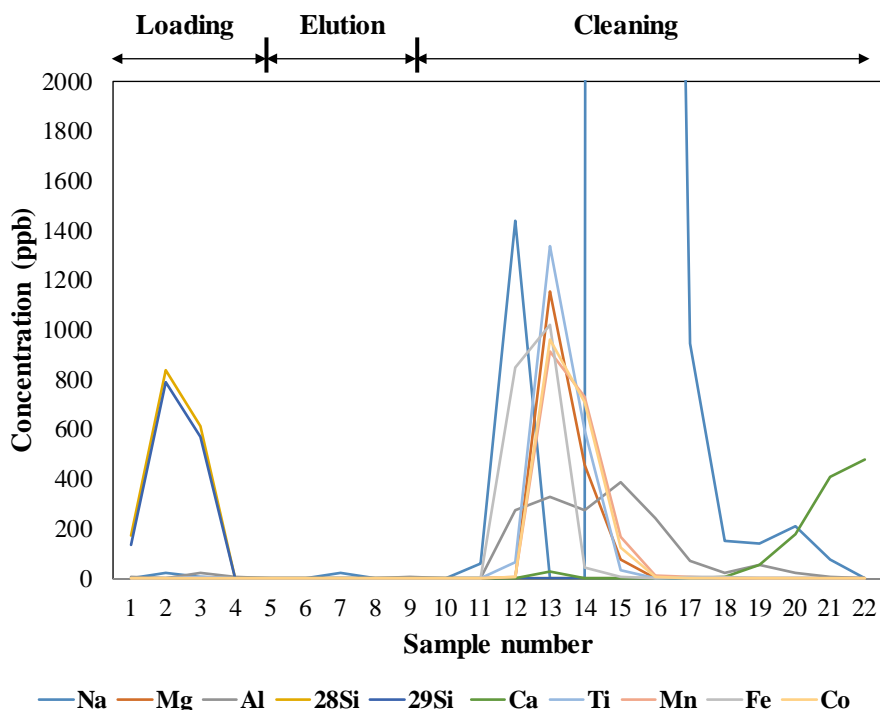


Figure 2.7. Concentration of Si and cationic species in the aliquots obtained during column chromatographic steps for the sample elution and cleaning of cationic exchange resin.

2.9.4 Silicon isotope measurement techniques

Stable silicon isotope measurements ($\delta^{30}\text{Si}$) are one of the most challenging analyses performed for this thesis. In this decade, IRMS was extensively used to measure silicon isotopes which included tedious efforts with far less data accuracy than present mass spectrometric techniques (De La Rocha et al., 2000; Ding et al., 2005). The major disadvantage of this technique was associated with the hazardous sample preparation, where the silica was initially converted to SiF_4 reacting with F_2 using the fluorination technique, which itself is prone to the fractionation during sample preparation (Ding et al., 2005). Few labs worldwide still measure silicon isotopes using IRMS (Beucher et al., 2007) as the fluorination technique was abandoned with the development of mass spectrometry and prepared the sample offline using mild HF, which efficiently converts a major portion of the silica to SiF_4 . However, this sample preparation technique itself introduces fractionation to

the silica since reacting silica with HF volatiles the samples. It poses a fractionation that could cause precision deformities in the sample datasets.

The advent of the latest mass spectrometric techniques and sample preparation methods eliminated the hazard associated with the sample preparation (Grasse et al., 2017). The result of the recent development in the latest mass spectrometry improved the efficiency of the measurement in the form of high sample throughput and improved precision (De La Rocha et al., 2000). Despite the recent developments, several measurement challenges, such as the polyatomic interferences of $^{14}\text{N}^{16}\text{O}$ to ^{30}Si and $^{15}\text{N}^{16}\text{O}$ to the ^{29}Si exist (Table 2.2), which require high resolving power of the instrument, thus reducing the sensitivity of the measurements. However, measurement using MC-ICP-MS in the samples is the most advanced and reliable technique available. The advancement of mass spectrometry and the development of MC-ICP-MS further development encouraged the measurement and application of silicon isotopes in various fields of interest. The MC-ICP-MS is a plasma-based measurement technique that facilitates the ion beam separation using a high-intensity induced magnetic field and allows them to collect in the focal plane of the mass spectrometer simultaneously and detected by the 11 movable faraday detectors. The silicon isotope measurement using MC-ICP-MS proved time-efficient and required a smaller sample volume (Wieser and Schwieters, 2005).

Table 2.2. Polyatomic interferences associated with the mass of Si isotopes 28, 29, and 30

Isotope	Hydrides	Nirtogen based	Carbon based	Doubly charged ions
^{28}Si		$^{14}\text{N}_2^+$ (960) ^e	$^{12}\text{C}^{16}\text{O}^+$ (1560) ^e	$^{56}\text{Fe}^{2+}$ (-2960) ^e
^{29}Si	$^{28}\text{SiH}^+$ (3510) ^e	$^{14}\text{N}^{15}\text{N}^+$ (1090) ^e	$^{12}\text{C}^{16}\text{OH}^+$ (1100) ^e	$^{58}\text{Fe}^{2+}$ (-2940) ^e
		$^{14}\text{NH}^+$ (770) ^e	$^{12}\text{C}^{17}\text{O}^+$ (1280) ^e	$^{58}\text{Fe}^{2+}$ (-3280) ^e
			$^{13}\text{C}^{16}\text{O}^+$ (1330) ^e	
			$^{13}\text{C}^{17}\text{O}^+$ (1044) ^e	$^{60}\text{Ni}^{2+}$ (-3580) ^e
^{30}Si	$^{29}\text{SiH}^+$ (2840) ^e	$^{12}\text{N}^{16}\text{O}^+$ (1240) ^e		
		$^{14}\text{N}^{15}\text{NH}^+$ (810) ^e		
		$^{14}\text{N}^{15}\text{ND}^+$ (650) ^e		

^evisible in Higher mass resolution ^bnegative values represents the interference fall on lower mass side Numbers in () indicates the required mass resolution (m/ Δm)

2.9.5 Working parameters of MC-ICP-MS

Several analytical challenges were encountered during Si isotope measurement and instrument optimisation. Sample introduction mode was one of the major challenges due to the lower sample amount. The standard sample bracketing technique of three replicate measurements requires a large volume of standard for each sample analysis while using the wet plasma mode. On the other hand, the dry plasma mode, which is the comparatively advanced technique of sample introduction, removes the sample solvent before introducing it to the plasma, thus requiring a lower sample amount and providing better sensitivity and precision (Oelze et al., 2016). The major challenge encountered during the measurement with the dry plasma mode (Aridus III) is the memory effect due to possible silica precipitation in the transfer tubes. The memory effect was initially removed using mild HF (0.1 M) followed by HNO₃ flow for long hours to obtain the silica-free and HF-free system before measurement. Once the silica is removed from the system, the memory effect was not encountered even during the long run of measurement. Instrument tuning was performed before each session of analysis for maximum optimised signal. The better optimisation help to reduce the instrument-induced isotope fractionation. Before each analytical session, a warm-up time of ~3 hrs is utilised at optimised parameters. With the improvement in the instrument sensitivity by tuning parameters such as torch positions, inlet gas pressure through desolvator, peak shape and flatness was specially optimised for better precision. Basic details and instrument operating parameters are described in Table 2.3.

One of the most common challenges of isotopic measurement through mass spectrometry is the isobaric interferences introduced into the plasma through Ar, N₂, hydrides, and NO_x. For silicon isotopes, these isobaric interferences prominently affect all three isotopic peaks, as shown in table 2.2, and remain unresolved in the low-resolution mode of the Neptune MC-ICP-MS. These interferences were visible in the medium resolution ($m/\Delta m$) of 1000; however, the peaks were not completely resolved. Thus, the measurement were performed left half shoulder of the plateau (Figure 2.8). The high-resolution modes were avoided since the isotope signals significantly reduced with deterioration in the precision of the measurement (Cardinal et al., 2003; Cardinal et al., 2005; Grasse et al., 2017).

Table 2.3. Instrument operating parameters for the analysis of silicon isotopes using Neptune plus MC-ICP-MS coupled with Aridus-III desolvating nebulizer

Instrument parameters	Operating details/magnitude
Hardware	
Instrument	Thermo Neptune Plus
Injector	ESI™ Quatrz (1.8 mm I.D)
Sample Cone	Jet spary
Skimmer Cone	Ni-X
Faraday cup	H3 (³⁰ Si), C(²⁹ Si), L3 (²⁸ Si), [L2(²⁴ Mg), C (²⁵ Mg)
Plasma	Dry plasma (Aridus III without N ₂)
Autosampler	ESI™ prepFAST 2DX
Inlet system	
RF power	1200W
Argon cool gas flow rate	15.5 L/min
Argon Auxiliary gas flow rate	1.0 L/min
Argon sample gas flow rate	0.7 L/min
Other parameters	
Mass resolution	Medium
Number of blocks	1
Number of cycles	30
Integration time	4.13 s/ 8.389 s
Idle time	3 s for 10 ¹¹ ohm
Number of integrations	1
Peristaltic pump speed	3 rpm for waste
Sample aspiration	Self (dry plasma)
Sample Matrix	0.1 M HCl
Uptake time	60s
Analysis time	250 second
Washout time	250 second

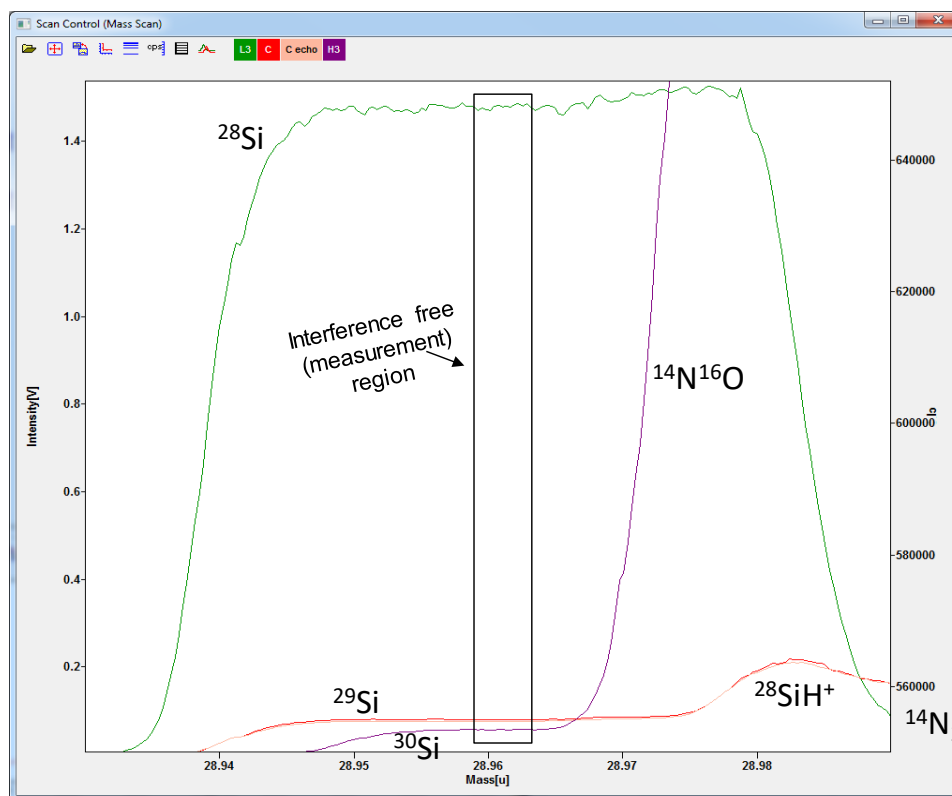


Figure 2.8. Isobaric interference observed for the Silicon isotopes in the medium resolution ($m/\Delta m=1000$).

In addition to instrument tuning and optimisation, sample measurement sequence is also critical to estimate the mass bias during measurement. The typical sequence order used for each sample includes ‘Blank-Standard-blank-sample-blank-standard’ with three measurements of indicated sequence for each sample analysis. The mean $\delta^{30}\text{Si}$ value observed from each analysis sequence is reported with 2SD. Samples diluted in 0.1M HNO_3 matrix were introduced to the mass spectrometer using self-aspirating Aridus-III (CETAC) desolvating nebulizer (temperature 140°C), inbuilt spray chamber (temperature 110°C) with Ar sweep gas flow rate of 4 ml/min. The 50 $\mu\text{l}/\text{min}$ micro-centric nebulizer was used in the desolvation unit to minimise the sample uptake and enhanced sensitivity. Approximately 3 times sensitivity ($16\text{V}/\mu\text{g}$) was obtained using this setup than the wet plasma system ($6\text{V}/\mu\text{g}$). The jet sample cone, Ni-x skimmer cone with quartz injector was used to obtain the better sensitivity.

2.9.6 Mass Bias correction

Mass bias uncertainties introduced in the silicon isotope data are mainly due to internal mass shifts during long batch analysis and polyatomic interferences. Thus for achieving high precision isotope data, these mass bias becomes essential to be corrected with adding the internal standard such as Mg (Cardinal et al., 2003). Magnesium is established as an ideal internal standard for mass bias corrections as it possesses the required physical, chemical, and isotopic properties. Two isotopes of the Mg (^{24}Mg and ^{25}Mg) are free from polyatomic interferences as the contribution of $^{24}\text{MgH}^+$ as hydride interferences are negligible (0.02‰) (Vanhaecke and Moens, 2004) and with high relative abundances. The introduction of Mg as an internal standard poses another challenge for the simultaneous measurement using Neptune MC-ICP-MS since it only allows up to 17% of mass difference, whereas the difference between the mass of Si and Mg exceeds this limit (Weyer and Schwieters, 2003). Thus the measurement of two was performed in a dynamic mode where the mass at the magnet shift between Mg and Si simultaneously during each line of measurement. Two cup configurations as (main and sub configurations) where ^{28}Si , ^{29}Si , and ^{30}Si were monitored in the main cup configuration as C, L3 and H3 whereas ^{24}Mg and ^{25}Mg were monitored in the subconfiguration as C and L2 cup configuration. The concentration matching (Mg and Si) was supposed to be another challenge for measurement and producing high-quality data. To minimise the matrix-related uncertainties, concentration match was kept within $\pm 10\%$, although it does not show potential influence on the data up to 40% of mismatch (Oelze et al., 2016). Dynamic measurement of the Si and Mg increases the measurement time (almost double) compared to Si analysis without Mg using dry plasma mode. Steps for offline estimation and correction of mass bias include the calculation of f_{Mg} , which is a factor that represents the mass bias occurs during the analyses (equation 1) (Cardinal et al., 2003). Mass ^{25}Mg and mass ^{24}Mg here represent the natural atomic abundance of the two isotopes, respectively.

$$f_{\text{Mg}} = \ln \frac{\left(\frac{^{25}\text{Mg}}{^{24}\text{Mg}}\right)_{\text{true}}}{\left(\frac{^{25}\text{Mg}}{^{24}\text{Mg}}\right)_{\text{measured}}} \bigg/ \frac{(\text{Mass } ^{25}\text{Mg})_{\text{true}}}{(\text{Mass } ^{24}\text{Mg})_{\text{measured}}} \quad (1)$$

The estimated mass bias factor obtained using Mg isotopes is then applied to correct the Si isotopic data to find the mass bias-corrected Si isotopic ratios ($^{30}\text{Si}/^{28}\text{Si}$), also denoted as the true isotopic ratio in equation 2.

$$\left(\frac{^{30}\text{Si}}{^{28}\text{Si}}\right)_{true} = \left(\frac{^{30}\text{Si}}{^{28}\text{Si}}\right)_{measured} \times \left(\frac{Mass\ ^{30}\text{Si}}{Mass\ ^{28}\text{Si}}\right)^f \quad (2)$$

The mass bias-corrected isotopic ratios are then utilized to estimate the $\delta^{30}\text{Si}$ relative to the bracketing standard (NBS-28 used in this study).

$$\delta^{30}\text{Si} (\text{‰}) = \left(\frac{\left(\frac{^{30}\text{Si}}{^{28}\text{Si}}\right)_{true}}{\left(\frac{^{30}\text{Si}}{^{28}\text{Si}}\right)_{NBS28}} - 1 \right) \times 1000 \quad (3)$$

2.9.7 Three isotope plot

A three isotope plot is constructed between $\delta^{29}\text{Si}$ and $\delta^{30}\text{Si}$ values obtained for Diatomite, Big Batch and IRMM-18a to assess the deviation from true mass-dependent fractionation line (Figure 2.9). The analytical precision of $< 0.1\text{‰}$ helps to assess the differentiation between the two mass-dependent fractionation i.e., kinetic and equilibrium. Molecular and/or isotopic movement control kinetic fractionation whereas equilibrium isotope fractionation depends solely on the isotope mass (Engström et al., 2006). Slope of three isotope plot also differentiate between kinetic and equilibrium fractionation as the calculated slopes for two are reported as 1.93 and 1.96 respectively (Reynolds et al., 2006). Inaccurate mass bias estimate and polyatomic interference to Si isotopes cause major deviations from the reported slopes, hence slope deviation from the theoretical boundaries are used to interpret the data robustness (Cardinal et al., 2003; Grasse et al., 2017; Hendry and Brzezinski, 2014; Zambardi and Poitrasson, 2011). In natural silicon isotope systematics, the slope deviation helps to assess the type of mass dependent fractionation and natural processes. The silicon isotope datasets obtained for this thesis are determined for the slope i.e., 1.952 ± 0.01 which is well within the theoretical limits set for equilibrium and kinetic mass dependent fractionation (Figure 2.9).

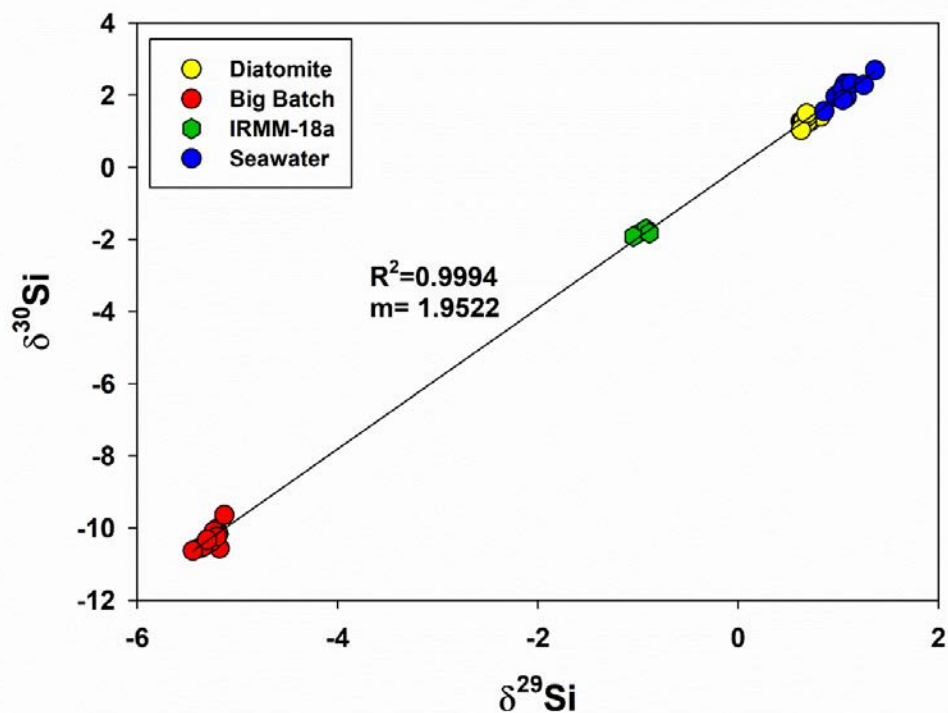


Figure 2.9. Three isotope plot constructed for the data obtained during analysis between $\delta^{29}\text{Si}$ and $\delta^{30}\text{Si}$ to assess the mass dependent fractionation of the silicon isotopes following Young et al., 2002.

2.9.8 Standard reproducibility

Uncertainties during the silicon isotope measurements are important as they are most likely to be controlled by mass dependent fractionation. Interpretation of the several natural processes such as diffusion and adsorption require the precise estimation of isotopic characteristics. In context of silicon isotopes, internal reproducibility is indicated by the standard error of analytical session during a complete block which affect largely by the sensitivity and instrument optimisation. The long term reproducibility for $\delta^{30}\text{Si}$ measurements are reported here for three isotopic standards i.e. Diatomite, Big batch and IRMM-18a. Among these, two of the isotopic standards (BB and Diatomite) were obtained from the Prof M. A. Brzezinski, California University, Santa Barbara, USA. All the $\delta^{30}\text{Si}$ analytical uncertainties of the measurements are provided as twice the standard deviation (2σ SD) of all the SSBs, where each sample was measured in triplicate. The $\delta^{30}\text{Si}$ are well reproduced for replicate measurements and found as IRMM-18a ($1.57 \pm 0.15\%$, $n=27$), Big batch ($-10.2 \pm 0.25\%$, $n=11$) and Diatomite ($-1.24 \pm 0.1\%$, $n=21$) as presented in the Table 2.4.

Table 2.4. Standards for the silicon isotopes analysed during seawater sample measurements

	$\delta^{30}\text{Si}$	$\delta^{29}\text{Si}$	n	$\delta^{30}\text{Si}$	$\delta^{29}\text{Si}$
	measured			reported	
IRMM-18a	-1.70 ± 0.09	-0.95 ± 0.07	27	-1.73 ± 0.13	-0.95 ± 0.07
Diatomite	1.34 ± 0.12	0.68 ± 0.05	18	1.34 ± 0.12	0.68 ± 0.05
Big batch	-10.34 ± 0.21	-5.30 ± 0.05	19	-10.38 ± 0.20	-5.40 ± 0.23

Chapter-3

Dissolved major ions, Sr and $^{87}\text{Sr}/^{86}\text{Sr}$ of coastal lakes from Larsemann Hills, East Antarctica: Solute sources and chemical weathering in a polar environment

3.1 Introduction

Antarctica, the southernmost continent of the Earth, is mostly (~98% of its area) covered by ice with an average thickness of about 2 km (Fretwell et al., 2013; Morlighem et al., 2019). Chemical weathering processes in this vast continent and its role in solute supply to Antarctic lakes, surrounding oceans and atmospheric CO₂ consumptions could be important. Further, this cold and semi-arid desert could serve as a terrestrial analogue for the Martian surface, making it an ideal location to understand the land surface processes on Mars (Dickinson and Rosen, 2003; Gibson et al., 1983; Heldmann et al., 2013). The rock weathering in Antarctica is dominated by glacial/wind induced physical weathering (Campbell et al., 1995; Robert and Kennett, 1997) and chemical rock-water interaction, mostly in the hyporheic zone of streams (Nezat et al., 2001). The glacial action such as freeze-thaw cycle is considered as one of the strong agents of mechanical breakdown of rocks (Foster and Vance, 2006; Gibbs and Kump, 1994). Chemical weathering in this seasonal ice-free region is promoted by intense physical erosion due to waxing and waning of glacial ice sheets and frequent exposure of bedrock with fresh mineral surfaces. Available studies on the Antarctica weathering have reported that the weathering rates in these sub-zero temperature regions are comparable to that of the temperate rivers (Cuozzo et al., 2020; Lyons et al., 2015; Nezat et al., 2001). Hence, Antarctica weathering might have played a significant role in regulating past global seawater chemistry during warmer conditions, when large areas of Antarctica was exposed (Zachos et al., 1999). Despite its planetary and oceanographic significance, detailed investigations on the Antarctica weathering rates have been limited mainly due to remoteness and inaccessibility to the regions.

The ice-free areas of Antarctica mostly occur in coastal regions, which are relatively warmer than inland and receive a significant amount of glacial melt-water input during the austral summer. Repeated waxing and waning of the glacial ice sheets and their movement caused strong physical erosion in the past, that lead to the formation of small to medium size depressions which eventually formed permanent lakes (Hodgson et al., 2012). In absence of perennial rivers/streams, these lakes are the only archive to study solute dynamics, biogeochemical cycling and on-going surficial process in Antarctica. A large numbers of surface and

subglacial lakes (~10,000) have been reported from Antarctica, however, only a few of them have been studied to understand water chemistry and their solute sources (Lyons et al., 2017; Lyons et al., 2005; Lyons et al., 2003; Sabbe et al., 2003). Multiple factors may contribute to the solute chemistry of these lakes which include chemical weathering of the bedrocks, biogeochemical processes, snow-ice melting, evaporation, precipitation, aerosol induced dust deposition, sea salt spray and anthropogenic activities (Sabbe et al., 2004; Verleyen et al., 2011b; Wilson, 1979). Chemical weathering in the West Antarctic peninsula indicate that the rate of chemical weathering per unit area in these regions could be significant compared to temperate regions (Lyons et al., 2015; Lyons et al., 2002). Recently, Torres, Moosdorf, Hartmann, Adkins, and West, (2017) have demonstrated based on the global compilation of hydro-chemical data that weathering fluxes yield from the glacierized catchments are higher than the global average and therefore highlighted dominant role of glacial weathering. However, in this compilation, most of the hydro-chemical data of the glacierized catchments are only available from the tropical and subtropical regions. Therefore, considering the vast glacierized area of Antarctica and absence of any anthropogenic activities, this region provides us a unique opportunity to understand glacial mediated chemical weathering in a pristine environment.

The objectives of the present study are to investigate lake water chemistry and chemical weathering processes in the Larsemann Hills region, East Antarctica during austral summer. Based on chemical (dissolved major ions, Sr and $^{87}\text{Sr}/^{86}\text{Sr}$) datasets and their inverse modelling, we have apportioned solute sources and quantified their contributions to chemical budgets of these lake waters. Finally, these results have led us to estimate silicate weathering rates (SWR) and their corresponding atmospheric CO_2 consumptions in the catchments of the East Antarctic lakes. We have also investigated primary controlling factors of chemical weathering processes in the Larsemann Hills, East Antarctica.

3.2 Results

Major ions, Sr concentration and its isotopic ratio for ten lakes from the Larsemann Hills, East Antarctica are provided in Table 3.1. The pH of these samples vary between 6.3 and 8.9 (mean: 7.3 ± 0.8 ; $n = 24$). Water samples from

eight (out of ten) lakes exhibit strong pH-alkalinity co-variation ($r = 0.95$; $p < 0.01$; $n = 19$). The other two lakes (Fisher and L7 lakes) are characterized by significantly higher alkalinity ($3989 \pm 900 \mu\text{M}$; 1σ) compared to that of the eight lakes ($684 \pm 548 \mu\text{M}$; 1σ). Water temperatures of all samples range from 2.6 to 9.0°C (average: $6 \pm 3^\circ\text{C}$). These values broadly follow a bi-modal ($\sim 3^\circ\text{C}$ and 8°C) variation with relatively higher temperatures observed for semi-enclosed lakes with limited oceanic connections. The average total dissolved solid (TDS) in these lakes with warmer water (250 mg/L) is higher than those with colder water conditions (50 mg/L). Chemistry of these lake waters is mostly Na-Cl type (Figure 3.1), indicating the dominance of solute inputs from oceanic sources. Dissolved Na, on average, accounts for about 70% of the total cationic (TZ^+) load, whereas Mg and Ca contribute about 18% and 11% of the TZ^+ . The Na concentrations vary widely from 880 μM to 15643 μM , and the lower Na values were observed for lakes with relatively lower temperatures. The average Cl/Na ratio (1.06 ± 0.10) of these samples is marginally lower than that of the seawater (1.166; Drever (1997)). The median value of Mg (360 μM) for these lakes is significantly higher than the global average (123 μM ; Meybeck (2005)). In contrast, the median value of Ca for these lakes (281 μM) and global rivers (297 μM ; Meybeck (2005)) are similar. The K content (29-562 μM ; Table 3.1) in these lakes accounts for only $\sim 2\%$ of the total TZ^+ . The dissolved Si for most of the lakes (9 out of 10; excluding L7) vary between 1.8 and 21.6 μM , with an average value of $10 \pm 6 \mu\text{M}$. This average Si value is lower by an order of magnitude compared to that of reported value for global rivers (145 μM ; Meybeck (2005)).

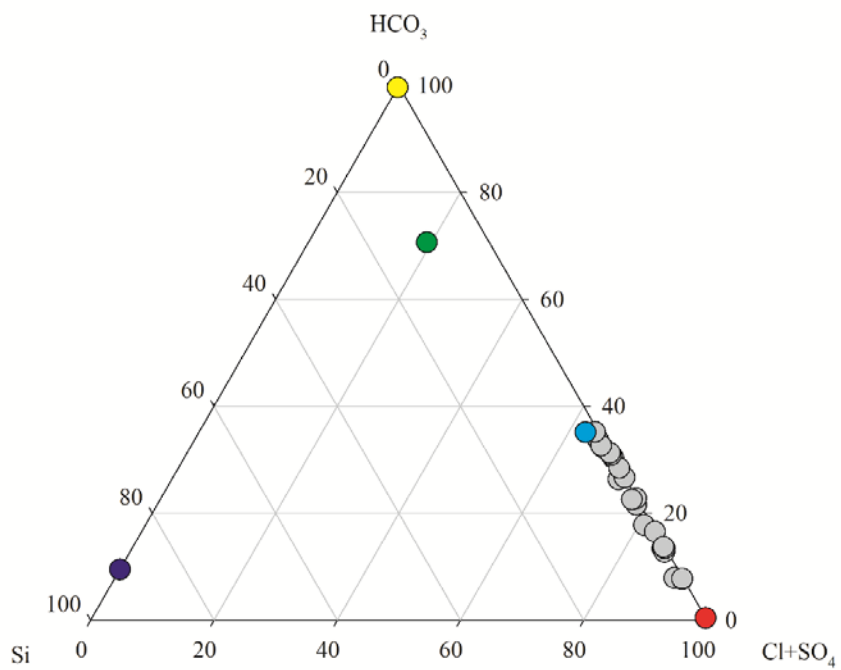
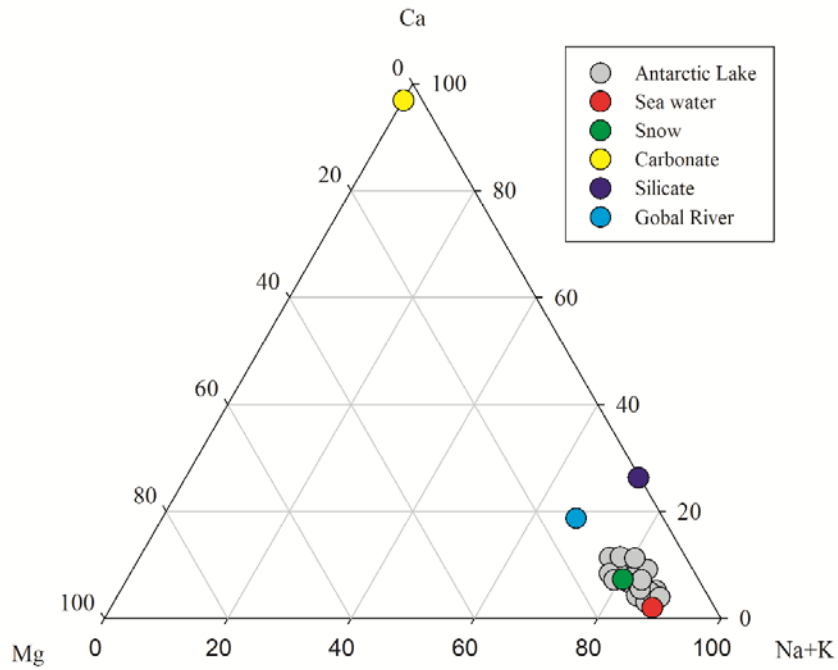


Figure 3.1. Ternary diagram for major cations and anions of the Antarctic lakes. For reference, average composition of possible major solute sources (seawater, Antarctica snow and silicate rocks) is also shown; See text for data source for the end-member compositions. The data distribution indicates dominance of oceanic sources in regulating the lake water chemistry.

The Si content of the L7 lake (122-123 μM ; $n = 2$) is anomalously higher than that of other Antarctic lakes ($10 \pm 6 \mu\text{M}$; Table 3.1). Among the anions, dissolved Cl^- ion accounts for about 70% of the total anionic load (TZ⁻). Alkalinity and sulphate in these lakes, on an average contribute, 21% and 8% of the TZ⁻. The sulphate concentrations of these lakes vary from 44 to 1046 μM . It is worth mentioning here that the highest sulphate concentration is observed for the Lake L7, for which the anomalously higher Si concentration was also observed. The average $\text{SO}_4/(\text{SO}_4+\text{HCO}_3)$ ratio, a possible tracer for carbonic versus sulphuric acid-mediated weathering intensity, for these lakes (excluding two outliers with extremely higher values (~ 0.7) from Unnamed lake) is found to be 0.15 ± 0.09 . Despite large spatial variability in lake chemistry, most of the chemical constituents (*e.g.* Na, Mg, Cl, SO_4 , Si and TDS) show minimal (less than 10%) depth variability in these lakes. In contrast, dissolved Ca and HCO_3 show (on an average) about 20% depth variability with relatively higher concentrations in the surface (than deep) water samples. Further, contrary to its general trend of insignificant variability, the sulphate concentrations in one of the (Progress Lake) lakes show about 40% change within a depth of 20 m (Table 3.1).

The dissolved Sr concentrations of these lakes vary between 91 and 2832 nM, with a median value of 503 nM. This median value is significantly lower than that of reported for seawater (89 μM) and global rivers (1.27 μM ; Peucker-Ehrenbrink et al. (2010). The average Sr concentration is the lowest for the Discussion Lake, whereas it is highest for the Fisher Lake. Despite of its large variability, the Sr concentrations show strong co-variation with their corresponding Ca ($r = 0.87$; $p < 0.01$; $n = 24$) and alkalinity ($r = 0.83$; $p < 0.01$; $n = 24$) values.

Table 3.1. Chemical and Sr isotopic data for the coastal lakes from the East Antarctica.

Lake (Lat.; Long.)	Sample ID	Depth (m)	pH	Temp. (°C)	Na	K	Mg	Ca	Cl	HCO ₃	SO ₄	NO ₃	Si	PO ₄	TZ+	TZ-	NICB (%)	CSI	Sr (nM)	⁸⁷ Sr/ ⁸⁶ Sr
					μM															
Lake L7 (69° 24' 34.48"S 76° 11' 40.38"E)	L7_CS	Surface central	8.2	9.0	14938	562	2097	2290	19007	3122	1046	0.8	123	0.06	24274	24222	0.2	0.58	2483	0.71567
	L7_15	15	8.1	8.8	15643	509	2241	1271	19044	2956	1015	0.5	122	0.06	23176	24029	-3.6	0.21	1583	0.71568
Lake L67 (69° 23' 10.98"S 76° 20' 44.87"E)	L67_S1	Surface margin	7.1	8.7	5596	221	511	636	5915	956	238	0.1	11	0.07	8111	7347	9.9	-1.43	2832	0.71405
	L67_S2	surface central	7.2	8.7	4441	145	564	299	4613	956	207	0.1	11	0.09	6310	5982	5.3	-1.64	651	0.71405
	L67_C5	5	7.3	8.4	4485	170	517	401	4751	789	207	0.3	11	0.08	6492	5954	8.7	-1.50	632	0.71405
Fisher lake (69° 23' 28.26"S 76° 14' 58.28"E)	F_S2	Surface (margin)	8.5	8.7	10061	360	1594	1358	11431	4289	350	0.3	3	0.04	16323	16419	-0.6	0.83	2499	0.71251
	F_CS	Surface (central)	8.4	8.3	9748	179	1608	1480	11014	4956	370	0.3	3	0.05	16103	16710	-3.7	0.83	2437	0.71252
	F_10	10	8.4	8.5	9925	346	1605	1134	11292	4622	355	0.2	3	0.04	15748	16624	-5.4	0.69	2431	0.71251
Reid lake (69° 23' 08.83"S 76° 22' 42.36")	RL S	Surface central	8.8	8.1	12627	550	1461	577	14270	2122	301	0.2	6	0.08	17252	16994	1.5	0.43	1558	0.71126
	RL 3	3	8.9	8.1	13127	512	1528	460	14084	1956	258	0.1	6	0.06	17615	16556	6.2	0.39	612	0.71126
Unnamed lake (69° 24' 27.24"S 76° 15' 44.64"E)	BPL_S	Surface central	6.8	7.6	2901	97	535	325	2853	289	612	0.1	6	0.06	4717	4366	7.7	-2.54	519	0.72107
	BPL_3	3	6.8	7.6	2940	131	533	280	2792	289	639	0.3	6	0.10	4696	4360	7.4	-2.60	487	0.72068
Merd lake (69° 24' 53.43"S 76° 12' 46.66"E)	ML	Surface margin	8.0	6.4	1932	81	209	282	1950	1122	98	0.7	18	0.14	2994	3268	-8.7	-0.79	647	0.71101
Progress Lake (69° 24' 07.07"S; 76° 23' 17.85"E)	PG_S0	Surface central	6.4	4.4	1076	39	138	108	1264	289	53	0.3	22	0.05	1605	1659	-3.3	-3.38	167	0.71571
	PG_10	10	6.5	3.0	1161	44	150	49	1311	122	97	0.4	21	0.07	1605	1627	-1.4	-4.02	168	0.71577
	PG_25	20	6.3	2.7	1162	40	151	67	1203	456	52	0.4	21	0.09	1638	1763	-7.3	-3.52	170	0.71561
Nella Lake	NL_S2	Surface (margin)	6.9	2.6	1315	60	181	77	1341	622	48	0.1	2	0.08	1890	2060	-8.6	-2.73	164	0.71626

(69° 23' 35.44"S 76° 22' 17.12"E)	NL_CS	Surface (central)	6.8	3.6	1292	41	183	67	1318	622	47	0.1	2	0.06	1833	2034	-10.4	-2.88	174	0.71625
	NL_S3	Surface (margin)	6.8	3.6	1364	56	175	50	1498	456	44	0.1	2	0.07	1870	2042	-8.8	-3.14	171	0.71629
Discussion lake (69° 23' 21.27"S 76° 21' 07.24"E)	DL_S2	Surface margin	6.7	2.8	989	31	93	61	817	456	65	0.1	11	0.09	1328	1403	-5.5	-3.15	95	0.71298
	DL_CS	Surface central	6.5	3.0	919	33	100	54	910	289	70	0.2	12	0.09	1261	1340	-6.1	-3.59	91	0.71299
	DL_C2	2	6.7	2.7	990	30	92	46	854	456	76	0.2	12	0.06	1296	1461	-12.0	-3.27	100	0.71295
Lake L5 (69° 24' 27.63"S 76° 11' 03.36"E)	L5_S	Surface central	7.0	2.6	953	38	119	76	894	456	54	0.3	11	0.04	1382	1458	-5.4	-2.76	126	0.71344
	L5_5	5	6.9	2.9	880	29	107	69	987	289	54	0.3	9	0.07	1260	1385	-9.4	-3.09	131	0.71343
Sea Water	-	-	-	-	-	-	-	-	-	-	-	-	-	-	-	-	-	-	-	0.70921

Excluding L7 Lake, the Sr concentrations show no major change (within 10%) with water depths in these lakes. The $^{87}\text{Sr}/^{86}\text{Sr}$ ratios for the lake samples vary between 0.71105 and 0.72111, with an average of 0.715 ± 0.003 . The average $^{87}\text{Sr}/^{86}\text{Sr}$ is found to be the highest for the Unnamed Lake, whereas it is lowest for the Merkwater Lake. These isotopic values are intermediate to that of the seawater (0.7092; and regional lithology (0.76; Sheraton et al. (1984)). We observed that the Sr isotope profiles do not show depth variations and therefore suggest Sr isotope behave conservatively in these lake systems (Table 3.1).

3.3 Discussion

Chemical and Sr isotopic compositions of the LH lake waters are mostly regulated by the relative contribution from its major solute sources, which include seawater, precipitated snow/glacial meltwaters and chemical weathering of bed-rocks present in the basin (Angino and Armitage, 1963). The major rock-types observed in this basin are granitic/gneissic in nature. There have been no reports of carbonate exposure in this region. However, the presence of trace amounts of carbonates, owing to their faster dissolution kinetics, can influence the surface water chemistry significantly even in crystalline terrains (Jacobson and Blum, 2000; Lyons et al., 2005; Lyons et al., 2003). Average elemental ratios for these major sources are compiled from available literature and provided in Table 3.2.

Table 3.2. *a-priori* values and associated uncertainties^a

	Silicates ^{b,c,d}	Seawater, ^{e,f,g}	Carbonates ^h	Snow ^{i,j}
Cl/Na	0.01 ± 0.007	1.2 ± 0.006	0.01 ± 0.01	1.1 ± 0.09
Ca/Na	1.0 ± 0.2	0.02 ± 0.002	50 ± 20	0.1 ± 0.05
Mg/Na	2.1 ± 0.3	0.12 ± 0.0009	20 ± 8	0.1 ± 0.04
Sr/Na	2.7 ± 1.8	0.19 ± 0.008	80 ± 30	1.2 ± 0.9
$^{87}\text{Sr}/^{86}\text{Sr}$	0.82 ± 0.08	0.7092 ± 0	0.7090 ± 0.001	0.7097 ± 0.0007
Alk/Na	1.8 ± 0.4	0.01 ± 0.0001	100 ± 40	0.3 ± 0.22

^aUncertainties are in $\pm 2\sigma$, Sr/Na in nM/ μM units, ^bSheraton et al. (1984), ^cGrew et al. (2013),

^dMaas et al. (2015), ^eCarpenter and Manella (1973), ^fVeizer (1989), ^gCulkin and Cox (1966),

^hMillot et al., (2003), ⁱDelmonte et al. (2013), ^jGrotti et al. (2015)

In addition to these major sources, freezing of seawater in polar regions may precipitate mirabilite (Na_2SO_4), hydrohalites ($\text{NaCl} \cdot 2\text{H}_2\text{O}$) and Ca-Mg rich salts

(Bein and Arad, 1992; Lyons et al., 2017; Wilson, 1979). Dissolution of these minerals may also supply solutes to these lakes.

3.3.1 Possible solute sources for major ions

Ternary diagram of chemical datasets can provide qualitative information about possible sources and their relative contribution to the LH lakes. Figure 3.1 depicts the ternary plot for major cations and anions for these lakes. These data are mostly Na-Cl type, and distinctly different compared to that observed for the global average composition of rivers (Figure 3.1). In contrast, the lake data fall closer to the seawater end-member value, indicating the dominance of oceanic input of solutes to these aquatic systems. This observation is consistent with the trends of both the cations and anions (Figure 3.1). To better constrain these sources, we have evaluated the co-variation of dissolved chloride with key ionic species (*e.g.* Ca, Mg, alkalinity, and sulphates; Figure 3.2). The dissolved chloride ion is mostly supplied through oceanic sources and is almost absent in major rocks present in the catchments. This makes Cl^- ion a reliable tracer to assess seawater influence on lake water chemistry. Figure 3.2 indicates that the Ca, Mg and HCO_3^- data fall above the average seawater values. This observed enrichment in these elements is attributable to their appreciable supply from the chemical weathering of bedrocks. However, the degree of enrichment due to chemical weathering input is observed to be different for these elements. The enrichment is found to be more prominent in the case of dissolved Ca (than Mg). The non-oceanic sources that can supply Ca are weathering of silicate and carbonate rocks and/or supply from Ca-Mg salts. In contrast to this, most of the dissolved sulphate data fall on the seawater line (Figure 3.2), indicating dominant contribution of seawater input for sulphate ion. This observation further ascertains the minimal impact of sulphide oxidation in supplying dissolved sulphate to these lakes. However, two data from the unnamed lake fall above the seawater line (Figure 3.2). These data hint at the additional supply of sulphate, possibly from the dissolution of Gypsum and/or sulphide oxidation. As there have been no gypsum exposures in the basin, we attributed these enriched sulphate values of the unnamed lake to oxidation of sulphides.

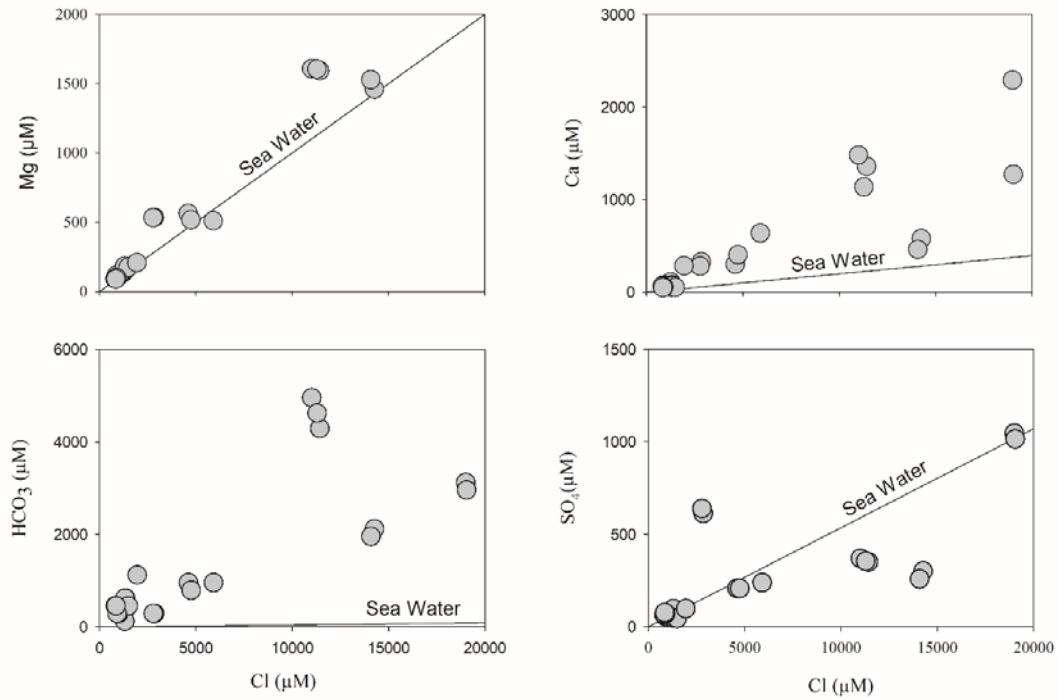


Figure 3.2. Co-variation of dissolved Mg, HCO₃, Ca and SO₄ with chloride ion. The straight line represents the average seawater composition. Enriched Ca and Mg with respect to the seawater line indicate their supply also from other sources, such as chemical weathering of bed-rocks and/or Ca-Mg rich salts.

In contrast, a few SO₄ data also (from Fisher and Reid lakes) fall below the seawater. This lower dissolved sulphate concentration compared to seawater has been interpreted as removal of SO₄ through Na₂SO₄ precipitation during the freezing of seawater (Dickson et al., 2013; Herut et al., 1990).

Like for any chemical constituent, the dissolved (Ca+Mg) concentrations of these LH lakes are likely to be supplied through oceanic sources and/or weathering processes (Lyons et al., 2017). To better constrain the weathering process, we estimated the non-sea-salt component of all the elements using the following equation

$$X_{NSS} = X_{lake} - (Cl_{lake} \times (X/Cl)_{SW}) \quad (1)$$

where, the subscripts *lake*, *SW* and *NSS* stand for the measured lake water composition, seawater composition and non-seasalt component of the element, X (= Na, K, Ca, Mg, SO₄, HCO₃ and Sr) respectively. The average non-seasalt components for Ca and Mg in these lakes are found to be $71 \pm 13\%$ and $20 \pm 14\%$,

respectively. These components are lower compared to that computed for the alkalinity ($98 \pm 1\%$), which is predominantly supplied through non-oceanic sources. Dissolved alkalinity in aquatic systems is mostly supplied through CO_2 -mediated weathering processes and these land-surface processes supply (Ca+Mg) and alkalinity in a fixed proportion of 2:1 ratio (in molar units; (Jacobson et al., 2002)). We have compared the seawater-corrected (Ca+Mg) and alkalinity (in Eq units) for the lakes investigated in the present study (Figure 3.3). Most of the lake samples fall below the 1:1 line and the average (Ca+Mg)/alkalinity ratio for these samples is found to be ~ 0.78 which is lower than the expected value of 1.0.

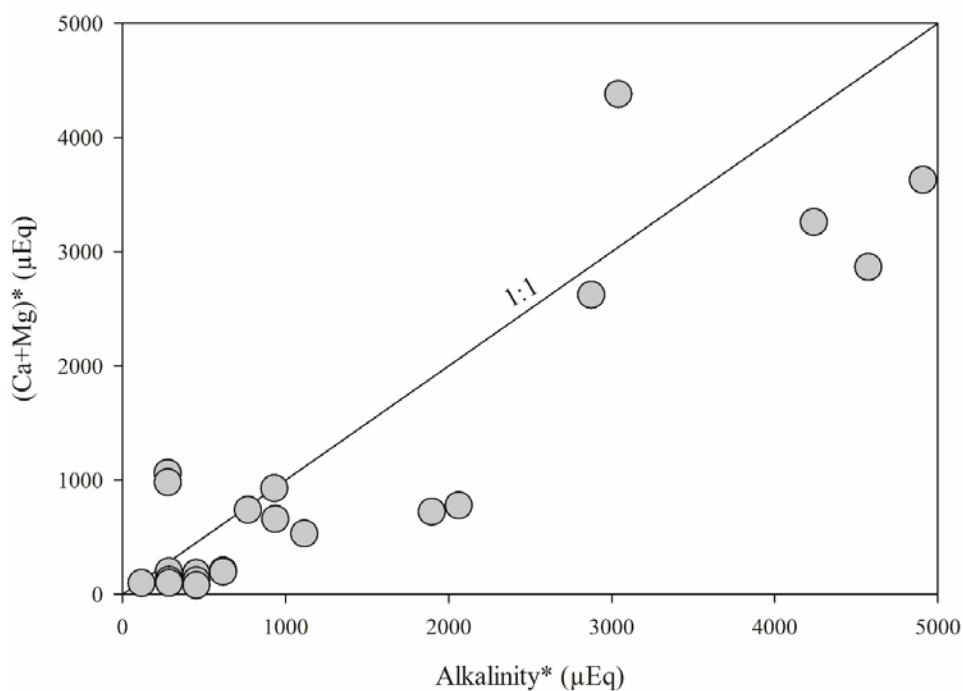


Figure 3.3. Correlation plot between seawater-corrected alkalinity and (Ca+Mg) for the Antarctic lakes. The straight line represents the 2:1 line, a trend expected for chemical weathering of bed rocks.

The exact cause for this depleted ratio is not known; we, however, hypothesize that the estimation of the non-oceanic component by assuming all dissolved chloride from seawater sources may not be strictly valid. The computation of X_{NSS} with the assumption of all dissolved Cl is, therefore, underestimate the non-oceanic sources. A large number of studies have reported the supply of dissolved Ca and Cl ions from the dissolution of Ca-Mg rich salts (Dickson et al., 2013; Lyons et al., 2017; Wilson, 1979) to the Antarctic lakes. It is, therefore, likely that the LH lakes also

receive an appreciable amount of Ca, Mg and Cl from these salts, produced during freezing-thawing of the seawater. This proposition is also consistent with the higher $(\text{Ca}+\text{Mg})_{\text{NSS}}/\text{Alkalinity}_{\text{NSS}}$ ratios (3.5 to 3.8) observed for the unnamed lake (Figure 3.3). This observed excess (Ca+Mg) cannot also be attributed to dissolved sulphate ion and hence, need to be accounted for chloride-rich sources, such as CaCl_2 or MgCl_2 salt/brines. Consistent with this proposition, the impact of calcium-rich salts on water chemistry has already been reported for various Antarctica lakes, groundwater and subsurface waters. The occurrence of these CaCl_2 salts in these watersheds is primarily linked to cation exchange processes during the downward transport of Na-Cl rich brines (Toner and Sletten, 2013).

3.3.2 Sources for dissolved Sr and $^{87}\text{Sr}/^{86}\text{Sr}$

Dissolved Sr and $^{87}\text{Sr}/^{86}\text{Sr}$ found frequent applications in constraining sources and weathering pattern of watersheds (Bickle et al., 2005; Dalai et al., 2002; Galy and France-Lanord, 1999; Palmer and Edmond, 1992; Rai et al., 2010; Tripathy et al., 2012). The Sr isotopic compositions of major rock-types, such as silicates and carbonates, are characterized with distinct isotopic values and hence, serve as a reliable proxy to apportion their contribution. We have used $^{87}\text{Sr}/^{86}\text{Sr}$ ratio to infer about its possible sources and their relative contributions. Figure 3.4 depicts a mixing plot between Sr/Ca and $^{87}\text{Sr}/^{86}\text{Sr}$ ratios for the LH lakes. This plot also includes source compositions and their mixing trends. It may be noted that the Sr isotopic ratios are distinctly higher for the silicates compared to those for seawater and carbonates (or, Ca-rich minerals). The LH lake samples fall closer to the seawater end-member, confirming the dominance of the oceanic sources in supplying Sr to these lakes. In addition to seawater, the dataset fall closer to the seawater-carbonate mixing trend, suggesting an appreciable supply of Sr from these minerals with faster dissolution kinetics. The data, however, fall far from the silicate end-member indicating minimal Sr contributions from silicate weathering to the lake.

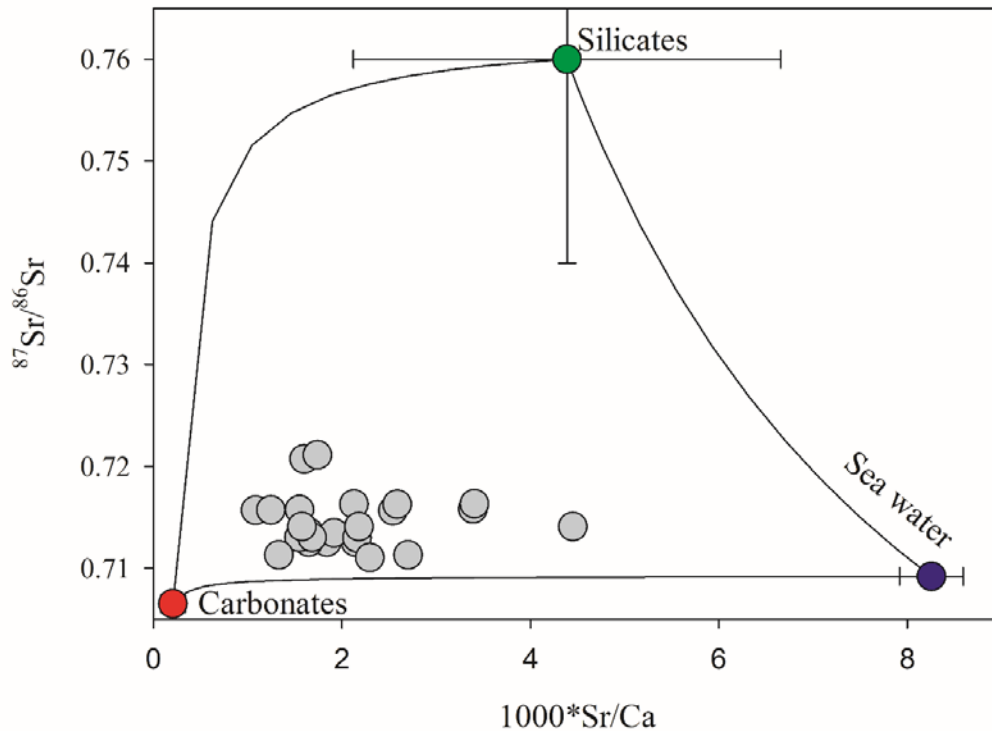


Figure 3.4. Mixing diagram between Sr/Ca (molar ratio) and $^{87}\text{Sr}/^{86}\text{Sr}$ ratios of the Antarctic lakes. Chemical compositions for major solute sources (*cf.* text for data source) are also shown here. The data fall closer to the seawater end-member, hinting at dominance of oceanic solute supply to the lake.

Seabirds and penguins excreta have also been invoked as a possible source to the chemistry of Antarctic lake water (Spurr, 1975). Further, the significance of this source in regulating the sedimentary Sr isotopic data was established by (Liu et al. (2007)) through investigation of $^{87}\text{Sr}/^{86}\text{Sr}$ data for lacustrine sediments and seabird excreta. These excreta are often enriched in P, C and N and may supply about 2.5 wt% of the animal body part per day (Scherer et al., 1995). Efforts are made in this study based on the distribution of PO_4 and PO_4 - $^{87}\text{Sr}/^{86}\text{Sr}$ variation to assess the importance of this solute source to the dissolved Sr isotopic budget. The dissolved phosphate in these samples is ($6.7 \pm 2.1 \mu\text{g/L}$; Table 3.1) lower than that of the earlier reported values for the glacial waters influenced by seabird excreta ($\sim 35 \mu\text{g/L}$; Scherer et al. (1995)). Further, the phosphate shows no systematic trend with Sr. Based on these observations, we infer that the minimal impact of excreta supply to the dissolved Sr budget of these lakes in East Antarctica.

3.3.3 Source-apportionment modelling

We have used an inverse model involving mass balance calculations of chemical and Sr isotopic datasets to apportion solute sources for the LH lakes. The inversion approach has been successfully used to quantify source contribution to rivers and estimating erosion rates for these basins (Millot et al., 2003; Moon et al., 2007; Negrel et al., 1993; Rahaman and Singh, 2012; Tripathy and Singh, 2010; Wu et al., 2005). Unlike rivers, the lake water chemistry is linked to various complex processes, which includes the intensity of chemical weathering, hydrological (evaporation and condensation) changes, biological activities, residence time of lake water and chemical constituents. The residence time of subglacial lake water from Eastern Antarctica have reported varying between 5000 and 125000 years (Jean-Baptiste et al., 2001; Kapitsa et al., 1996). Therefore, estimating erosion rates for the drainage basin of a lake system using a chemical mass balance approach is not straightforward. Although we recognize the limitation of this approach, attempts were made to estimate erosion rate in the lake catchments of LH, for which no literature data exists. The present approach based on the inverse model assumes that the LH lakes are in steady-state and all the chemical species used in the calculation have similar residence time for these lakes. Further, it was assumed that the biological activities in the LH lakes only influence the dissolved silica content of the lake and its impact is minimal for major ions and Sr concentrations. Based on these assumptions, this approach is expected to yield first-order chemical erosion rates averaged over the residence time of the elements.

Details on the method and the computational code adopted in this study are provided in Tripathy and Das (2014). Briefly, this method relies on a set of chemical mass balance equations which relates the measured data (lake water) and model (possible sources and their relative fractions) parameters:

$$\left(\frac{X}{Na}\right)_{lake} = \sum_i^4 \left(\frac{X}{Na}\right)_i \times f_i(Na) \quad (2)$$

$$\left[\frac{{}^{87}Sr}{{}^{86}Sr} \times \left\{\frac{Sr}{Na}\right\}\right]_{lake} = \sum_{i=1}^4 \left(\frac{{}^{87}Sr}{{}^{86}Sr}\right)_i \times \left(\frac{Sr}{Na}\right)_i \times f_i(Na) \quad (3)$$

$$1 = \sum_{i=1}^4 f_i(Na) \quad (4)$$

where, the subscript, *lake* stands for lake water composition whereas i (= 1, 2, 3, 4) stands for the four major solutes sources, which are seawater, snow, silicates and Ca-rich minerals (e.g. carbonates and Ca-Mg salts). The $f_i(Na)$ represents the fraction of dissolved Na derived from the source i . The model uses a non-linear Quasi-Newton optimization algorithm (Tarantola (2005)) to find the best fit between the observed data and model parameters. This iterative algorithm starts from a set of *a-priori* information for the model parameters and finds the best possible *a-posteriori* results which explain the Eq. (2-4) with the least residual. *A-priori* values (and associated uncertainties) for the Na-normalized ratios and $^{87}\text{Sr}/^{86}\text{Sr}$ for the end-member were compiled from the literature and are listed in Table 3.2. Average silicate composition has been ascertained using the bedrock data reported earlier for the Larsmann Hills (Sheraton et al., 1984; Stüwe et al., 1989). Besides, the leaching of aerosols can also be a source of solutes to these lakes. Earlier studies have shown that these sources mostly supply solutes similar to carbonate weathering (Lyons et al., 2017) and hence, are considered to be part of the “*Ca-rich mineral*” end-member. Two samples, one from L67 and Reid Lake, show anomalous results and hence, are not included in constraining the general trend of Antarctic lake chemistry. The anomalous samples from L67 are characterized with relatively higher Ca, Cl and Na compared to the other two samples from the lake, whereas the Reid lake sample has significantly lower Sr content with no change in $^{87}\text{Sr}/^{86}\text{Sr}$ when compared to other samples (Table 3.1). The dissolved cations of these lakes (Figure 3.5) is dominantly supplied by seawater ($63 \pm 15\%$), with additional contributions from snow ($15 \pm 7\%$), silicates ($13 \pm 8\%$) and Ca-rich minerals ($9 \pm 5\%$).

Results from the inverse model on dissolved cations and Sr supplied from major sources are provided in Table 3.3.

Table 3.3. Percent contribution of cations and Sr in Antarctic lakes

Lake_Name	Sample ID	% Catsw	% CatCar	% CatSnow	% Catsil	%Sr _{sil}	%Sr _{sw}	%Sr _c	%Sr _{snow}
Lake L7	L7_CS	56	4	14	26	4	27	3	67
	L7_15	75	5	5	16	4	56	5	36
L67	L67_S1	14	3	63	19	1	2	1	94
	L67_S2	71	6	12	12	2	36	5	58
	L67_C5	70	4	11	16	3	37	4	58
Fisher lake	F_S2	40	10	24	25	3	13	5	79
	F_CS	36	12	24	27	3	12	6	79
	F_10	42	12	24	21	2	14	6	78
Reid lake	RL S	79	5	8	8	1	47	4	48
	RL 3	-	4	0	7	2	139	10	2
Unnamed lake	BPL_S	58	1	15	23	3	26	1	69
	BPL_3	62	1	14	21	3	30	1	66
Merkwater lake	ML	25	16	38	21	2	6	6	88
Progress lake	PG_S0	63	7	13	18	3	31	5	62
	PG_10	77	3	11	8	1	39	2	58
	PG_25	68	12	11	9	1	34	9	56
Scandrett lake	NL_S2	68	14	7	10	1	41	13	45
	NL_CS	68	14	9	7	1	38	12	49
	NL_S3	76	10	8	6	0	44	9	47
Discussion lake	DL_S2	76	15	4	8	1	57	17	27
	DL_CS	78	10	4	10	2	57	11	32
	DL_C2	78	15	4	6	1	55	16	31
Lake L5	L5_S	64	14	9	14	2	37	12	50
	L5_5	66	9	12	13	2	33	7	58

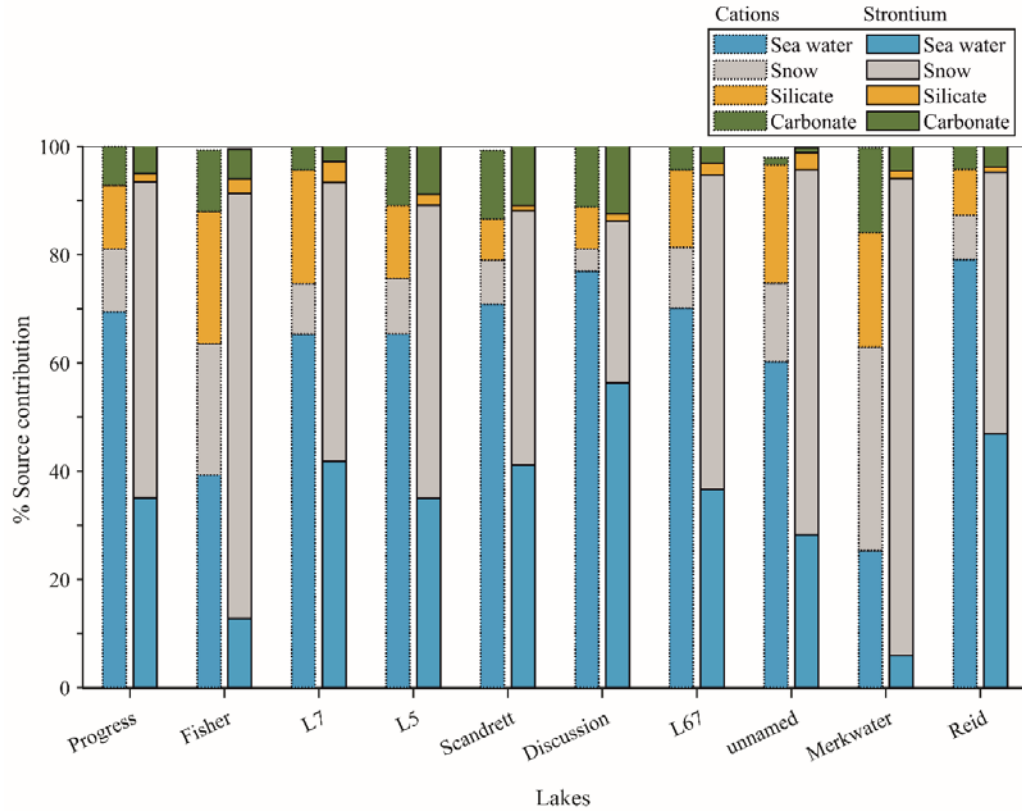


Figure 3.5. Results from the inverse model on relative supply cations and strontium to the lakes from different sources.

In the case of dissolved Sr, these lakes mainly receive Sr through oceanic sources ($91 \pm 4\%$) with minor contributions from silicate/Ca-rich minerals ($10 \pm 4\%$). These results are consistent with our earlier discussions based on chemical and isotopic data distributions. The average silicate derived cations (Cat_s) for individual lakes vary between 8 and 24% (Figure 3.5). The higher Cat_s value is observed for the Fisher lake, with relatively warmer ($\sim 8.5^\circ\text{C}$) water column temperature. The lower Cat_s values are observed for Reid, discussion and Scandrett lakes.

3.3.4 Silicate weathering rates and controlling factors

Efforts are made in this study to estimate the silicate weathering rates (SWR) and CO_2 consumption rates (CCR) for these basins from Eastern Antarctica. There has been very limited hydrological information on these lakes and hence, we recognize that the present estimates are likely to be associated with large uncertainties. The SWRs and CCRs have been calculated using the following equations (Dalai et al., 2002):

$$SWR = \frac{Q}{A} \times (Na_{sil} + K_{sil} + Ca_{sil} + Mg_{sil} + SiO_2) \quad (5)$$

$$CCR = \frac{Q}{A} \times (Na_{sil} + K_{sil} + 2 \times (Ca_{sil} + Mg_{sil})) \quad (6)$$

where Q is the water discharge to the lakes, whereas A stands for the drainage area for the watershed. The results obtained from the inverse model for silicate-derived Na, K, Ca and Mg are used in the equations (5-6) to estimate the erosion rates. The SWR estimated using equation 5 also accounts for the dissolved silica of the LH lake samples. We show in a subsequent discussion that a significant fraction of silica from the lake gets removed due to biological activities and hence, our SWR estimate is only a lower limit for the weathering intensity for silicates. Representative data on drainage area and water discharge is only available for the Scandrett lake (Shevnina and Kourzeneva, 2017) and hence, the weathering rate has been calculated for this lake system. Shevnina and Kourzeneva (2017) have reported water outflow (0.079 m³/s) and creek catchment area (1.14 km²) for this lake. Assuming a comparable amount of water flux into the lake and discharge for selected seasons (about three months), we have computed an annual water discharge of 5.4×10⁸ L/yr for this lake. The estimated silicate weathering rates for the Scandrett lake basin is 3.6 ± 0.3 tons/km²/yr, which corresponds to 1.4 ± 0.1 mm/yr. These weathering rates are lower than that reported for the average global river basins (Figure 3.6) (5.4 tons/km²/yr (Gaillardet et al., 1999), Amazon (13.0 tons/km²/yr), and Ganga (8.9 tons/km²/yr; Krishnaswami and Singh (2005)). The estimated CO₂ consumption rates of the Scandrett lake basin (0.5 ± 0.2 × 10⁵ moles/km²/yr) is also found lower compared to that reported for the global average for rivers (0.9 × 10⁵ moles/km²/yr; Gaillardet et al., 1999). These lower weathering rates are consistent with the colder climatic regimes particularly in the polar conditions, which is less conducive for weathering of resistant silicate minerals. In an interesting observation of the present study, the dissolved silica concentrations in these Antarctic lakes (range from 3 μM to 100 μM with an average 18.94 μM; Table 3.1) were found systematically lower by an order of magnitude than that of the average global rivers (Gaillardet et al., 1999). Dissolved silica in any aquatic basin is mainly derived from silicate weathering, however, later could be altered by biological activities. To better understand the silicon cycle, we estimated the CO₂ consumption rates independently by using Si concentration of the lakes and its behaviour during the alumino-silicate weathering process. , based on global riverine

datasets, have suggested that the amount of CO₂ consumed from basins is equal to twice the silica concentrations.

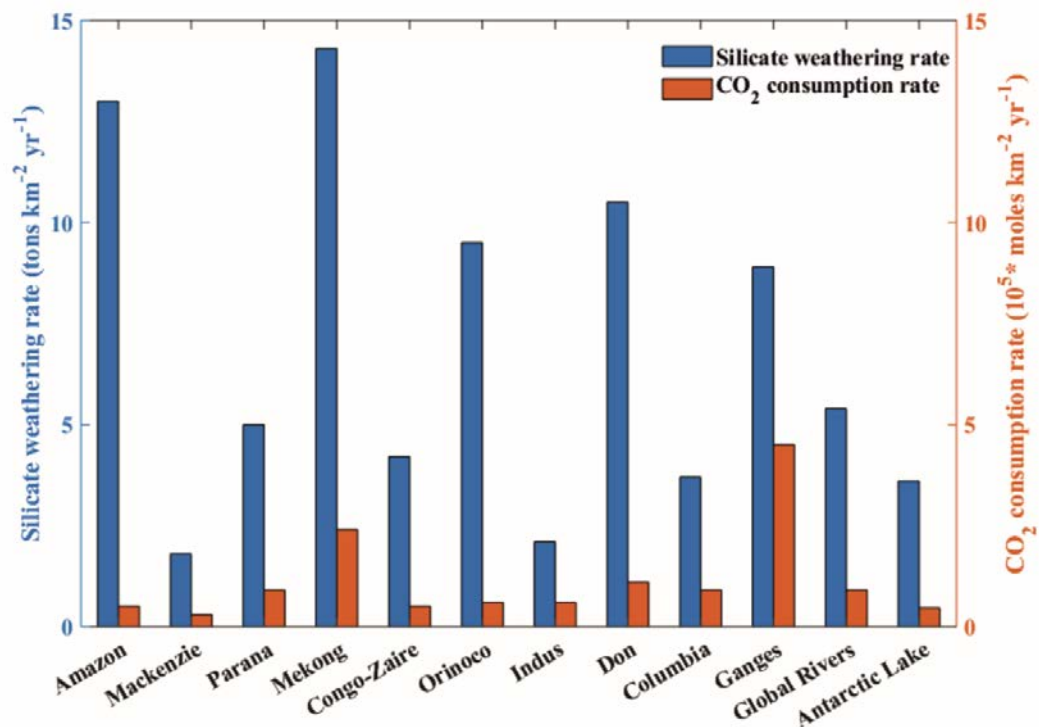


Figure 3.6. Results from the inverse model on relative supply cations and strontium to the lakes from different sources.

This approach yields a CO₂ consumption rate of $(0.02 \pm 0.001) \times 10^5$ moles/km²/yr. This rate is about 95% lower than that estimated using silicate-derived cations in the present study. The exact cause of this difference is unclear. A possible explanation is removal of dissolved silica through biological pathways to support lake productivity which is needed to be understood in more detail, however, it is beyond the scope in the present study. Recent study by Hawkins et al. (2017) has highlighted export of amorphous silica to ocean produced by the Greenland ice sheet during aqueous weathering processes such as dissolution-precipitation mechanism in sub glacial environments. Similar processes have already been invoked for large river systems. For instance, Fontorbe et al. (2013), based on silicon isotopic investigations, have suggested about 50% removal of dissolved silica from the Gangetic plain. We suggest similar processes to explain about 95% lower silica content in the Scandrett Lake. This proposition, however, needs to be tested thoroughly and a systematic study of silicon isotopes in dissolved and its counter phase i.e. lake sediments of water-bodies from Antarctica.

3.4 Conclusions

In this contribution, we have investigated the chemical and Sr isotopes of ten coastal lakes from East Antarctica to decipher solute sources, and estimate the rate of glacial induced chemical weathering in their catchments. Our important findings and their implications are concluded below.

The $^{87}\text{Sr}/^{86}\text{Sr}$ of these lake waters is close to global seawater and Antarctica snows, indicating a dominant role of seawater and snow precipitation in regulating the solute chemistry. Results of inverse modelling show that the cations are dominantly supplied from oceanic sources ($80 \pm 5\%$), with a less but significant contributions from weathering of carbonates and silicates (together contributing $20 \pm 10\%$). Computations of the results from the inverse model yielded SWR of 1.4 ± 0.1 mm/yr which is lower than the global average (2.08 mm/yr).

Our estimate of SWR and corresponding CO_2 consumption rates are slightly lower (~ 0.6 times) that of the global average reported for the global river basins. Though chemical weathering is lower, but, considering vast regions of Antarctica that went through glacial waxing and waning in areal coverage; for example exposure of large ice-free regions during the last interglacial and mid-Pliocene warm periods. This could be a potential region for silicate weathering and atmospheric CO_2 consumptions, unaccounted so far in the global estimates and hence could be a source of uncertainty.

Anomalous removal of silica ($\sim 95\%$) produced during weathering, for which the reason is still unknown which could be the scope for future investigations.

Chapter-4

Sources, distribution and biogeochemical cycling of dissolved trace elements in the coastal lakes of Larsemann Hills, East Antarctica

4.1 Introduction

Trace elements in natural aquatic systems play an important role in sustaining life, dominantly through their utilization as essential micronutrients and by controlling multiple biogeochemical processes across the trophic levels. Trace metals like Mn, Cu, Mo, Ba and Cd are important for metabolic functions, enzyme formations, and primary productivity (Brand et al., 1986; Horner et al., 2013; Lane et al., 2005; Maldonado et al., 2006; Peers and Price, 2006; Takano et al., 2014; van den Berg et al., 1987; Wu et al., 2014). Whereas, heavy metals like Pb, Cr, As and U are widely utilised to source fingerprint and to trace the reactive-transport pathways of contaminants, and to assess the pollution stress in the aquatic environments (Maceda-Veiga et al., 2013; Wang et al., 2011). Multidecadal research initiative through an international programme “GEOTRACES” (Trace elements and isotopes studies in ocean) has demonstrated the importance of key trace elements (e.g. Fe, Mn, Zn, Cu and Cd) as essential micronutrients in the ocean. For example, dissolved Fe in the Southern Ocean is known to be the key limiting factor for primary productivity (Lyons et al., 2015) leading to the formation of high nutrient low chlorophyll (HNLC) regions. However, only a few studies have investigated the coastal regions of Antarctica and the Southern Ocean to highlight the role of trace elements in controlling primary productivity (Lecomte et al., 2016; Lecomte et al., 2020; Lyons et al., 2015; Wadham et al., 2010). Satellite observation has identified ~65,000 supraglacial lakes in the East Antarctic ice sheet (Stokes et al., 2019). Note, that despite the presence of thousands of proglacial freshwater and saline lakes in Antarctica, primary productivity and nutrient dynamics, particularly role of these trace elements as an essential micronutrient, have not been investigated so far.

Antarctic (freshwater) lakes are mostly oligotrophic in nature; however, our recent study, based on multiple Larsemann Hills (LH) lakes, demonstrated significant removal of dissolved silica (up to 95%) from the lake water and suggested a possible role of biological uptake (Nuruzzama et al., 2020). This hypothesis is corroborated by the widespread occurrence of algal mats (Sabbe et al., 2004). However, the exact mechanism and extent of silica removal, and the limiting factors driving these lakes oligotrophic are not yet established. Therefore, to understand the type of biogeochemical processes, and to assess the role of the micro and macro-

nutrients in these pristine Antarctic lakes, a coupled investigation of the water column and sediment chemistry is necessary. Additionally, Antarctic lakes are relatively pristine and hence provide a suitable natural archive to gather baseline information on assessing the possible impacts of anthropogenic pollution and pollution driven stress in natural water bodies elsewhere. Anthropogenic sources of metals and their contribution to any reservoirs/aquatic systems can only be assessed if natural baselines, their variability, and processes controlling their mobility are fully understood and well characterized.

Selected dissolved trace metals (Mn, Cu, Ba, V, Mo, As, Cr, Co, Sr, Pb, U and Cd), major nutrients (NO_3 , SiO_2 and PO_4), and key biological parameters (DOC, *Chlorophyll-a*) were studied in the coastal lakes of Larsemann Hills, East Antarctica. The key objectives were to decipher their sources, understand geochemical behaviour and their role on the primary productivity in the extreme polar aquatic environment. The Larsemann Hills (LH) region comprises of ~100 lakes spread across 35 km² area. This area receives approximately 16% of total meltwater input from East Antarctic ice melt (Hodgson et al., 2016). The absence of any direct anthropogenic contamination source in this area will allow for this study to reveal novel insights into trace metal transport and their role in regulating biogeochemistry in extreme aquatic environments. Additionally, the observations will help quantify the role of Antarctic weathering in supplying dissolved trace metals to the surrounding oligotrophic Southern Ocean.

4.2 Results

4.2.1 Trace metals, nutrients, DOC and chlorophyll-*a* in water samples

The concentration data of dissolved trace metals (V, Cr, Mn, Co, As, Rb, Cd, Ba, Pb, U, Cu, Mo and Sr), major nutrients (NO_3^- , Si, PO_4^{3-}), Chlorophyll-*a* and DOC of ten lakes from the Larsemann Hills, East Antarctica are provided in Table 4.1. Among the major nutrients, average dissolved nitrate (NO_3^-) and phosphate (PO_4^-) concentrations range from 0.1–0.8 μM (average $0.27 \pm 0.19 \mu\text{M}$) and 0.04–0.14 μM (average $0.07 \pm 0.02 \mu\text{M}$) respectively. This range of values is much lower compared to the global rivers (Gaillardet et al., 2003). The dissolved silica concentration of these lakes ranges from 3 to 22 μM with an average value of

9.5±6.4 µM (Table 1) which is almost an order of magnitude lower than the average global rivers (145 µM; Meybeck (2005)) with the exception of the lake L7 (123 µM) (Nuruzzama et al., 2020). Dissolved Chlorophyll-a measured in these lakes ranges from 0.02–0.54 mg m⁻³, which is similar to the oligotrophic Southern Ocean (0.3–0.4 mg m⁻³) (George et al., 2013). DOC varies from 11 to 350 µM with an average concentration of 154±96 µM, which is lower than that of the lakes (250–800 µM) from west Antarctic Peninsula (Takacs et al., 2001).

The dissolved trace metal concentrations determined in this study are in sub-nanomolar level (Table 4.1); an order of magnitude lower than that of the global rivers (Gaillardet et al., 2003). A few of these trace metals (As, U, Pb, Co and Cr) that are generally used as a tracer for anthropogenic sources were found at extremely low concentrations (sub-nM level) in the lake waters compared to that of global rivers or seawater (Table 4.1). Among them, dissolved Arsenic (As) varies from 0.73-17.6 nM with an average concentration of 5.2 nM, which is almost five times lower than the average seawater value (23 nM) (Cutter et al., 2001). It is important to note that As concentration shows a significant positive correlation with the water temperature, higher As concentration are observed in warm waters (8.7°C, 17.6 nM); whereas, lower concentrations are observed in cold waters (2.6°C, 0.74 nM), except for the samples from Lake L67 (8.7°C, 4.40 nM). The Pb concentration in the samples from lake L67 was found to be highest among all the lakes studied. Dissolved Pb in the lake waters varies from 14.5-651.5 pM with an average of 170 ± 160 pM, which is ~20 times lower than the average seawater concentration (~9.94 nM).

Among the nutrient-type trace metals (Ba, Cd, Mn, Cu and Mo), Ba concentration in the lake waters was high, with values ranging from 1-55 nM and an average of 15 nM; whereas, the lowest concentration was observed for Cd with an average of 0.14 nM. The dissolved trace metal concentrations display a bimodal distribution pattern when all the lakes are taken into consideration; the five lakes viz., Progress, L5, L7, Scandrett and Discussion lakes show an order of magnitude lower than rest of the lakes (Table 4.1). Redox sensitive metals such as dissolved Mo in the all of the lakes vary from 0.5-8.6 nM with an average concentration of 2.4 nM which is ~50 times lower than seawater (104 nM) (Table 4.1; Morris (1975)). Whereas, dissolved Mn in the lakes varies from 5-68 nM with an average

of 22 ± 18 nM which is lower than the average rivers (618 nM) and an order of magnitude higher than global seawater (0.4nM) (Table 4.1).

4.2.2 Major oxides and trace elements abundances in sediments

The major oxides of the bulk sediments, collected from lakes and their catchments, are given in Table 4.2. The bulk sediment compositions, based on SiO_2 and Al_2O_3 abundances of 64.7 ± 2.8 wt% and 14.5 ± 0.5 wt%, indicate a primarily granitic source. The SiO_2 and Al_2O_3 abundances are similar to the average upper continental crust (UCC) abundances (Taylor and McLennan, 1995; Table 4.2). The rest of the major oxides in descending order of concentration are Fe_2O_3 , K_2O , Na_2O , CaO , MgO , P_2O_5 and MnO with abundances of 5.3 ± 2.8 , 3.70 ± 0.68 , 2.02 ± 0.49 , 1.74 ± 0.63 , 1.32 ± 0.40 , 0.13 ± 0.07 and 0.09 ± 0.07 wt % respectively (Table 4.2). Among these oxides, most of them (CaO , Na_2O , Fe_2O_3 , TiO_2 , K_2O , P_2O_5 , Fe_2O_3) have concentrations similar to average UCC values (Table 4.2) except for CaO (1.74 ± 0.63 wt%; for lake sediments) which is approximately half of the UCC value (4.0 wt%). In contrast, MnO shows a higher abundance (0.22 wt %) in the sediments of lake L67 compared to UCC value (0.08 wt%) (Table 4.2). The Sr concentration of the lake sediments ranges from 60-190 mg kg^{-1} with an average concentration of 128 ± 67 mg kg^{-1} ; whereas, in the catchment sediments it ranges from 80-370 mg kg^{-1} with an average of 183 ± 110 mg kg^{-1} . Both these ranges are slightly lower than the UCC value (350 mg kg^{-1}). The Ba concentration of the lake sediments ranges from 780-1630 mg kg^{-1} with an average concentration of 1234 ± 404 mg kg^{-1} (Table 4.2); whereas, for the catchment sediments, it varies from 790-1450 mg kg^{-1} with an average of 1445 ± 218 mg kg^{-1} . The Ba concentrations in the lake and catchments are almost 2-3 times higher than the average crustal abundance (550 mg kg^{-1} ; Taylor and McLennan (1995)).

Table 4.1. Trace metals and biological parameters analysed from coastal lake waters of Larsemann Hills, East Antarctica.

Lake Name (Lat. Long.)	Sample ID	Temp (°C)	pH	Mn	Cu	Ba	V	Mo	As	Cr	Co	Sr	Pb	U pM	Cd	nM				DOC	<i>Chl-a</i> (mg m ⁻³)
																SO ₄ ⁻²	NO ₃ ⁻	SiO ₂	PO ₄ ⁻ ₃		
Progress Lake																					
69° 24' 07.07"S 76° 23' 17.85"E	PG_S0	4.4	6.4	32	4.8	2.7	1.9	0.6	1.2	1.1	0.6	167	72	17	89	53	0.3	22	0.05	80	0.09
	PG_10	3	6.5	31	4.5	3.1	1.9	0.7	1.8	1	0.5	168	82	13	80	97	0.4	21	0.07	124	0.12
	PG_25	2.7	6.3	32	7.3	3.1	1.8	0.7	1.4	0.5	0.6	170	130	17	205	52	0.4	21	0.09	81	0.36
Fisher lake																					
69° 23' 28.26"S 76° 14' 58.28"E	F_S2	8.7	8.5	8.7	13	24.7	8	0.7	11	2.5	3.2	2499	92	311	BD	350	0.3	3	0.05	350	0.06
	F_CS	8.3	8.4	9.3	13	25.3	8.2	0.8	9.9	7.2	3.1	2437	14	319	125	370	0.3	3	0.04	114	0.04
	F_10	8.5	8.4	9	13	25.2	8	0.8	10	2.3	3.2	2431	256	319	44	355	0.2	3	0.04	65	0.02
Lake L7																					
69° 24' 34.48"S 76° 11' 40.38"E	L7_CS	9	8.2	8.3	27	24.8	8.2	8.6	10	2.3	3.2	2483	58	302	36	1046	0.8	123	0.06	127	0.04
	L7_15	8.8	8.1	5.7	26	19.4	28.1	7.7	15	4	2.4	1583	68	272	BD	1015	0.5	122	0.06	81	0.03
Lake L5																					
69° 24' 27.63"S 76° 11' 03.36"E	L5_S	2.6	7	17	5.3	1.8	1.6	0.9	0.7	41.7	0.4	126	179	26	BD	54	0.3	11	0.04	11	0.15
	L5_5	2.9	6.9	11	4.2	2.6	1.6	1.8	0.9	3.3	0.3	131	246	21	80	54	0.3	9	0.07	109	0.18
Scandrett Lake																					
69° 23' 35.44"S 76° 22' 17.12"E	NL_S2	2.6	6.9	17	11	2.2	2.2	0.5	1.2	0.3	0.2	164	82	21	80	48	0.1	2	0.08	108	0.19
	NL_C S	3.6	6.8	18	12	3.6	2.3	0.6	1.3	1.8	0.3	174	579	17	160	47	0.1	2	0.06	197	0.15
	NL_S3	3.6	6.8	19	10	2.6	1.7	0.6	1.2	0.4	0.4	171	72	26	BD	44	0.1	2	0.07	70	0.14
Discussion lake																					
69° 23' 21.27"S 76° 21' 07.24"E	DL_S2	2.8	6.7	9.4	12	1.1	1.8	4.6	1.1	0.6	0.5	95	130	26	80	65	0.1	11	0.09	68	0.44
	DL_C S	3	6.5	9.1	12	1.2	1.6	4.1	0.7	1.2	0.5	91	97	34	125	70	0.2	12	0.09	176	0.5

	DL_C2	2.7	6.7	12	11	1.2	1.6	4.1	0.9	2.5	0.5	100	357	26	205	76	0.2	12	0.06	176	0.54
Lake L67	L67_S1	8.7	7.1	13	15	54.5	15.5	1.1	18	37.2	1.3	2832	217	885	80	238	0.1	11	0.07	244	0.24
69° 23' 10.98"S 76° 20' 44.87"E	L67_S2	8.7	7.2	37	13	5.3	5.5	0.9	4.4	2.9	0.8	651	652	60	80	207	0.1	11	0.09	56	0.33
	L67_C5	8.4	7.3	35	12	2.9	4.6	0.9	4.6	1.2	0.4	632	63	34	BD	207	0.3	11	0.08	116	0.4
Unnamed lake																					
69° 24' 27.24"S 76° 15' 44.64"E	BPL_S	7.6	6.8	68	33	13	2.8	0.8	2.5	3	63	519	87	30	374	612	0.1	6	0.06	308	0.01
	BPL_3	7.6	6.8	67	23	14.1	3.7	0.9	3	1.9	64	487	92	34	507	639	0.3	6	0.1	367	0.08
Merkwater lake																					
69° 24' 53.43"S 76° 12' 46.66"E	ML	6.4	8	8.2	26	11.9	8	7.2	4.5	2.3	0.5	647	130	515	44	98	0.7	18	0.14	218	0.57
Reid lake																					
69° 24' 08.83"S 76° 22' 42.36"E	RL_S	8.1	8.8	35	26	3	4.5	4.9	4.3	1.6	0.4	1558	48	34	BD	301	0.2	6	0.08	255	0.49
	RL_3	8.1	8.9	5.2	24	19.2	27.2	4.4		3.6	2.4	612	179	247	116	258	0.1	6	0.06	212	0.53
<hr/>																					
*Global Rivers		-	-	618	23	168	14	4	8	13	3	685	381	2605	712	-	-	-	-	-	-
^{b,c,d} Seawater		-	-	0.4	2.4	109	39	104	16.0	4.04	0.02	89021	13	13444	623	-	-	-	-	-	-
r									2												

*BD=below detection limit, pM=picomolar, nM=nanomolar, μM=micromolar

^aGaillardet et al. (2003)); ^bBruland and Franks (1983)), ^cChan et al. (1976)), ^dMorris (1975))

Table 4.2. Major oxides, bulk Sr and Ba composition of lake sediments and catchment sediments from LH, East Antarctica.

<i>Lake sediments</i>	Lat; Long	SiO ₂	TiO ₂	Al ₂ O ₃	Fe ₂ O ₃	MnO	MgO	CaO	Na ₂ O	K ₂ O	P ₂ O ₅	Sr	Ba
		wt %										(mg kg ⁻¹)	
Lake L7	69° 24' 34.48"S 76° 11' 40.38"E	59.6	0.611	15.23	4.341	0.054	1.913	2.286	2.234	3.557	0.139	190	1590
Discussion lake	69° 23' 21.27"S 76° 21' 07.24"E	64.8	0.541	15.58	3.235	0.043	1.169	1.271	1.947	4.406	0.082	130	1330
Lake L67	69° 23' 10.98"S 76° 20' 44.87"E	62.4	0.918	14.06	10.28	0.22	1.241	0.989	1.286	2.618	0.067	60	840
Merkwater Lake	69° 24' 53.43"S 76° 12' 46.66"E	63.8	0.491	15.05	4.161	0.059	1.462	2.457	2.023	3.947	0.243	200	1630
Progress lake	69° 24' 07.07"S 76° 23' 17.85"E	68.8	0.387	14.48	4.386	0.067	0.815	1.707	2.622	3.99	0.106	60	780
<i>Average</i>		63.9 ±3.4	0.59 ±0.2	14.9 ±0.6	5.3 ±2.8	0.09 ±0.07	1.32 ±0.40	1.74 ±0.63	2.02 ±0.49	3.70 ±0.68	0.13 ±0.07	128 ±67	1234 ± 404
<i>Catchment sediments</i>													
Dry Lake Grovnes S	69° 24' 31.50"S 76° 12' 06.03"E	64.07	0.332	12.93	2.577	0.033	0.63	1.175	1.79	3.993	0.077	80	790
SOIL 10cm		67.21	0.615	15.07	5.548	0.102	1.143	2.127	2.139	3.983	0.164	110	1110
LOC 02 DP CE	69° 25' 05.26"S 76° 13' 32.02"E	65.38	0.579	14.96	4.579	0.077	1.302	2.182	1.944	4.088	0.158	140	1450
LOC 02 SS		67.02	0.584	15.19	4.999	0.086	1.066	2.354	2.209	3.848	0.165	140	1260
LOC 08	69° 24' 07.07"S 76° 23' 17.85"E	58.75	0.381	12.15	3.624	0.055	1.345	11.85	1.251	3.414	0.214	370	1080
Polar Ice	69° 25' 01.23"S 76° 13' 55.51"E	67.65	0.575	14.99	4.938	0.094	1.449	3.18	3.127	2.575	0.158	260	1180
<i>Average</i>		65.01 ± 3.35	0.51 ±0.12	14.22 ±1.32	4.38 ±1.09	0.07 ±0.03	1.16 ±0.29	3.81 ±3.99	2.08 ±0.62	3.65 ±0.58	0.16 ±0.04	183 ±110	1145 ± 218
*UCC		66.9	0.5	15.2	5	0.08	1.33	4.0	2.39	3.4	0.16	350	550

*Average upper continental crustal compositions (UCC) of these elements obtained from Taylor and McLennan (1995)

4.3 Discussion

In the previous study, major ions, dissolved Sr and $^{87}\text{Sr}/^{86}\text{Sr}$ ratio were studied in these lakes to decipher their possible sources and to understand weathering patterns in the lake catchments (Nuruzzama et al., 2020). The inverse model-based estimates suggested that the major cations are mostly derived from the ocean via sea-spray ($80 \pm 5\%$) and the remainder is derived from chemical weathering of rocks in the lake catchments ($20 \pm 10\%$) which yield a chemical weathering rate of 3.4 moles/km²/yr for this region (Nuruzzama et al., 2020). This suggests that in spite of lower chemical weathering rates in this glacial environment compared to the global average, it supplies a substantial amount of major ions and nutrients to these lakes (Lecomte et al., 2020). In this study, we have focused on selected trace metals and key nutrients to decipher their possible source(s), and to understand their role in biogeochemical processes in these lakes. Overall, nutrients and trace metals data shows bimodal distribution pattern in the LH Lakes (Table 4.2), where five of the lakes (L7, Fisher, Reid, L67 and Unnamed lake) have an order of magnitude higher concentrations than rest of the lakes (Scandrett, Merkwater, L5, Progress and Discussion lake) (Table 4.1). Multiple factors and processes like locations, geological settings and geohydrological conditions, are recognised as important factors to decide the geochemical characteristics of these lakes (Gasparon and Matschullat, 2006a). Distance from the sea, altitude and wind conditions (strength and directions) are the important factors for the supply of metals, ions and nutrients through sea spray and aeolian dust depositions (Magesh et al., 2020; Nuruzzama et al., 2020). In addition, geohydrological and climatic conditions such as extent and duration of ice cover in these lakes, precipitation, water temperature, interconnectivity between lakes and with the sea, melt water input and endorheic conditions can also influence chemical characteristics of these lakes (Gasparon et al., 2002; Gasparon and Matschullat, 2006a, b; Magesh et al., 2020; Nuruzzama et al., 2020). Further, biogeochemical processes are also known to influence the distribution of major ions, trace elements and nutrients compositions of these lakes (Verleyen et al., 2011a). The lower concentrations of dissolved solutes in west Antarctic lakes have been explained in terms of ice-cover in the lakes which control the supply of dissolved solutes to these lakes (Lecomte et al., 2016). In the

following sections, we have investigated sources, factors and processes which play an important role in controlling biogeochemical characteristics of these LH lakes.

4.4 Data analysis using statistical methods

We employed multiple Statistical tools to decipher metal sources and to infer about the processes that regulate biogeochemical parameters and environmental conditions in these lakes. Principle component analysis (PCA) and Hierarchical Cluster Analysis (HCA) were performed to simplify the complex data set, and to identify groups of samples with similar characteristics (Zelano et al., 2017). Details of the PCA and HCA are well established (Giacomino et al., 2011). These statistical methods enabled us to explore correlations among the variables in the same sample and among different samples for the same set of elements. PCA results were further validated with Kaiser-Meyer-Olkin sample adequacy and the Bartlett sphericity test (Giacomino et al., 2011). Along with PCA, Hierarchical Cluster Analysis (HCA) on all 24 samples were performed using an add-on of Microsoft Excel (XLSTAT) and Primer-e. Prior to HCA. Sample standardization was done by autoscaling procedure (Zelano et al., 2017). Square root method of resemblance was used before calculating the similarity between the objects (variables). Euclidean distances in which results were filtered out from manifold embedding were used to calculate percentage similarities between variables and samples. Results obtained from HCA are displayed in the dendrogram plot.

4.5 Sources of trace elements to the LH lakes

The LH lakes are in the proximity to the sea, and therefore, solute compositions of these lakes are strongly influenced by sea spray (Magesh et al., 2020; Nuruzzama et al., 2020). Almost 80% of the total dissolved solute supply to these lakes is contributed by sea spray (Nuruzzama et al., 2020). Further, strong covariations of the major cation (Na^+ , Ca^{2+} , Mg^{2+} , K^+) with dissolved Si (Table 4.3) indicate that a significant amount of these elements are also derived from chemical weathering of exposed rocks in the lake catchments. The previous study based on Sr isotopes and the inverse model suggests that chemical weathering of the exposed rocks in the catchments contribute ~20% of the total dissolved solutes to LH lakes (Nuruzzama et al., 2020). In order to assess contributions of trace elements from the sea spray

against other sources, we have plotted trace elements with Cl^- concentrations (Figure 4.1).

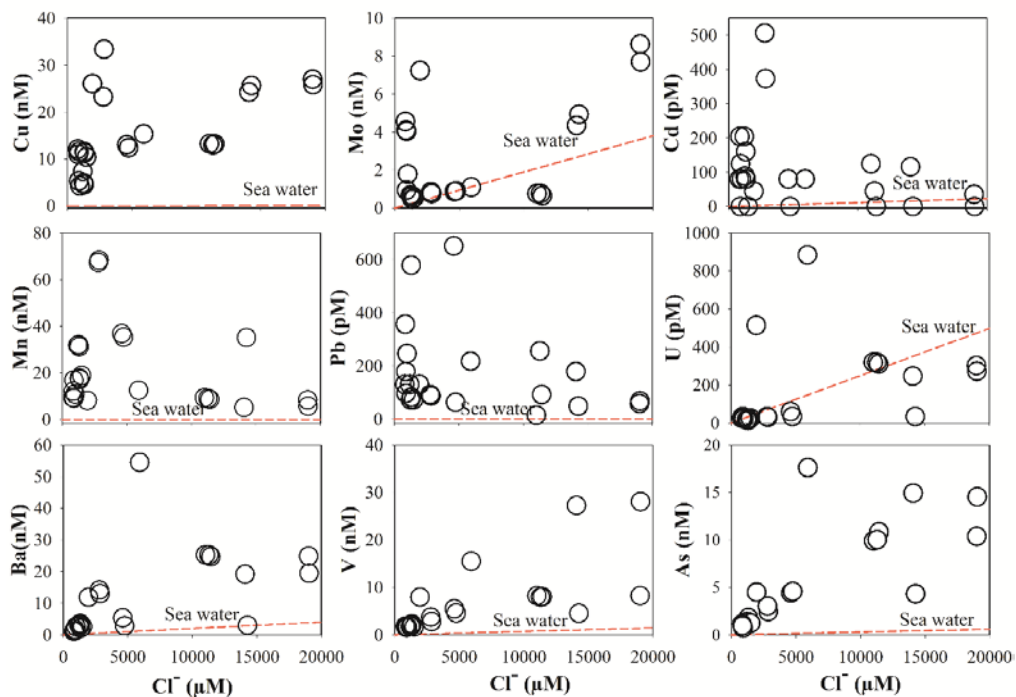


Figure 4.1. Dissolved trace metal concentration in LH lakes are plotted with Cl^- . The red dashed line represents the average seawater compositions. Any deviations from the seawater line indicate either supply from additional sources and removal/gain of these trace elements due to processes operating the water column.

Since evaporites/saline/alkaline soils are not present in the catchments of these lakes, all Cl^- is expected to be derived mainly from sea spray. Therefore, any deviation with respect to seawater ratio of elements/ Cl^- (Figure 4.1) would indicate contributions from other sources and/or processes operating in the water column responsible for the gain/ loss of those elements in/from lake waters (Figure 4.1). Most of the trace metals data fall above the seawater line, whereas, a few samples fall below the seawater line in the Cl^- vs Mo and Cl^- vs Ba plots (Figure 4.1). The higher ratios of trace metals (Cu, Cd, Mn, Pb, As and Ba) and Cl^- indicate weathering of the exposed rocks in the LH or release of these metals from the lake sediments through desorption and ion exchange processes which are commonly reported from global rivers and estuaries (Rahaman et al., 2014; Rahaman et al., 2010; Sholkovitz, 1978). Whereas for Mo and Ba, adsorption of Ba onto lake sediments and biological uptake of dissolved Mo may be responsible for their deviation (removal) of a few samples from the seawater line (Figure 4.1). The

covariation of dissolved Ba and HCO_3 ($r=0.6$, $p<0.01$, $n=24$), and Ba enrichment in sediments indicate that changes in the carbonate chemistry in the water column might play a significant role for the Ba distribution in these lake waters. Therefore, co-precipitation under favourable pH and temperature conditions could be the dominant processes to explain the above observations. Pearson correlation matrix between these elements shown in Table 4.3 highlights significant correlations between pollutant indicator metals such as Cr, As, Cu, Pb and Co and lithogenic elements (Rb, Ba, Mn and U) and suggests lithogenic sources of these heavy metals.

Further, these heavy metals fall within the permissible limits defined by the World Health Organization for drinking water (WHO, 2017). Recent studies reported from few lakes in the Grovnes Peninsula and LH indicate that despite increasing anthropogenic activities globally as well as in Antarctica, the pristine condition is still maintained in these lakes (Magesh et al., 2020). The dust depositions in these lakes and their catchments, based on the back trajectory analysis of air parcel shows (Figure SA2) that the majority of the dust supply comes from arid-semi arid regions of the nearby continents such as the South American deserts (Patagonian) (Laluraj et al., 2020; Rahaman et al., 2016) and the Australian deserts. These regions are known as the potential dust source regions for Southern Ocean and Antarctica (Revelrolland et al., 2006). However, the previous study in these lakes suggests that contributions from the dissolution of aeolian dust to the dissolved solutes in the lake is less than 10% flux of (Nuruzzama et al., 2020). Therefore, we suggest that the supply of trace metals from anthropogenic sources and dust deposition are almost insignificant compared to other sources, i.e. sea salts and chemical weathering of catchments rocks.

Table 4.3. Pearson correlation coefficient matrix (at 95% significance level) Bold numbers indicate significant correlations.

Variables	Temp.	pH	Na ⁺	K ⁺	Mg ⁺²	Ca ⁺²	Cl ⁻	HCO ₃ ⁻	SO ₄ ²⁻	NO ₃ ⁻	Si	PO ₄ ⁻³	DOC	<i>Chl-a</i>	V	Cr	Mn	Co	As	Rb	Cd	Ba	Pb	U	Cu	Mo	Sr	
Temp.	1																											
pH	0.7	1																										
Na ⁺	0.8	0.9	1																									
K ⁺	0.8	0.9	1	1																								
Mg ⁺²	0.8	0.9	1	0.9	1																							
Ca+2	0.7	0.7	0.8	0.8	0.9	1																						
Cl ⁻	0.8	0.9	1	1	1	0.9	1																					
HCO ₃ ⁻	0.6	0.8	0.8	0.7	0.9	0.9	0.8	1																				
SO ₄ ²⁻	0.7	0.5	0.7	0.7	0.8	0.8	0.8	0.5	1																			
NO ₃ ⁻	0.3	0.2	0.5	0.4	0.5	0.7	0.5	0.3	0.7	1																		
Si	0.3	0.2	0.6	0.5	0.6	0.6	0.6	0.3	0.8	0.8	1																	
PO ₄ ⁻³	-0.2	-0.4	-0.3	-0.2	-0.4	-0.4	-0.3	-0.6	-0.1	-0.2	-0.1	1																
DOC	0.4	0.2	0.2	0.2	0.2	0.1	0.1	0.1	0.3	-0.2	-0.2	0.2	1															
<i>Chl-a</i>	-0.2	-0.1	-0.2	-0.1	-0.3	-0.4	-0.2	-0.4	-0.5	-0.4	-0.3	0.5	0	1														
V	0.6	0.6	0.8	0.7	0.7	0.5	0.7	0.5	0.5	0.2	0.5	-0.2	0.1	0	1													
Cr	0	0	-0.1	-0.1	-0.1	0	-0.1	-0.1	-0.1	-0.1	-0.1	-0.3	-0.1	-0.1	0.1	1												
Mn	0.1	-0.3	-0.3	-0.2	-0.3	-0.3	-0.3	-0.4	0.1	-0.1	-0.2	0.4	0.4	-0.1	-0	-0	1											
Co	0.2	-0.1	-0.1	-0.1	0	0	-0.1	-0.2	0.4	-0.1	-0.1	0.2	0.6	-0.3	-0	-0	0.8	1										
As	0.8	0.7	0.8	0.8	0.8	0.7	0.8	0.7	0.6	0.2	0.4	-0.3	0.2	-0.2	0.9	0.3	-0	-0	1									
Rb	0.8	0.7	0.8	0.7	0.8	0.9	0.8	0.8	0.6	0.3	0.3	-0.4	0.3	-0.4	0.6	0.2	-0	0	0.9	1								
Cd	0	-0.4	-0.3	-0.3	-0.3	-0.3	-0.3	-0.3	0.1	-0.2	-0.2	0.3	0.5	-0.1	-0	-0	0.7	0.8	-0	-0	1							
Ba	0.7	0.5	0.6	0.5	0.6	0.6	0.5	0.6	0.5	0.2	0.2	-0.3	0.3	-0.3	0.6	0.4	-0	0.1	0.9	0.9	0	1						
Pb	-0.1	-0.2	-0.2	-0.2	-0.2	-0.3	-0.2	-0.2	-0.3	-0.3	-0.2	0.1	-0.1	0.2	-0	0.1	-0	-0	-0	-0	0.1	-0	1					
U	0.6	0.4	0.5	0.5	0.5	0.6	0.5	0.5	0.3	0.1	0.2	-0.3	0.2	-0.2	0.6	0.5	-0	-0	0.9	0.8	-0	1	-0	1				
Cu	0.7	0.5	0.6	0.7	0.6	0.5	0.6	0.3	0.8	0.2	0.4	0.1	0.5	-0.1	0.5	-0	0.3	0.6	0.5	0.5	0.3	0.4	-0	0.2	1			
Mo	0.2	0.4	0.6	0.6	0.5	0.5	0.6	0.2	0.6	0.5	0.8	0	0	0.2	0.5	-0	-0	-0	0.3	0.2	-0	0.1	-0	0.1	0.5	1		
Sr	0.8	0.7	0.8	0.7	0.8	0.9	0.8	0.8	0.6	0.3	0.3	-0.5	0.2	-0.4	0.6	0.2	-0	-0	0.9	1	-0	0.9	-0	0.9	0.4	0.2	1	

4.6 Identification of dominant factors

To identify the dominant controlling factors that regulate biogeochemical characteristics and trace metal distribution in these lakes, statistical tools were employed on these geochemical data sets and biogeochemical parameters obtained in the present study. Principal components (PCs) derived from principal component analysis (PCA) indicate possible sources and processes/factors that control supply and distribution of major ions, dissolved metal concentrations and biological parameters in these lakes.

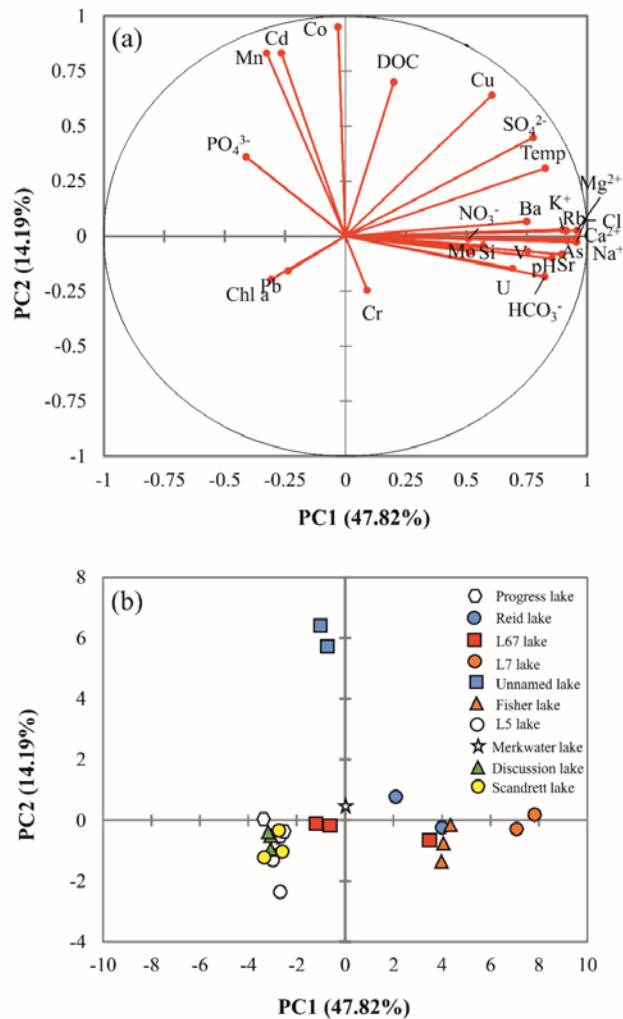


Figure 4.2. Results derived from PCA are plotted: (a) Biplot between two principle factors (PC1-PC2) of factor loadings obtained for variables (b) Biplot between two principle factors (PC1-PC2) for scores obtained for samples.

We plotted the significant components PC1 versus PC2 (Figure 4.2); together, they explain 62% of the total variance in these geochemical data and biological parameters (Table 4.4). Major ions (Na^+ , Mg^+ , K^+ , Ca^{2+} , Cl^- , SO_4^{2-} , and HCO_3^-) along with temperature and total dissolved solids (TDS) load onto PC1, indicates a dominant influence of sea-salt spray that alone explain ~48% of the total variance in these parameters (Figure 4.2a; Table 4.4). Thus PC1 is identified as a source related factor, i.e. sea-salt spray, which is consistent with the earlier reports (Magesh et al., 2020; Nuruzzama et al., 2020).

Table 4.4. Factor loading after varimax rotation ($p < 0.05$)

	PC1	PC2	PC3	PC4
Temp	0.68	0.25	0.52	-0.03
pH	0.75	-0.16	0.37	0.06
Na	0.91	-0.10	0.30	-0.01
K	0.86	-0.06	0.28	0.09
Mg	0.94	-0.06	0.24	-0.13
Ca	0.88	-0.08	0.27	-0.19
Cl	0.93	-0.12	0.25	-0.01
HCO₃	0.73	-0.23	0.32	-0.34
SO₄	0.86	0.38	0.07	0.02
NO₃	0.61	-0.08	-0.18	0.36
Si	0.74	-0.12	-0.17	0.25
PO₄	-0.34	0.15	-0.11	0.79
DOC	0.03	0.68	0.37	0.16
<i>Chlorophyll-a</i>	-0.36	-0.27	0.03	0.72
V	0.58	-0.13	0.51	0.21
Cr	-0.12	0.01	0.88	0.00
Mn	-0.19	0.84	-0.25	-0.11
Co	0.04	0.98	-0.04	-0.07
As	0.60	-0.12	0.76	-0.02
Rb	0.65	0.01	0.68	-0.29
Cd	-0.25	0.84	-0.07	-0.05
Ba	0.38	0.09	0.87	-0.13
Pb	-0.34	-0.14	0.12	-0.07
U	0.25	-0.13	0.88	0.16
Cu	0.59	0.53	0.19	0.45
Mo	0.57	-0.19	-0.07	0.73
Sr	0.63	-0.10	0.70	-0.25

Few trace metals (Rb, Sr, Ba, U, Mo and V) also load onto the PC1 suggesting a sea salt input; however, these elements show strong correlations with Si (Figure 4.2) indicating influence of chemical weathering on the supply of these metals to the LH lakes. The DOC, SO_4^{2-} , Cu, Mn and Co show maximum loading onto the PC2, which explain 14% of the total variance (Figure 4.2a; Table 4.4). These elements (Cu, Mn and Co) and SO_4^{2-} are sensitive to the changes in redox condition in the water column (Rahaman et al., 2010). Therefore, loading of these elements with DOC and SO_4^{2-} onto PC2 (Figure 4.2) indicate that organic matter decompositions and thereby consumption of dissolved oxygen from the water column might influence redox conditions and distributions of these trace elements. Thus PC2 is suggested to be a factor related to organic matter decomposition in the lakes. Higher DOC concentrations in the lake waters ($154 \pm 97 \mu\text{M}$; Table 4.1) compared to Southern Ocean ($50 \pm 10 \mu\text{M}$; Fang et al. (2020)) indicates an active biological decomposition during the austral summer, particularly those lakes where ice-free conditions are more prevalent. The trace elements Rb, As, V, Sr, Cr and U along with physical parameters, i.e. water temperature load onto the PC3 that explain 10% of the total variance (Table 4.4). These elements are primarily derived from the weathering of granitic rocks and hence PC3 is regarded as a factor related to the source i.e. chemical weathering of rocks in the catchments.

Dissolved Mo, nutrient (PO_4) and *Chlorophyll-a* load onto PC4 that explains 8% of the total variance (Table 4.4), suggesting that Mo and PO_4 play a significant role in controlling primary productivity in these lakes and hence PC4 is identified as a factor related to productivity. In summary, four principle factors (PC1 to PC4) identified in our investigations are sea salt spray (PC1), biological decomposition (PC2), chemical weathering (PC3), and primary productivity (PC4). These are dominant factors controlling biogeochemical characteristics of the LH Lakes.

Another statistical tool, Hierarchical Cluster Analysis (HCA) was employed to these geochemical data sets, which also corroborate some of the conclusions derived from the PCA. In addition, HCA also enabled us to group these lakes based on their chemical

characteristics and to explain the intra-lake variations of multiple parameters. Samples and measured parameters (variables) were classified based on their percentage similarity. The results of HCA are shown in the R-mode dendrogram (Figure 4.3) in which three major groups have been identified.

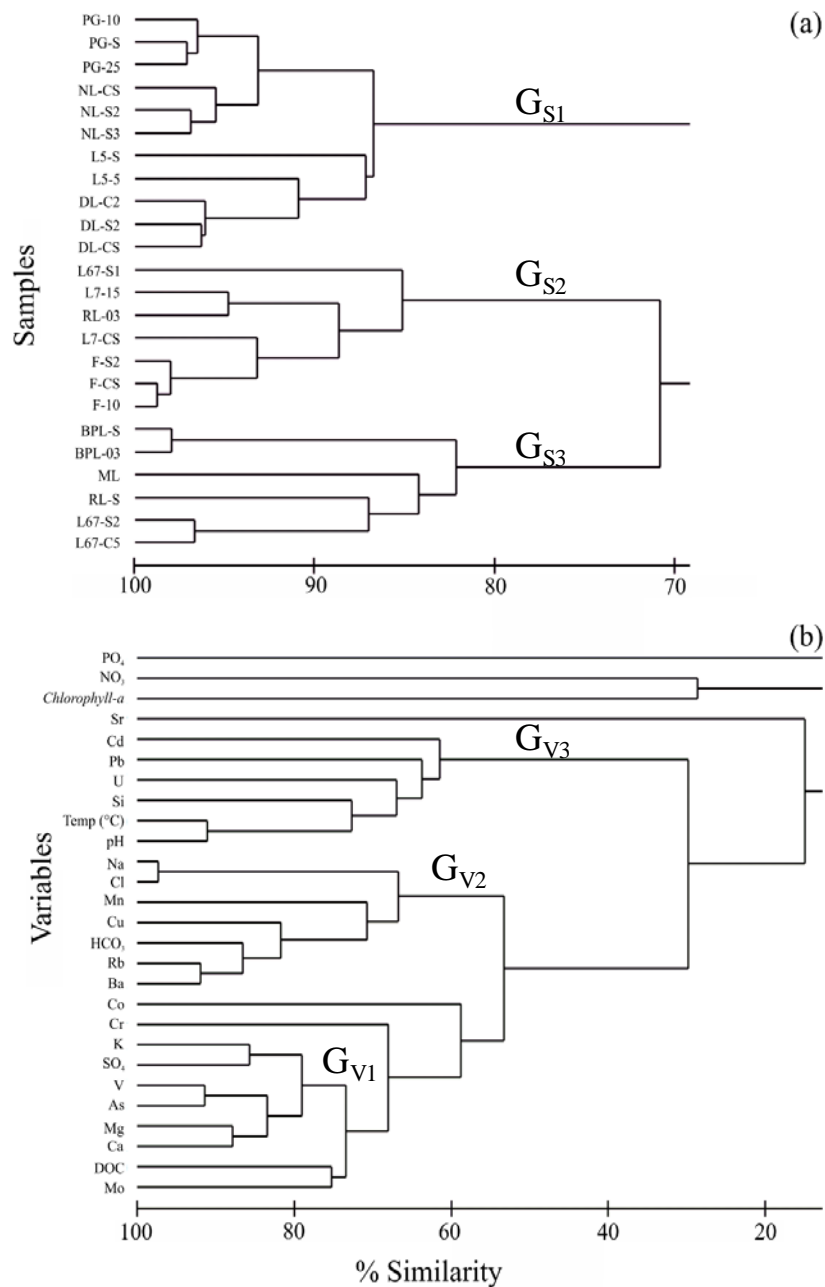


Figure 4.3. Element concentration in lake water samples: (a) Samples and (b) Variables classification obtained by HCA.

For variables, the first group (G_{V1}) where the similarity between variables are close to 75%, includes Mo, DOC, Ca, Mg, As, V and SO_4 (Figure 4.3b). A possible reason for their higher similarity could be due to their redox-sensitive behaviour in the water column which is known to be influenced by organic matter decompositions in the lakes (identified as PC2 in the PCA). The second group (G_{V2}) comprises of Mn, Cu, HCO_3 , Rb, Ba and Co shows 60% similarity (Figure 4.3b) and Na^+ and Cl^- with ~65% similarity. This suggests that the G_{V2} group could be formed due to their common source, i.e. sea salts and weathering of the rocks, which is identified as PC3 in the PC analysis. The third group (G_{V3}) comprises of physicochemical parameters (i.e. temperature and pH), heavy metals (Pb, U, and Cd) and dissolved Si (Figure 4.3b) shows less than 60% similarity. Rest of the parameters measured in these lakes (PO_4^{3-} , NO_3^- , *Chlorophyll-a*, Sr and Cd) do not form any group (less than 30% similarity; Figure 4.3b). These parameters are mainly related to biological processes, thus may have a complex relation with the factors related to nutrient supply and availability such as extent and duration of ice cover in the surface of these lakes and their catchments.

We have identified three sample groups (G_s) based on the percentage similarity in the dendrogram derived from HCA (Figure 4.3a). The first group (G_{S1}) includes four lakes (Progress, Scandrett, L5 and Discussion Lake) with 85% similarity. The formation of this group with such high similarity could be due to their close geographical locations and influence of the common source of dissolved metals. The second group (G_{S2}) includes Fisher, L7, L67 and Reid lakes with 85% similarity (Figure 4.3a). These lakes are closed and isolated water bodies, and therefore the similar extent of endorheic conditions prevailed over these lakes could be the reason to form this group. The third group (G_{S3}) comprises of four lakes viz., Merkwater, Unnamed, Reid, and the Lake L67 with a similarity of ~80%. The exact reasons or factors to form this group are not clear; however, the Unnamed and Merkwater lakes have identical geohydrological settings due to their close proximity could be the possible reason.

4.7 Biogeochemical processes

Several biogeochemical processes in the LH lakes like biological uptake, remineralisations and scavenging of trace metals through organic/inorganic processes

and changes in redox conditions in the water column are known to have significant control on the distributions of dissolved metals (Brand et al., 1983; Danielsson et al., 1985; Donat et al., 1994). We have investigated biogeochemical processes/mechanisms and environmental conditions in the lake water column that influence chemical behaviour and distributions of specific trace elements and nutrients in the water column.

4.7.1 Productivity

LH Lakes are mostly ultra-oligotrophic (Sabbe et al., 2004; Sabbe et al., 2003); however, thick diatom rich algal mats were found widespread onto the lake bottoms indicating benthic diatom productivity. The lower *Chlorophyll-a* concentration ($<0.2 \text{ mg m}^{-3}$) supports the oligotrophic character of these lakes. Limited availability of micronutrients and/or macronutrients, along with the restricted photosynthetic active solar radiation (PAR) (Obryk et al., 2014) could be the limiting factors for productivity and thereby the oligotrophic character of these lakes. Most of the nutrient type trace metals (Co, Mn, Cd and Ba) do not show significant relations with the primary productivity indicator pigment, *Chlorophyll-a*. However, dissolved Mo shows a strong correlation with the *Chlorophyll-a* concentration ($r=0.90$ $p<0.0001$, $n=19$; Figure 4.4a) indicating biological uptake and its possible role in controlling primary productivity. The concentration of dissolved Mo in most of these lake waters are below 4 nM (1.7 ± 1.5 , 1σ , $n=21$) except Merkwater Lake (7.2 nM) and L7 lake (8 nM). Further, significant correlation ($r=0.6$, $p<0.005$) between dissolved Mo and silica (Figure 4.4b) indicates dependence of biological producer (i.e. diatoms) on Mo as a micronutrient. Dissolved Mo is known to be utilised as an essential cofactor in enzyme formations (Glass et al., 2012; Smedley and Kinniburgh, 2017). In the ocean, Mo is not a limiting factor for biological productivity in spite of its large uptake as a micronutrient because of its higher concentration and excess availability of Mo over the biological requirement (Morris, 1975; Sohrin et al., 1998). In freshwater lakes and marine systems, where the concentration of dissolved Mo is below 10 nM, it could act as a limiting factor for primary productivity (Glass et al., 2012). Most of the samples (6 out of 10 lakes) have Mo concentration close to 1 nM; ~ 100 times lower than that of

seawater concentration and therefore biological requirement may exceed the availability of Mo in these lakes.

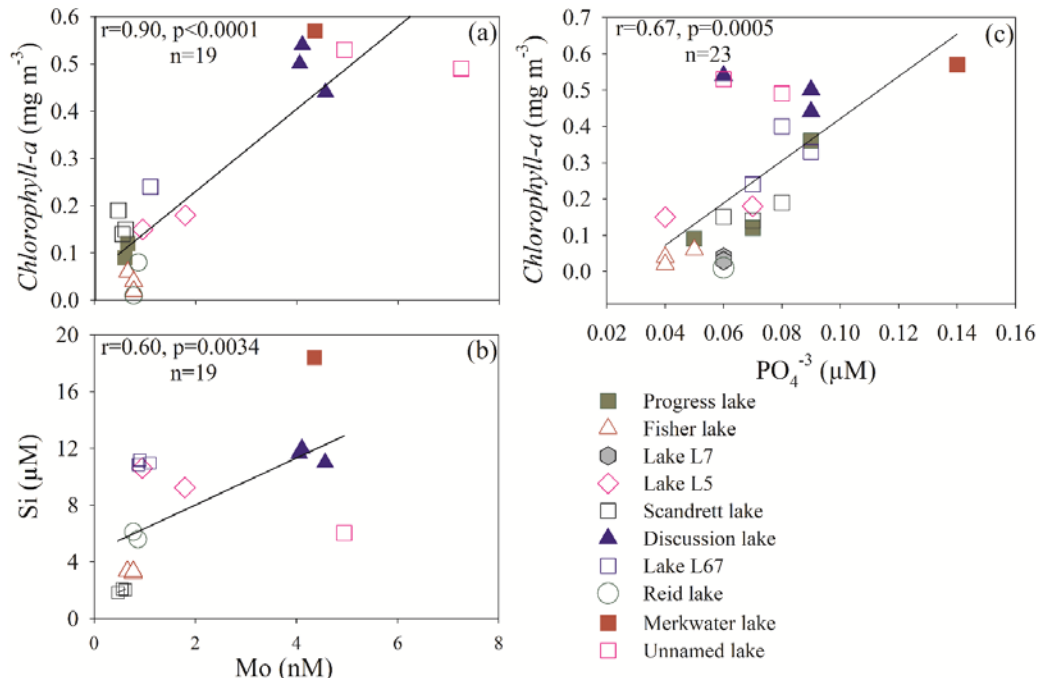


Figure 4.4. Micronutrient behaviour of dissolved Mo in 9 out of the total 10 lakes studied. (a) Correlation plot between *Chlorophyll-a* of water samples from lakes with dissolved Mo. (b) Correlation between dissolved Mo and Si suggesting common sources and identical behaviour in the lake water columns (c) Correlation between dissolved PO_4^{3-} and *Chlorophyll-a* in the lakes.

This suggests that dissolved Mo play an important role in regulating primary productivity in the LH lakes and also act as a limiting factor in most of these lakes. In addition to dissolved Mo, one of the macronutrients, i.e. PO_4^{3-} also shows a strong correlation with *Chlorophyll-a* ($r=0.6$, $p<0.05$; Figure 4.4c) indicating its role on primary productivity in these lakes. The primary source for dissolved phosphate is weathering of the catchment rocks since the possibility of a significant contribution from bird droppings and penguin excreta have been ruled out in the previous study (Nuruzzama et al., 2020). The occurrence of phosphate bearing minerals such as apatite (P_2O_5 up to 2.3 wt%) in the exposed gneissic rocks has been reported from the Larsemann Hills which could be the source for the dissolved PO_4^{3-} supply to these lakes (Grew et al., 2013). The LH lakes are usually covered with ice throughout the year

except for the summer months. In absence of ice cover during austral summers, sunlight penetrates through the water column and reaches the lake bottom, which provides conducive conditions for flourishing the benthic productivity. Thus, ice cover in the lake surface (extent and duration) together with dissolved Mo and PO_4^{3-} play important role in regulating benthic productivity of the LH lakes.

Among the nutrient type trace metals, dissolved Ba does not show significant correlation with *Chlorophyll-a* ($r=-0.3$, $n=24$ Table 4.3), therefore, seems to suggest that it does participate in any of the biological processes in these lakes. However, the role of inorganic processes in dissolved Ba distributions could not be ruled out. In the following section 5.4, we have discusses how the inorganic processes control Ba dynamics in the LH lakes.

4.7.2 Biological decompositions

Bacterial mediated organic carbon decomposition has been reported for several polar and global lacustrine systems (Sobek et al., 2007). The lower water yield (Shevnina and Kourzeneva, 2017) together with restricted interaction with the atmosphere during ice-covered conditions (Gasparon et al., 2002) inhibits the allochthonous supply of organic carbon and effective in-situ decompositions in these lakes. These processes can affect the redox conditions and thereby distributions of the redox-sensitive elements in the lake water column. DOC in the LH lakes shows a significant positive correlation ($r=0.79$, $n=23$, $p<0.001$) with dissolved Cu (Figure 4.5a) and therefore indicate their close association with the processes occurring in the water column. The higher Cu concentration in any enclosed marine/lake ecosystems is known for promoting the metal tolerant bacterial population (heterotrophs) (Gough and Stahl, 2011). These bacterial induced processes further help in decompositions of organic matter and release of organic carbon from copper-sensitive components. The trace metals dependent *Actinobacteria* are also reported for the soils from the Larsemann Hills area (Bajerski and Wagner, 2013). Thus, bacterial mediated organic carbon decomposition could be considered as an important process controlling the distribution of dissolved trace metals (Cu, Mn and Co) in these lakes.

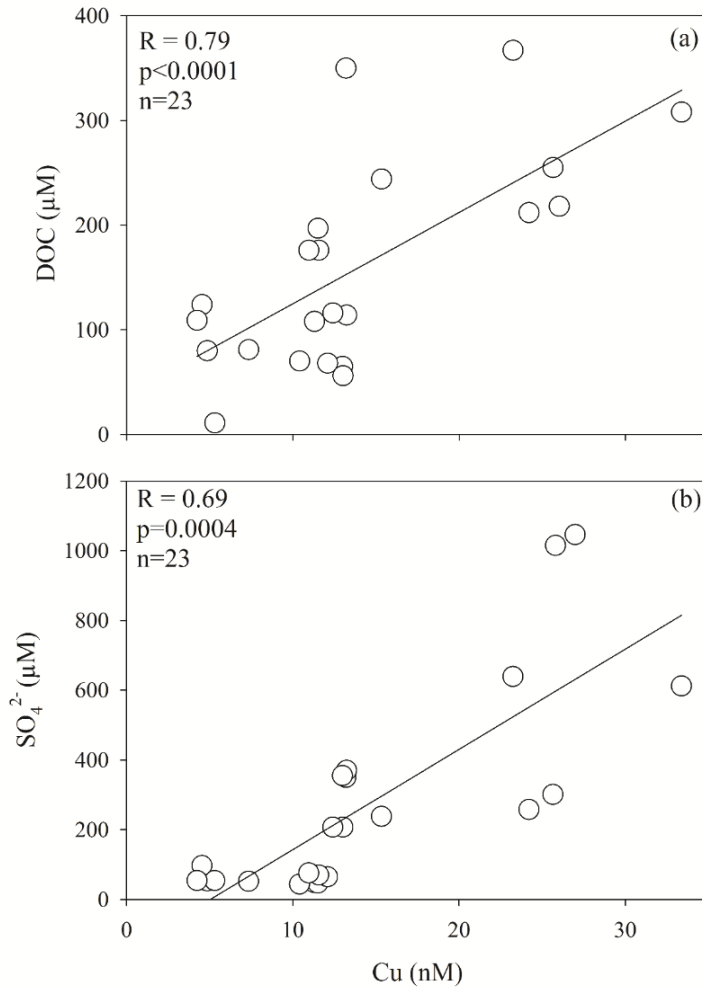


Figure 4.5. Correlation plot for Cu vs dissolved organic carbon (DOC) and SO_4 in lake waters indicating for bacterial mediated organic decomposition in the lakes.

4.8 Inorganic versus biological processes controlling Ba dynamics in the LH Lakes

4.8.1 Dissolved Ba

Dissolved Ba concentration in the LH lakes is lower than that of reported value for most of the global aqueous systems such as lakes, rivers and seawater. The average Ba concentration (29 ± 12 nM) in few lakes like L7, L67 and Fisher lake is close to that of the rivers (48 nM) draining old cartons (Gaillardet et al., 2003). The anomalously higher Ba concentrations are observed in three lakes viz., L7, L67 and Fisher lakes compared to rest of the lakes. Ba dynamics in Antarctic environments

depend on various factors, including diurnal temperature fluctuations and biological induced attenuation (Saelens et al., 2018). Such high Ba concentrations could be due to the desorption of Ba from the lake sediments or release of Ba through ion exchange with Mg^{+2} at the water-sediment interface in an acidic environment (Edmond et al., 1985). Dissolved Ba is strongly correlated with water temperature ($r=0.98$, $p<0.05$, $n=22$; Table 4.3), however, few samples from L67 and Reid lakes do not follow this relationship (outliers) and hence were not considered in the correlation. Our observation of temperature-dependent variations in dissolved Ba is consistent with the earlier report of the Ba dynamics in west Antarctic streams, where a large proportion of the dissolved Ba gets precipitated in lake catchments due to diurnal temperature fluctuations (Saelens et al., 2018). Temperature-induced inorganic precipitations of the dissolved salts are found widespread in cold Antarctic environments (Gooseff et al., 2002; Murray et al., 2012; Toner and Sletten, 2013). Micro-precipitation of Ba usually occurs when the solution is supersaturated with dissolved Ba. To further understand the effects of inorganic precipitation in the LH lakes, we have modelled the saturation indices for the possible mineral formations due to precipitations in the lakes using web-PHREEQ free software. Saturation indices (SI) for Barite ($BaSO_4$) in the lakes vary from -1.0 to -2.87 (Figure 4.7a) suggesting slightly undersaturated for Ba and therefore, Ba precipitation in these lakes through inorganic processes is unlikely. However, biological induced Ba precipitation cannot be ruled out (Saelens et al., 2018). In order to have more insights into the processes regulating Ba dynamics in these lakes, we have also analysed Ba in its counter phase, i.e. bulk sediments from lakes and catchments.

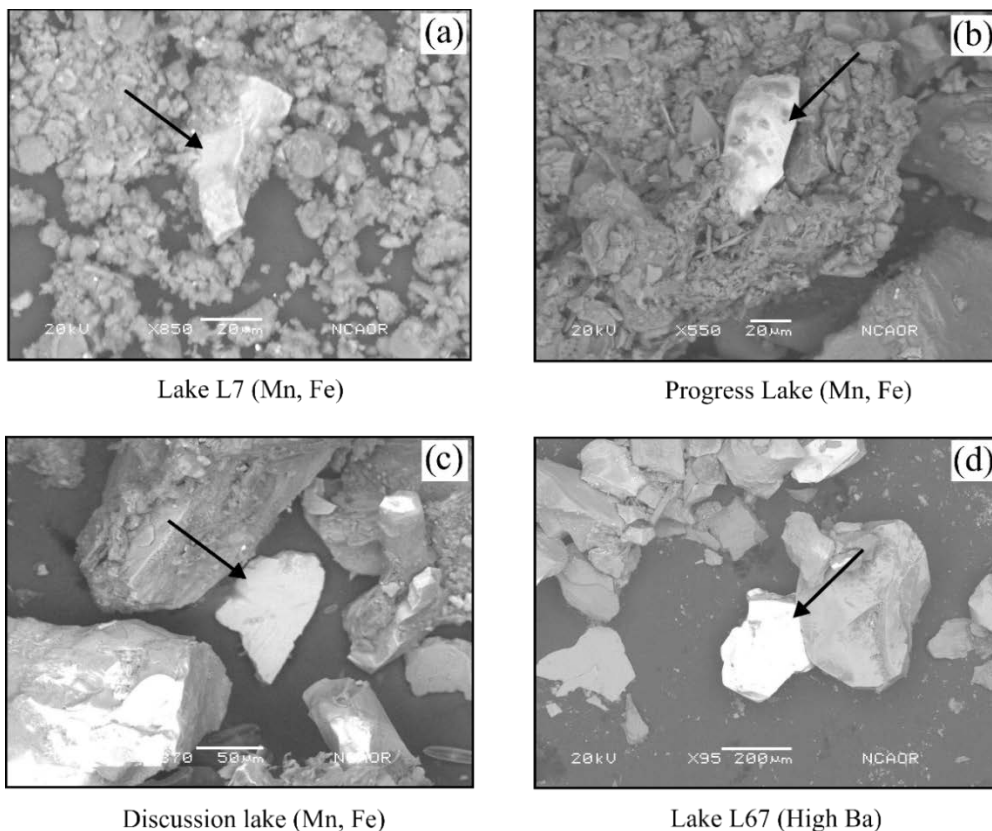


Figure 4.6. SEM images of sediments obtained from lake bottom showing an exceptionally high concentration of Ba, Mn and Fe in their micro-precipitates.

4.8.2 Particulate Ba

Lakes and their catchment sediments are granitic in nature of which major oxides abundances are similar to UCC values. However, Ba concentrations are anomalously higher than UCC value (Table 4.2). The geochemical data (Table 4.2) and SEM-EDS analysis (Figure 4.6b) indicate a presence of secondary minerals of Fe, Mn and Ba oxides/sulphides in the sediments. The source of these minerals could be either allochthonous supply from weathering of rocks in lake catchments or autochthonous (in-situ precipitations within lakes) or combined contributions from these two processes. The saturation indices estimated for Mn and Ba hosting minerals show undersaturation ($SI < 0$) in all the lakes except the Reid lake (Figure 4.7a). It is interesting to note that in spite of undersaturated conditions for the precipitation of the Ba hosting minerals (e.g. $BaCO_3$ and $BaSO_4$), anomalously higher Ba concentrations are observed in the sediments. To understand Ba accumulations and its extent, Ba

excess (Ba_{excess}) was calculated for the catchments sediments and lake sediments following the approach adopted from Eagle et al. (2003)).

$$Ba_{\text{terrigenous}} = Al_{\text{total}} \times (Ba/Al)_{\text{detrital}} \quad (1)$$

$$Ba_{\text{excess}} = Ba_{\text{total}} - Ba_{\text{terrigenous}} \quad (2)$$

The molar ratio of $(Ba/Al)_{\text{detrital}}$ for the sediments was considered as 0.008 (Klump et al., 2000). Estimated Ba_{excess} is significantly higher in catchment sediments (>50%) than for lake sediments (26% for AL-1 and 34% for Discussion lake; Figure 4.7b). Source of this excess of Ba in these sediments could be either due to allochthonous supply or inorganic/biologically induced precipitations in the lakes. However, the possibility of the inorganic precipitations could be ruled out due to undersaturation of Ba hosting minerals ($SI < 0$), as shown in Figure 4.7.

The inorganic precipitations of Ba hosting minerals are common in the west Antarctic streams due to their supersaturation (Saelens et al., 2018). Therefore, one of the possibility could be the transport of catchment sediments comprising Ba hosting minerals to these lakes. It is important to note that lake sediments with thick benthic mats show higher Ba_{excess} (Merewater lake and L7) compared to those with limited occurrences of benthic mats (Discussion lake and L67). This suggests a biological factor that influences the anomalous Ba accumulation onto lake sediments. However, the role of biological induced precipitations of Ba is not yet confirmed. More detailed studies are required to unequivocally explain the mechanisms and individual processes and their quantitative roles in controlling Ba dynamics in these lakes of LH.

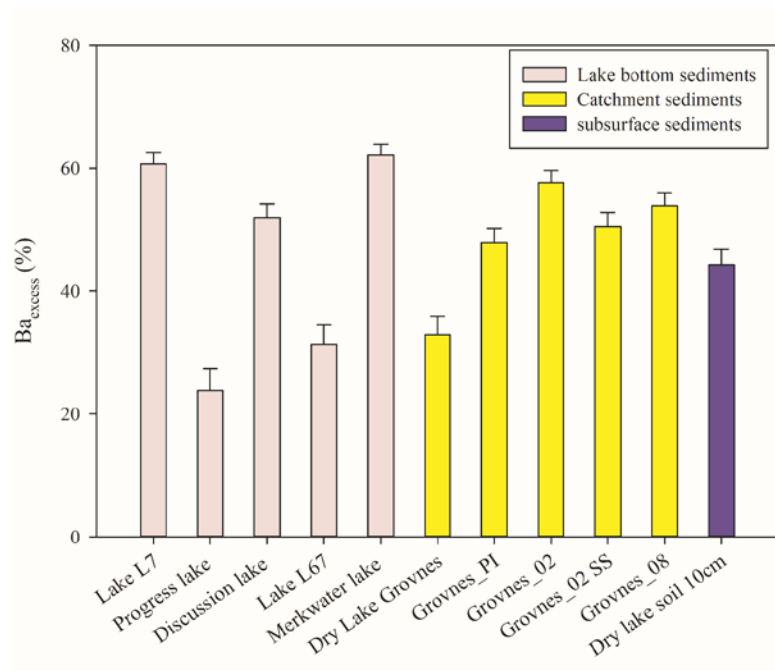
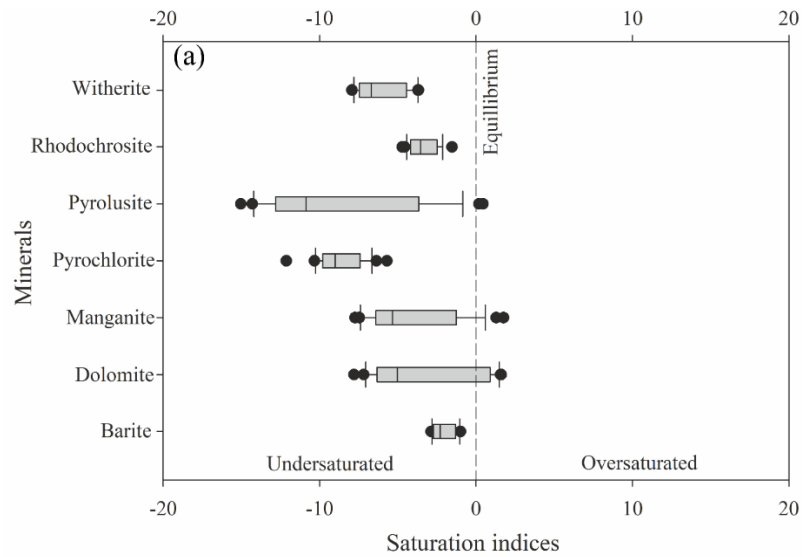


Figure 4.7. (a) Saturation index for minerals in the lake waters using PHREEQ (Mitchell and Brown, 2007; Parkhurst, 1995) (b) Bar plot for estimated Ba_{excess} in lake sediments and catchment sediments.

4.9 Conclusion

Dissolved trace metals, nutrients, *Chlorophyll-a*, DOC, along with major oxides, trace elements and microscale imaging and semi-quantitative compositions of the complimentary phases, i.e. lake and catchments sediments were studied to investigate sources and biogeochemical processes that regulate trace metals and nutrient cycling

in the East Antarctic lakes. Dominant sources for the supply of trace elements and nutrients to the LH lakes and the processes regulating their distribution in the water column are depicted in Figure 4.8.

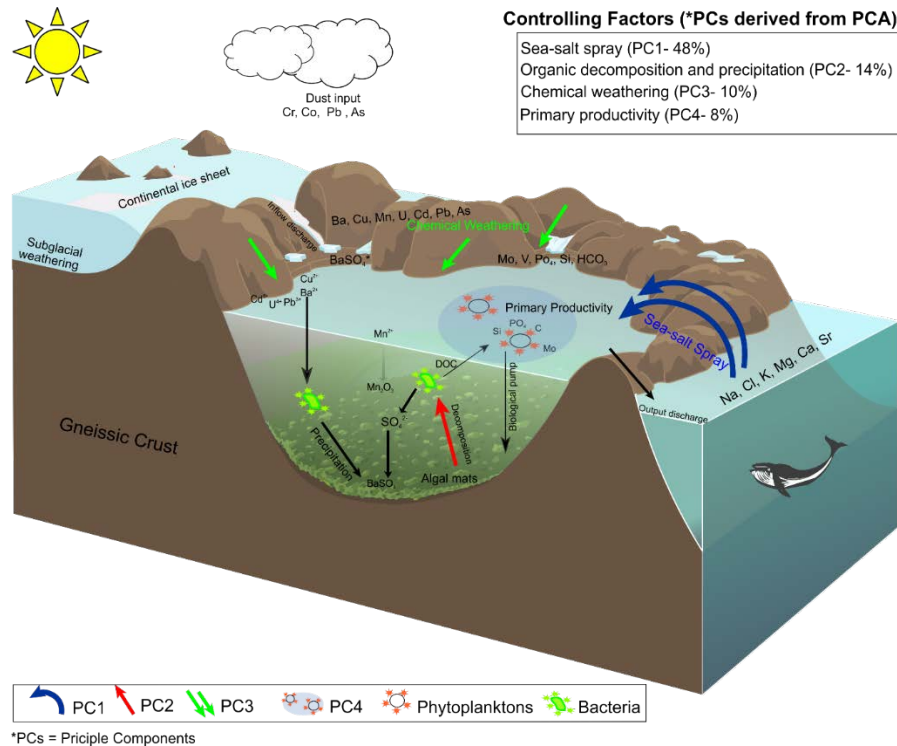


Figure 4.8. Various processes/factors are highlighted in the schematic to explain how they control dissolved trace metal and major ions, their sources and sinks in the lakes of the Larasemann Hills, Antarctica.

Key findings in the present study are as follows;

- Sea-salt spray together with chemical weathering of the catchment rocks are the dominant sources of trace elements and nutrients to the LH lakes.
- Dissolved PO_4 and Mo play a significant role in biological productivity and act as limiting nutrients in most of the Larasemann Hills lakes.
- DOC in the LH lakes shows a significant positive correlation ($r=0.79$, $n=23$, $p<0.001$) with dissolved Cu and therefore indicate their close association of the processes occurring in the water column.

- Bacterial mediated organic matter decomposition is evident in these lakes. Such bacterial activity is found to be controlled by dissolved Cu concentration in these lakes.
- Assessment of Ba in bulk sediments from the lakes and their catchments sediments show excess Ba up to 20-63%. This Ba excess could be either due to biologically induced precipitations of Ba hosting minerals or inorganic precipitations of Ba hosting minerals in the catchment sediments and later transported to these lakes. However, biological induced barite precipitation in the lakes is still unclear and which could be scope for future investigations.
- Geochemical data does not show any detectable evidence of anthropogenic influence. Therefore, these data sets could provide baseline information to investigate and assess anthropogenic stress in other global aquatic system.

Chapter-5

Biogeochemical cycling of Barium and Silica in the surface waters of the Indian sector of Southern Ocean

5.1 Introduction

The Southern Ocean accounts for ~40% of the global ocean's carbon uptake (Friedlingstein *et al.*, 2019; Gruber *et al.*, 2019). The pathway of carbon uptake is regulated by the physical and biological pump through photosynthetic processes subject to the bioavailability of dissolved macronutrients (Si(OH)_4 , NO_x , PO_4^{3-}), micronutrients (Fe, Zn, Cd, Mn, Mo), and sunlight (Honjo *et al.*, 2014). In the Southern Ocean, a paucity of these micronutrients limits primary productivity and leads to the enrichment of unutilized macronutrients, which is responsible for the high nutrient low chlorophyll (HNLC) state (Moore *et al.*, 2013). Photosynthetically active radiation (PAR) depth varies between 100-200m in the global ocean, thus restricting the primary productivity in the uppermost layer of the ocean. The surface Ocean, being the biological hotspot and major contributor to the ocean carbon cycle, becomes the vital zone for the trace metals involved in the ocean biogeochemical cycle. Although their variation throughout the water column is important to unravel the oceanographic processes, focusing on surface ocean variability would reveal the sources of trace metals, bioavailability, the effect of the spatial heterogeneity, and surface oceanic processes with the ultimate role in metabolic uptake processes.

The GEOTRACES initiative mainly focuses on the study of the essential micronutrients (Fe, Zn, Cd, etc.) and their isotopes to investigate the role of these micronutrients in global ocean primary productivity (SCOR working group; Group, 2007). Further, some of these trace elements have been employed as a potential proxy for paleo-productivity such as Barium. Despite the fact that the bulk accumulated Barium in ocean sediments serves as a reliable paleo-productivity proxy (Dehairs *et al.*, 1980; Paytan *et al.*, 1996; Jeandel *et al.*, 2000; Eagle *et al.*, 2003; Gonnee and Paytan, 2006) and Ba/Ca ratios in foraminifera shells are used as a proxy for paleo alkalinity through glacial-interglacial fluctuations (Lea and Boyle, 1989; Lea, 1993), Ba distribution and their relation with biological productivity are not well established in the Indian ocean. Dissolved Ba (Ba_d) behave as non-conservatively in the seawater column and shows large variations in the oceanic basin to sub-basins, it is imperative

to understand Ba distribution in the surface ocean and its relationship with the biological parameters e.g. Chlorophyll-*a*, Dissolved organic carbon (DOC).

Due to its nutrient type profile in the ocean water column (Paytan *et al.*, 1996), dissolved Barium (Ba_d) is recognized as a nutrient-intermediate element, with concentrations ranging from 35 to 140 nmol kg⁻¹ (Rubin *et al.*, 2003). The global ocean exhibits a strong Si(OH)₄-Ba correlation, which is most likely due to surface removal followed by regeneration at depths during the remineralization of particulate organic matter (Lea and Boyle, 1989; Jeandel *et al.*, 1996). In the surface waters (upper 200 m) the Si(OH)₄/Ba regression deviates from the global correlation which indicates a difference in the magnitude of the biological constraint of the Ba_d and Si(OH)₄. The direct metabolic uptake of the Ba_d is unknown, although various photoautotrophs taxa show significant Ba concentrations (Fisher *et al.*, 1991). In microenvironments, Ba associates with PO₄³⁻ through bacterial mediated processes which bind over the transparent exopolymeric particles (TEP) and extracellular polymeric substances (EPS). Later, this associated PO₄³⁻ is replaced with SO₄²⁻ available in the water column and commonly occurs in sediment through Ba-induced precipitation of Barite (BaSO₄) (Ganeshram *et al.*, 2003). Barite crystals are typically associated with organic aggregates and exported to deeper depths, thus regulating long-term Barium biogeochemical cycling in the ocean water column (Dehairs *et al.*, 1980; Dymond *et al.*, 1992). However, the association of Barium with PO₄³⁻ and organic matter and its role in the metabolic uptake has been yet poorly understood and poses an enigma to the Ba_d in the global ocean.

The Southern ocean depicts heterogeneity and biogeographical zonation along the major frontal zones (Pyle *et al.*, 2018). This provides an opportunity to investigate the role of the distinct ecological niche along frontal demarcations on the barium and macronutrient distribution. The presence of distinct features in the Indian sector of Southern Ocean (INSO), such as the Agulhas retroflection front (ARF), subtropical front (STF), islands, and potential upwelling zones offer an opportunity to understand the complexities of these factors on silica and Barium biogeochemical cycling in the INSO. Silica cycling in the Southern Ocean involves their sources from chemical

weathering of the continental rocks and deep water upwelling at large and, sinks such as biological uptake and inorganic binding/ adsorption (Derry et al., 2005; Gao et al., 2016; Treguer and De La Rocha, 2013). These processes control the long-term ocean and atmospheric CO₂ cycling and Southern Ocean in particular acts as an important CO₂ storage sink (Conley and Carey, 2015). The silicifying organisms discriminate against the heavier isotopes (³⁰Si) during silica uptake and thus produce comparatively positive δ³⁰Si signatures in the dissolved seawaters (Conley and Carey, 2015; Sutton et al., 2018). These fractionations are more prominent in surface waters of Southern Ocean and one of the highest Si isotope fractionations of modern seawater are reported for the Antarctic surface waters (AASW) (de Souza *et al.*, 2012a). The AASW are responsible for the formation of Antarctic Intermediate waters (AAIW) and Sub Antarctic Mode waters (SAMW). In this process, silica is stripped off from the surface waters and transfer to AAIW and SAMW which are supposed to be responsible for the silica supply and its isotopic signatures almost throughout the global seawaters through major upwelling zones (de Souza et al., 2014; Reynolds et al., 2006). Although, the surface water signature and its associated phenomenon are not well reported for the AASW in the Indian sector of Southern Ocean. Investigation of these signatures would further enhance the understanding of silica biogeochemical cycling and also account for the region-specific oceanic processes. The covariation of the Si(OH)₄-Ba_d cycling in the global seawater can also be focused through silicon isotopic investigations to assess the control of nutrient utilization on this geochemical variability.

In this study, Ba_d, δ³⁰Si, macronutrients, chlorophyll-*a* and dissolved organic carbon (DOC) were analysed in the surface waters of the INSO during the austral summer of the year 2017. This study will improve our understanding of the relative nutrient utilization of silica in the AASW and Ba_d cycling in the INSO. Assuming frontal variations, complex ocean currents, and regional upwelling/downwelling phenomenon of the INSO, this study will help to further simplify the enigmatic behaviour of the Ba_d in and its influence over other biogeochemical parameters. This will ultimately help paleoceanographers to better interpret the barium fluctuation with paleoclimate changes by considering the spatial changes and regional characteristics of Ba_d in the INSO.

5.2 Results

5.2.1 SST, SSS, and pH

Variations of sea surface temperature (SST) and sea surface salinity (SSS) (Figure 5.1) demarcate the frontal boundaries in the Southern Ocean. The SST and SSS exhibit a strong gradient along the N-S transect as depicted in the colour code (Figure 5.1); the water mass near 35° S has higher SST (~20° C) and salinity (35-36) than the water mass near the coastal region of Antarctica at ~70 °S (SST~0°C and SSS~33 – 34 psu). SST and SSS for the two corresponding transects T1 and T3 show close resemblance although they represent different phases of austral summer. This suggests the unchanged hydrodynamics of the surface waters throughout the austral summer. The pH values show a strong gradient along the two transects; (T1 and T3); the anomalously higher pH values are found in coastal Antarctica, primarily in the Prydz Bay region whereas the anomalous lower values were observed between 60 - 65° S in T1 (Table 5.1; Figure 5.1). The strong gradient with the lower pH anomalies can be linked to regional sea-ice melt supplying low pH freshwater as a result of freezing and thawing in the INSO (Srivastava *et al.*, 2007). In addition, the upwelling of Antarctic Intermediate Water (ABW) characterizes higher dissolved CO₂ and could be the reason for the lower pH anomaly in these waters.

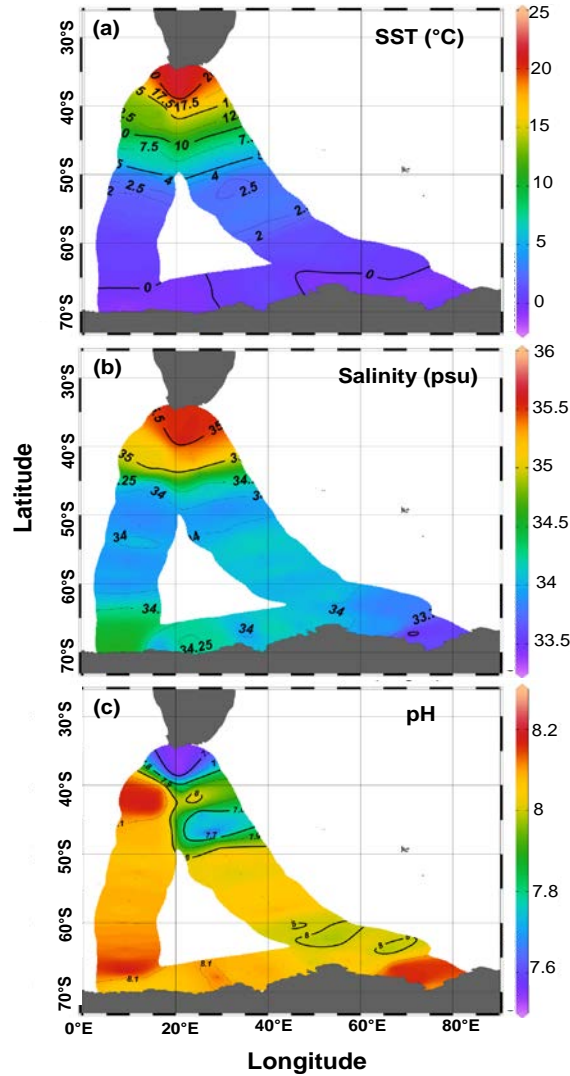


Figure 5.1. Variability of the insitu measured physical parameters (SST, SSS and pH) shows the clear frontal demarcations in the INSO.

5.2.2 Macronutrients (silicate, phosphate, nitrate), DOC and Chlorophyll-*a*

The macronutrients include Silicate ($\text{Si}(\text{OH})_4$), Phosphate (PO_4^{3-}), and Nitrates (NO_x) do not show any significant correlation with physical parameters (salinity and temperature). Bi-modal variations in the dissolved macronutrient concentrations have been observed along the Polar front zone (PF) (Figure 5.2). The distributions of the macronutrient concentrations in the sub-tropical zone (STZ; north of the Polar Front) are an order lower than the Antarctic surface waters (AASW; South of the Polar Front).

The observed bimodal macronutrient variation has previously been reported throughout the Southern Ocean and is attributed to the difference in community structures between the water masses in the North and South of Polar fronts (Kopczynska *et al.*, 1986). Anomalously high concentrations of the dissolved macronutrients were observed in the samples of the T1 near $\sim 60^{\circ}\text{S}$.

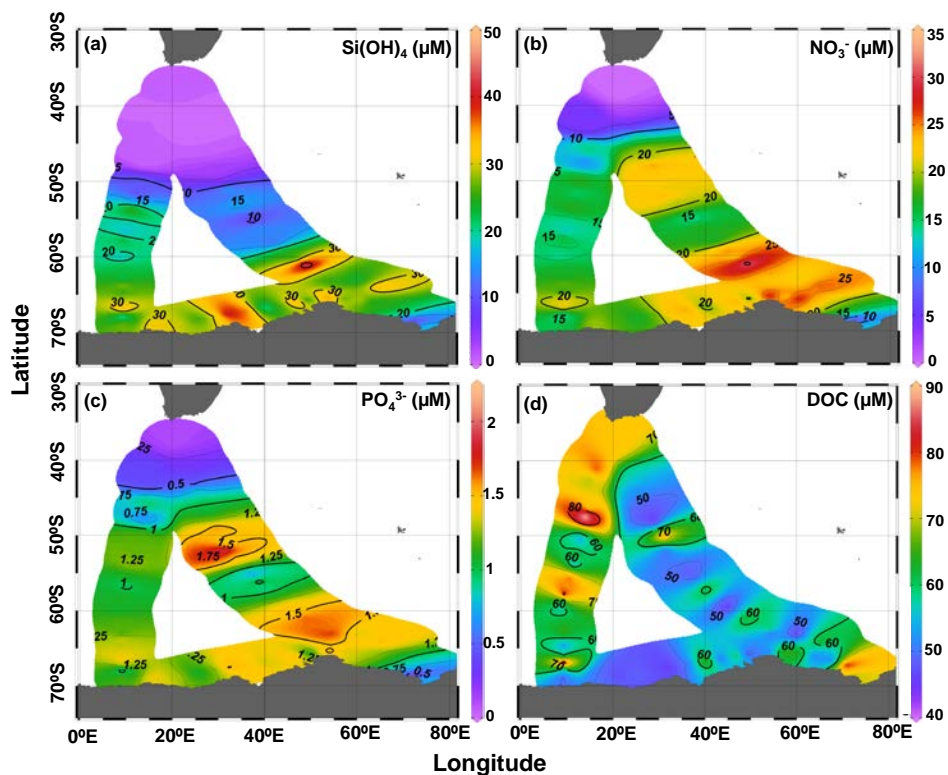


Figure 5.2. Dissolved macronutrients, and dissolved organic carbon (DOC) are spatially plotted to represent their latitudinal variability and differences in the three transects.

The variation of dissolved organic carbon (DOC) shows an opposite pattern to that of the distribution of macronutrients (Figure 5.2). The sub-Antarctic zone (SAZ) and STZ have higher DOC concentrations than the AASW zone. Higher DOC concentration ($95\mu\text{M}$) is observed in the samples of the T3 transect between 45°S and 55°S near Prydz Bay ($85\mu\text{M}$) whereas relatively lower concentrations are found in the coastal Antarctic samples (Figure 5.2).

Diatoms account for more than 70% of total primary productivity in the Southern Ocean (Malviya *et al.*, 2016). The primary productivity of diatoms is

indicated by chlorophyll-*a* concentration which shows a wide range from 0.5 to 6 mg m⁻³ (Table 5.1) measured in surface waters of INSO. The majority of the samples show a large range from 0.1-1 mg m⁻³. Anomalously high chlorophyll-*a* (approximately 6 mg m⁻³; Table 5.1) is observed in the samples collected from Prydz Bay. The two corresponding transects (T1 and T3) show significant differences in the chlorophyll-*a* concentrations; T1 shows twice higher concentrations than the T3 transect samples. The data for the dissolved chlorophyll-*a* are not consistent due to the unavailability of the samples at some locations in the transects T1 and T3.

5.2.3 Dissolved Barium (Ba_d)

The overall dissolved Barium (Ba_d) concentration varies between 40 and 90 nmol kg⁻¹ (Table 5.1) and represents the major frontal demarcations throughout the surface waters of INSO. The Bi-modal distribution pattern can also be seen along the polar front (50°S), with samples from the AASW (80 nmol kg⁻¹) having twice as much Ba_d as STZ (40 nmol kg⁻¹; Table 5.1). The Ba_d in the SAZ has an intermediate concentration (70 nmol kg⁻¹) and acts as the Barium transition zone. The occurrence of two abnormally higher Ba_d zones: (i) along 10°E, between 55-60°S, and (ii) in the Prydz Bay region. The Barite saturation index (SI) estimated (Monnin and Cividini, 2006) for these samples ranges from 0.75 to 1.75. The distribution pattern of the SI shows that SAZ is characterised by a supersaturated state (high SI) compared to STZ. The AASW zone shows a close variation of SI (1.1-1.3), indicating a slightly saturated state, except for the coastal Antarctic samples, where SI indicates highly under-saturated conditions (0.6-0.8).

Table 5.1. Sampling details, physical parameters, dissolved nutrients, chlorophyll-*a*, and DOC of the samples collected during the austral summer of the year 2017 from the Indian sector of the Southern Ocean

Sample ID	Latitude (S°)	Longitude (E°)	pH	Sea surface temperature (SST)	Sea Surface Salinity (SSS)	Trace metal	Nutrients				DOC	Chl. a	Si/N
							SiO ₄	PO ₄ ³⁻	NO ₃ ⁻	NO ₂ ⁻			
				(°C)	(psu)	Ba (nmol kg ⁻¹)	(µM)				(mg m ⁻³)		
Transect-1 From Capetown to Prydz Bay													
CT-PB 01	38.08	20.46	7.5	23	35.51		1	0.1	0.1	0.02	74	0.53	
CT-PB 02	39.12	21.34		21	35.8		1.3	0.2		0.02			
CT-PB 03	40.26	22.3	7.7	15.7	35.29	42	0.3	0.3	1.9	0.11		1.91	
CT-PB 04	41.3	23.21	8.1	15.1	35.39	40	0.3	0.3	2	0.11		0.15	
CT-PB 05	42.09	23° 52.463'	8.1	14.1	35.43	40	0.7	0.4	3.8	0.11	57	3.12	
CT-PB 06	43° 06.967'	24° 38.155'	8	13	35.2		1	0.4	5.2	0.13		0.19	
CT-PB 07	44.02	25.23	7.6	9.6	34.32	56	0.5	0.9	16	0.23	52	2.66	
CT-PB 08	46	27	7.8	7.7	34.02	46	0.8	1	20	0.27	48	0.04	
CT-PB 09	47	27.54	7.5	7.4	34.31	60	1.6	1	19	0.23		2.04	
CT-PB 10	48	28.49	7.93	4.5	33.89	72	4.2	1.2	26	0.2	43	3.74	
CT-PB 11	49	29.39	8.03	5.1	33.83	70	2.9	1.7	22	0.22		0.13	
CT-PB 12	50.08	30.54	8.1		33.9	62	3	1.5	22	0.2	82	1.35	
CT-PB 13	51	31.58	8.03	1.8	34.03	80	18	1.3	21	0.16		0.86	
CT-PB 14	52	33.15	8.02	2.4	33.96	75	11.5	2.1	24	0.18	46	2.46	
CT-PB 15	53	34.3	8.02	2.6	34.17	75	16.4	1.4	20	0.16		0.82	
CT-PB 16	55 20	37 38	8.04	3.2	34.2	71	7.3	0.6	13	0.11	47	1.62	
CT-PB 17	56 07	38 45	8.05	2.8	34.05	75	15.7	1.2	18	0.17		0.87	
CT-PB 18	57° 3.787'	40° 05.572'	8.04	2.2	34.03	76	14.2	0.8	17	0.22	63	0.84	
CT-PB 19	57° 56.755'	41° 49.587'	8.1		34.18		11.3	1.1	16	0.17		0.71	
CT-PB 20	59° 29.843'	44° 58.086'	8.02	1	33.99	78	25	1.5	26	0.27	45	0.96	
CT-PB 21	60° 11.128'	46° 24.115'	7.99	1.1	34.06	75	22.3	1.4	21	0.23		1.06	
CT-PB 22	60° 58.368'	48° 49.860'	8.01	1.1		73	47.9	1.7	33	0.16	63	1.45	
CT-PB 23	62° 23.125'	54° 06.572'	7.97	0.6	34.19	78	27.9	1.6	25	0.23	68	1.12	
CT-PB 24	62° 59.365'	56° 26.499'	8	1.2	33.92		24.1	1.8	22	0.23	42	1.1	
CT-PB 25	63.5	59.48	8.03	0.5	33.83	66	22.4	1.3	21	0.17	44	1.07	
CT-PB 26	64.2	65.1	7.98	0.5	33.81	80	33	1.5	26	0.18	64	1.27	
CT-PB 27					33.96		35.2	1.5	23	0.11	43	1.53	
Transect-2 Prydz Bay to India Bay													
PB-IB 01	69° 07.638'	75° 18.548'	8.098	0.1	33.58		18.8	0.8	13	0.16		6.37	
PB-IB 02	68° 27.224'	72° 51.377'	8.187	-0.6	33.64		6.7	0.3	5.7	0.08	69	4.36	
PB-IB 03	67° 15.041'	70° 51.202'	8.158	-0.9	33.33	75	21.2	0.8	17	0.15	88	6.96	
PB-IB 04	66° 35.720'	67° 34.666'	8.194		34.02	81	25.4	1.1	20	0.13	46	1.08	
PB-IB 05	66° 03.776'	63° 37.579'	8.025	-0.1	33.93		22.6	1.3	23	0.14	48	0.83	

PB-IB 06	65° 45.177'	60° 22.042'	8.003	-0.6	33.89	71	31.1		30	0.16	67	1.12	1.04
PB-IB 07	65° 28.289'	57° 15.374'	8.102	-0.3	34.09	78	23.9	1.3	21	0.13	69	1.44	1.14
PB-IB 08	65° 23.223'	53° 57.193'	8.018	-0.7	34.08	76	39.8	1.7	30	0.16	49	4.08	1.33
PB-IB 09	65° 42.451'	49° 20.173'	7.992	-0.7	34.18	75	20.7	0.8	16	0.11	45	1.89	1.29
PB-IB 10	65° 59.493'	46° 46.590'	8.052	0	33.99	74	38.9	1.7	26	0.15	65	0.54	1.5
PB-IB 11	66° 22.449'	43° 22.172'	8.068	0.5	34.21	61	25.8	1.4	23	0.14	45	1.67	1.12
PB-IB 12	66° 42.655'	40° 17.733'	8.105	1.2	34.24		16.7	1.3	17	0.13	70	0.59	0.98
PB-IB 13	67° 09.585'	35° 47.202'	8.086	0.6	33.91	75	38	1.5	25	0.12	49	0.8	1.52
PB-IB 14	67° 31.885'	32° 02.167'	8.058	0	34.24	84	43.6	1.6	24	0.09	45	0.47	1.82
PB-IB 15	67° 51.473'	29° 01.904'	8.153	0.3	34.25	68	28.1	1.2	18	0.07	47	1.68	1.56
PB-IB 16	68° 10.839'	25° 53.537'	8.08	-0.5	34.25	67	24.8	1	16	0.1	49	1.8	1.55
PB-IB 17	68° 39.316'	21° 01.731'	8.067	-0.5	34.29	76	29.7	1.3	18	0.13	47	1.39	1.65
PB-IB 18	69° 02.953'	16° 53.430'	8.054		33.98	74	31.4	1.4	20	0.13	50	1.79	1.57
Transect-3 India Bay to Capetown													
IB-CT 01	68° 52.289'	9° 08.756'	8.035	-1.2	34.59	58	28.1	1.2	16	0.14	47	0.98	1.76
IB-CT 02	67° 54.357'	9° 10.494'	8.102	0.1	34.53	64	16.3	0.8	12	0.16	46	0.55	1.36
IB-CT 03	66° 54.560'	9° 13.753'	8.225	-0.3	34.51	38	36.7	1.5	23	0.2	109	0.6	1.6
IB-CT 04	66° 00.570'	9° 14.772'	8.155	0.4	34.5	54	29.4	1.4	22	0.17	49	0.49	1.34
IB-CT 05	64° 32.807'	9° 13.522'	8.115	0	34.32	62	24.3	1.3	17	0.16	46	0.29	1.43
IB-CT 06	63° 45.700'	9° 14.324'	8.144	1.2	34.33	71	30.4	1.4	20	0.15	58	0.1	1.52
IB-CT 07	62° 58.572'	9° 13.877'	8.102	0.3	34.13	78	20.8	1.1	16	0.24	71	0.12	1.3
IB-CT 08	61° 56.015'	9° 02.548'	8.116	0.6	34.03	81	23.1	1.2	17	0.16	64	0.18	1.36
IB-CT 09	61° 03.747'	8° 37.925'	8.107	0.7	33.97	85	22.6	1.2	16	0.16	63	0.14	1.41
IB-CT 10	60° 02.700'	8° 39.572'	8.101	0.7	33.83	88	16.4	1	13	0.16	53	0.24	1.26
IB-CT 11	58° 51.316'	8° 44.164'	8.087	0.5	34.03	85	21.2	1.1	15	0.14	49	0.22	1.41
IB-CT 12	57° 47.937'	9° 16.933'	8.084	1.3	33.97	78	24	1.1	17	0.15	96	0.9	1.41
IB-CT 13	56° 44.209'	9° 52.489'	8.095	1.4	33.83	78	16.1	0.9	12	0.12	74	0.79	1.34
IB-CT 14	55° 41.894'	10° 29.411'	8.095	1.7	33.94	81	19.2	1.1	14	0.15	82	0.34	1.37
IB-CT 15	53° 36.394'	11° 27.078'	8.067	1.4	34.15	74	28.5	1.3	18	0.14	49	0.83	1.58
IB-CT 16	52° 38.892'	11° 52.345'	8.111	2	33.9	66	13.9	1.2	16	0.17	67	0.92	0.87
IB-CT 17	51° 32.081'	12° 19.068'	8.048	3.2	33.86	74	8.4	1.2	14	0.15		0.1	0.6
IB-CT 18	50° 29.938'	12° 43.185'	8.075		33.85	73	11	1.2	18	0.19	52	0.54	0.61
IB-CT 19	47° 21.136'	14° 02.980'	8.088	7	33.91	59	1.1	0.6	9.7	0.14	96		0.11
IB-CT 20	46° 14.161'	14° 40.422'	8.085	7.3	34.01	61	1.2	1	15	0.32	68		0.08
IB-CT 21	42° 30.433'	15° 53.348'	8.197	13.2	35.08	45	0.9	0.4	4	0.16	68		0.23
IB-CT 22	41° 07.339'	16° 15.759'	8.183	12.4	34.99	45	0.8	0.4	5.1	0.11	81		0.16

5.2.4 Dissolved Silica (Si(OH)₄) and $\delta^{30}\text{Si}$ in seawater samples from AASW

The Si(OH)₄ and $\delta^{30}\text{Si}$ of the Antarctic surface water (AASW) samples analysed show a wide variation from 6.7 to 48.0 μM and +1.74 to +3.2 ‰ respectively (Table 5.2). The Si(OH)₄ varies widely in the range between 0.1- 48 μM with a consistent increase from STZ to AASW and shows several gradients in the concentration throughout the INSO (Figure 5.2). The first gradient is visible at the Polar front (~50°S). North to PF, the concentrations limit to 5 μM , whereas, South to the PF, the concentrations reach up to 30 μM .

Table 5.2. The measured silica concentration and stable silicon isotope ($\delta^{30}\text{Si}$) characteristics of the samples collected from Antarctic surface waters (AASW)

Sample ID	Lat. Long.	Si(OH) ₄ (μM)	$\delta^{29}\text{Si}$	$\delta^{30}\text{Si}$		n
				Mean	2 $\sigma_{\text{SE(external)}}$	
PB-IB-01	69° 07.638'	18.8	1.13	2.33	0.06	3.00
	75° 18.548'					
PB-IB-02	68° 27.224'	6.7	1.62	3.16	0.03	3.00
	72° 51.377'					
PB-IB-04	66° 35.720'	25.4	1.05	2.08	0.09	3.00
	67° 34.666'					
PB-IB-05	66° 03.776'	22.6	1.07	2.12	0.07	3.00
	63° 37.579'					
PB-IB-06	65° 45.177'	31.1	0.91	1.73	0.06	2.00
	60° 22.042'					
PB-IB-07	65° 28.289'	23.9	1.05	2.10	0.01	3.00
	57° 15.374'					
IB-CT 01	68° 52.289'	28.1	1.00	2.01	0.03	3.00
	9° 08.756'					
IB-CT 02	67° 54.357'	16.3	1.280	2.56	0.02	3.00
	9° 10.494'					
IB-CT 03	66° 54.560'	36.7	0.88	1.80	0.02	3.00
	9° 13.753'					
IB-CT 04	66° 00.570'	29.4	1.00	2.06	0.08	2.00
	9° 14.772'					
IB-CT 05	64° 32.807'	24.3	1.05	2.12	0.05	2.00
	9° 13.522'					

Few anomalously high concentrations are also observed in the SAZ and AASW. The $\delta^{30}\text{Si}$ measured in AASW and SAZ samples on the transect-2 and transect-1 covering the longitudinal extent between Prydz Bay and India Bay (Figure 5.1). Samples from

the longitudinal extreme of the Prydz Bay region and India Bay region show a relatively higher $\delta^{30}\text{Si}$ signal (Table 5.2). The highly fractionated $\delta^{30}\text{Si}$ signal was observed in the sample near Prydz Bay (PB-IB-02; Table 5.2). Among all the surface water signatures, the sample possessing the highest fractionated Si isotopic signatures show enhanced nutrient utilization of the available silica pool. The $\delta^{30}\text{Si}$ signals reported in the AASW of INSO are similar to those reported for modern global oceanic systems (De La Rocha *et al.*, 2011; de Souza *et al.*, 2012b; Grasse *et al.*, 2013).

5.3 Discussion

The variation of the physical parameters such as the SST and SSS demarcates the known major frontal boundaries (Figure 5.1). Agulhas Retroflexion front (ARF) is recognized near $\sim 38^\circ\text{S}$ where the first gradient in the SST and SSS is observed (Figure 5.1). Further south, major potential gradients in the SST and SSS were identified as Subtropical Front (STF), Sub Antarctic Front (SAF), and Polar front (PF) at around 40°S , 45°S , and 50°S respectively. The SST and SSS show non-regular variations south of the PF (50°S), with no apparent potential gradients. The inverse relationship observed between the $\text{Si}(\text{OH})_4$ and SST indicates the control of SST on the nutrient utilization in surface waters of INSO.

5.3.1 Macronutrient stoichiometry, nutrient utilization, and biological decomposition

The dissolved macronutrients ($\text{Si}(\text{OH})_4$, NO_3^- , and PO_4^{3-}) play a vital role in photoautotroph metabolic uptake and siliceous frustule formation throughout the global ocean (Gruber *et al.*, 2019). Strong correlations observed between macronutrients indicate their common pathways during metabolic uptake. The stoichiometric ratios between macronutrients (Si/N and P/N) are sensitive to environmental changes and shifts in the ecological niche (Weber and Deutsch, 2010). Variations in the Si/N show a sharp contrast in the Fe-limited zones of the ocean and go up to ~ 3 (Hutchins and Bruland, 1998; Jin. *et al.*, 2006; Fu *et al.*, 2007) compared to the global mean (~ 1 ; (Jin. *et al.*, 2006)). The Si/N ratios in the samples vary between 0.04-1.82 (Table 5.1) which indicates the large variability in the biogeochemical

processes involving macronutrient dynamics throughout the INSO. The Si/N ratio in the SAZ and STZ is an order lower (0.1-0.5) than in AASW suggesting higher utilization in the SAZ and STZ whereas the limited micronutrient conditions prevail in the AASW zone results in higher unutilised silica. The Si/N of the samples from coastal transects show a close variation (1.3 ± 0.24 , 1σ) which is close to the global mean ocean indicating the balance between supply and uptake (Hutchins and Bruland, 1998). The Si/N in T1 samples ranges between 0.1 and 0.2, while it is higher in the T3 transect (0.2-0.8). This indicates intra-seasonal heterogeneities in controlling Si(OH)_4 and NO_3^- utilisation during the austral summer.

Dissolved macronutrient availability and their utilization in the Southern Ocean are controlled by various enrichment and biological uptake processes. The biological pump which drives the net pCO_2 drawdown depends on the ratio of nutrient utilization to its supply (Honjo *et al.*, 2014). To better understand the nutrient utilization in these samples, an index denoted by the N^* was estimated (Figure 5.2) based on the Redfield ratio of Nitrate and Phosphate in the global ocean (Harris, 2003; Ridgway and Dunn, 2003; Weber and Deutsch, 2010).

The N/P of the seawater mimics the metabolic uptake ratio (16:1) by photoautotrophs whereas the global mean of the N/P ratio is 14.5. Thus any deviation from the global N/P ratio indicates the relative nutrient utilization differences. N^* simplify the understanding of the relative nutrient utilization with the equation described below.

$$\text{N}^* = [\text{NO}_3^-] - 16 [\text{PO}_4^{3-}] \quad \dots\dots\dots (1)$$

Under optimum utilization conditions, the N^* is close to zero (0) which indicates a balance between the nutrient supply and uptake (Gruber and Sarmiento, 1997; Weber and Deutsch, 2010). Any deviation from the optimum utilization needs additional biogeochemical processes to explain.

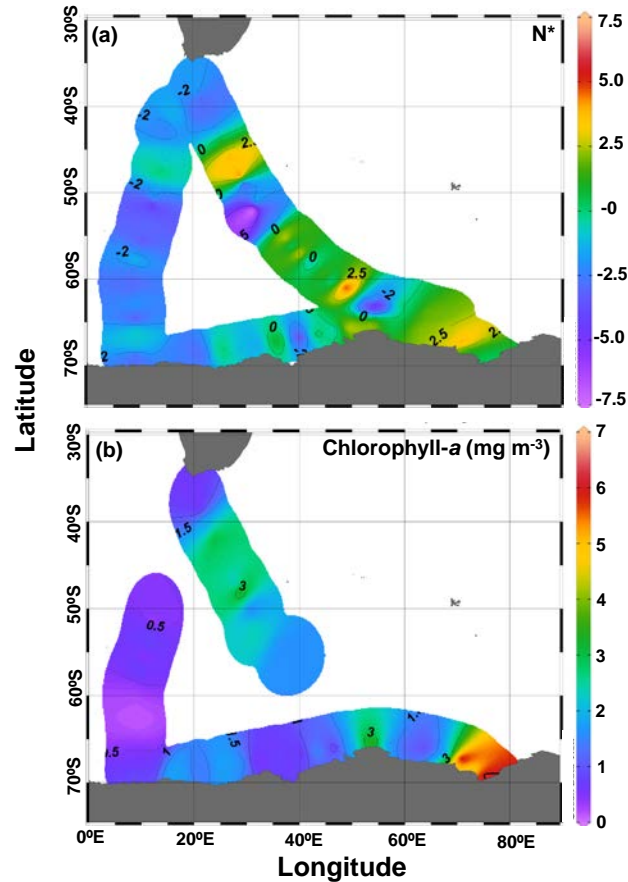


Figure 5.3. (a) The nutrient utilization, N^* ($= NO_3^- - 16 \cdot PO_4^{3-}$) in the surface waters of the Indian sector of Southern Ocean (b) In-situ Chlorophyll-*a* distribution in the INSO.

The variation in the N^* in the sampling region of INSO is attributed to three distinct processes, such as (i) high biological uptake with high chlorophyll-*a*, when N^* is less than 1, (ii) the denitrification zone where bioavailable dissolved nitrate converts to the NH_4 and NH_3 with low chlorophyll-*a*, when N^* is less than zero (0) and (iii) excess nutrient supply through upwelling/weathering with high chlorophyll-*a* when N^* is more than one (+1).

The N^* variation does not show any systematic variations with the fronts. A clear distinction between transects indicates that the processes related to nutrient dynamics are overshadowed by the intra-seasonal heterogeneity. The samples from the transect T1 show high N^* with higher chlorophyll-*a* than that of the T3 transects (Figure 5.3). This indicates the excess biological uptake with enriched supply during

the peak of austral summer. In general, N^* in the AASW zone is lower than PFZ and SAZ with the high chlorophyll-*a* concentrations (Figure 5.3) indicating the high biological uptake in the AASW. However, few samples of T3 in the AASW zone show low N^* with extremely low chlorophyll-*a*, although a potential subsurface water upwelling is observed in the region indicating active local denitrification (Gruber and Sarmiento, 1997). Samples from coastal Antarctica show anomalously higher chlorophyll-*a* with higher N^* (~2.5) in the Prydz Bay region resulting from strong upwelling of nutrient-rich waters and/or supply from active continental weathering in the Larsemann Hills (Nuruzzama *et al.*, 2020, 2021) and nearby ice-free regions.

The Dissolved organic carbon (DOC) reflects the extent of biological decomposition in the surface waters and supply through subsurface upwelling. DOC measured in the surface waters varies from 40-95 μM with an average of $58 \pm 13.7 \mu\text{M}$ (1σ) (Table 5.1). The variation of DOC shows a distinct distribution pattern compared to both physical parameters and dissolved macronutrients (Figure 5.2). The frontal demarcations are not visible however the samples from the two corresponding transects T1 and T3 show strong heterogeneity. This indicates control of intra-seasonal variations in DOC concentrations. While observing the latitudinal distribution, higher DOC concentrations are found in STZ and SAZ than in the PFZ and AASW zone. Unlike NO_3^- , anomalously high DOC was observed in the AASW samples of T3 near 58°S which further supports the possible subsurface water upwelling in the region. Another high DOC concentration is found in the Prydz Bay samples where an allochthonous supply of organic matter from the adjacent ice-free regions (Larsemann Hill and Vestfold Hill) and/or potential upwelling of subsurface waters could be responsible factors (Nunes Vaz and Lennon, 1996; Anilkumar *et al.*, 2010; Liu *et al.*, 2018; Guo *et al.*, 2019).

5.3.2 Dissolved Barium (Ba_d) distributions in Surface Ocean and controlling factors

Ba_d measured in the seawater samples of INSO ranges from 45-90 nmol kg^{-1} (Figure 5.4) which overprint hydrodynamics of the region identical to previously reported studies (Jeandel *et al.*, 1996). The latitudinal variation of Ba_d shows strong

frontal control and demarcates the major fronts up to $\sim 50^{\circ}\text{S}$. Further south, regional upwelling, continental supply through chemical weathering of Antarctica, and biogeochemical processes such as barite precipitation and/or biological uptake are important controlling factors responsible for Ba_d distribution in the INSO. The individual factors and their regional extent are discussed in the following sections.

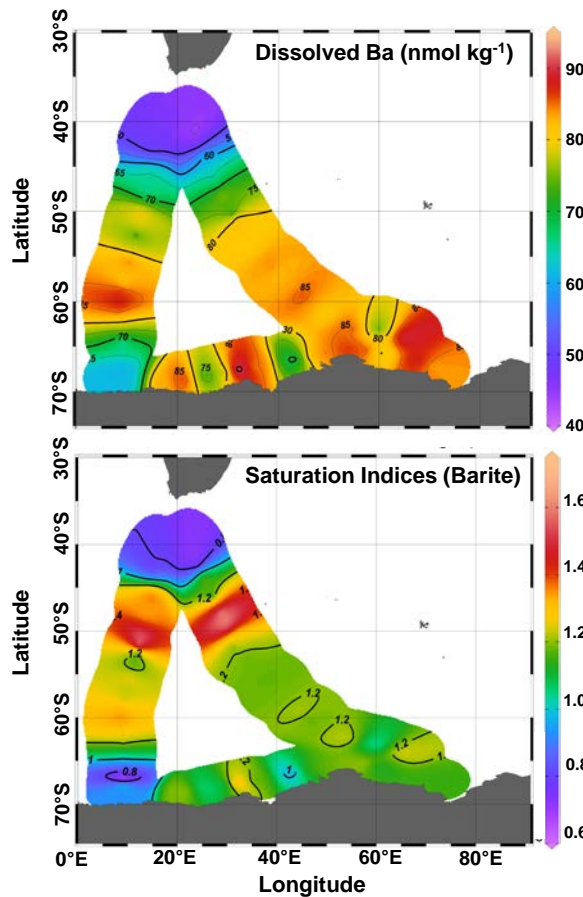


Figure 5.4. Distribution of the Ba_d in the sampling region of the Indian sector of the Southern Ocean representing the frontal (North of the 50°S) and non-frontal control (South of the 50°S).

Physical mixing across the fronts

The distribution pattern of the Ba_d follows the SST and SSS variations (Figure 5.4). The strong correlation of Ba_d with physical parameters (SST and SSS; Figure 5.5) indicates the role of the hydrodynamics in controlling the surface Barium distribution in the INSO. The Ba_d shows an inverse relation with physical parameters (SST and SSS) (Figure 5.5) with higher Ba_d in cold AASW than the warm SAZ and STZ waters.

In the open ocean waters, SST influences the dissolution kinetics and precipitation mechanism of Barite (Zhen-Wu *et al.*, 2016) such as the warm waters (STZ) foster Barite precipitation at a higher rate compared to cold waters (AASW). The Barite precipitation mechanisms remove the Ba_d from the surface waters which upon association with the decaying organic matters, exports to the intermediate depths (Gonzalez-Muñoz *et al.*, 2012).

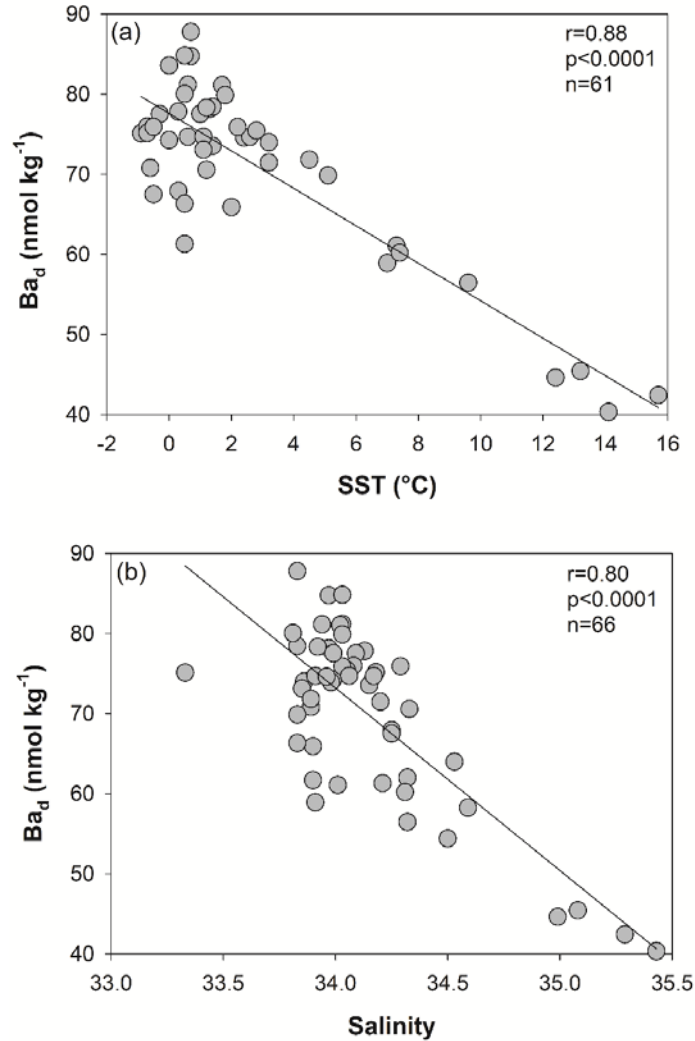


Figure 5.5. Inverse correlation observed between physical parameters (Salinity and SST) and dissolved Barium (Ba_d) indicates the control of the physical characteristics on Ba_d cycling in the INSO.

The inverse relation of Ba_d with the SSS (Figure 5.5) indicates non-conservative behaviour in the surface water resulting from the mixing of multiple water masses (endmembers) separated by frontal boundaries. The control of the frontal distribution

on the Ba_d distribution in the Southern Ocean is also reported in previous studies (Jeandel *et al.*, 1996; Pyle *et al.*, 2018). The potential gradients of SST and SSS demarcate the frontal locations in the INSO, thus a combination of these two physical parameters indicates the dominant role of frontal variations (physical mixing) in controlling the Ba_d distribution in the surface waters of INSO.

Circulation/Upwelling

Two zones of anomalously elevated Ba_d ($>80 \text{ nmol kg}^{-1}$) are observed in surface waters of INSO (Figure 5.4). These are located in the Prydz Bay region and AASW (T3, 55-60°S). Majorly, Ba_d varies between 35-50 nmol kg^{-1} which is close to the global mean ocean ($\sim 40 \text{ nmol kg}^{-1}$) (Singh *et al.*, 2013).

The Ba_d concentrations of the more than 80 nmol kg^{-1} are attributed to the excess supply through the chemical weathering processes (Dalai *et al.*, 2002) in the riverine/coastal systems, to ionic exchange processes in the estuarine/lake/lagoon system (Samanta and Dalai, 2016) and to the upwelling of the Ba_d rich subsurface waters in the open ocean systems (Pyle *et al.*, 2018). The Prydz Bay receives $\sim 16\%$ of the total freshwater melt from the East Antarctic ice sheet (Hodgson *et al.*, 2016) which could supply sufficient Ba_d produced during chemical weathering. The Prydz Bay region also acts as a potential upwelling zone, specifically, during the austral summer of 2017, a strong subsurface water upwelling is reported (Sabu *et al.*, 2021). This could bring the Ba_d rich cold subsurface waters to shallow depths and result in elevated concentrations. Thus a combined role of continental supply and subsurface water upwelling could be responsible for anomalous Ba_d in the Prydz Bay region.

Another region of the elevated Ba_d ($80\text{-}85 \text{ nmol kg}^{-1}$) is located in the open ocean along the 10°E in the samples of the T3 in the INSO (Figure 5.4). Since the contribution of continental supply is negligible, this anomaly can be solely attributed to subsurface water upwelling. It is further evident with World Ocean Atlas (WOA) data for the austral summer of the year 2017, where upwelling of nutrient-rich subsurface waters is observed in the defined section ($9\text{-}12^\circ\text{E}$; $55\text{-}60^\circ\text{S}$). In this section, the subsurface waters (200-600 m) exhibit anomalously colder water temperatures and elevated concentrations of the dissolved NO_3^- , Si(OH)_4 , and PO_4^{3-} than the

surrounding water masses (Figure 5.6) suggesting the presence of potential upwelling in the region.

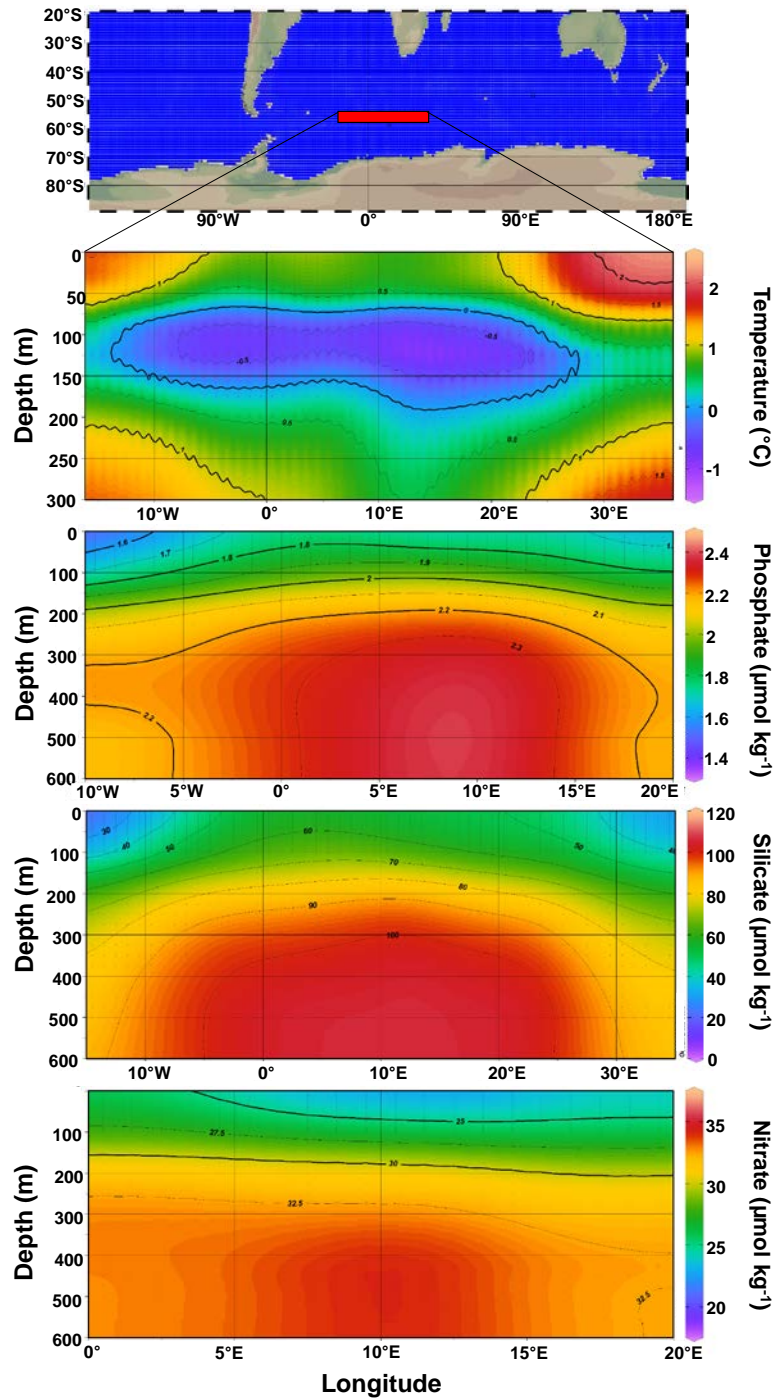


Figure 5.6. The physical (temperature) and macronutrient parameters are plotted in the section defined. This represents an upwelling zone in the highlighted region (57-59°S) along the 10°E latitudinal extent.

Although the exact mechanism of upwelling is not well understood, the bathymetry of the region indicates the presence of an extended flank of Mid Atlantic Ridge (MAR) which could act as a suitable barrier for the deep-water masses and trigger subsurface water upwelling.

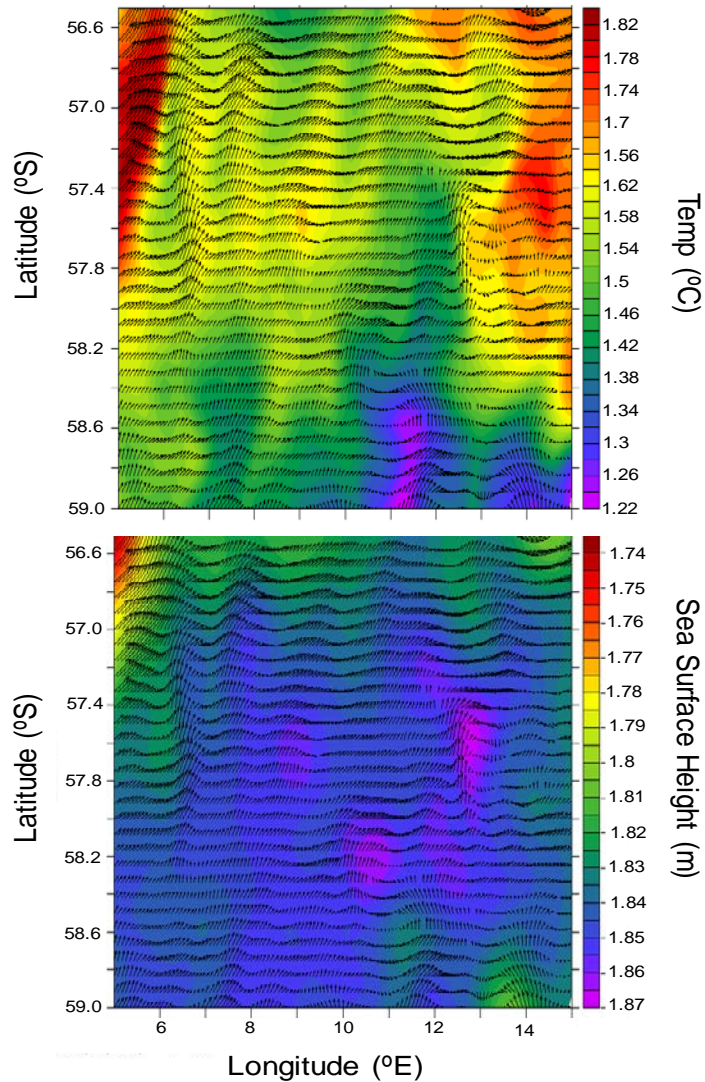


Figure 5.7. The SST shown with wind vectors represents the upwelling region in the sampling transect-3 near the 10°E in the Southern latitudes **(b)** The mesoscale sea-surface height of the region are shown along with the North and East wind vectors in the upwelling region.

We have also analysed the WOA data of Sea surface height (SSH) with the resolved wind vector and SST (Figure 5.7). Mesoscale eddies observed with the counter-clockwise rotation support the presence of active upwelling in the region and

sometimes reflect the bathymetry of the region (Ridgway and Dunn, 2003). However, the exact mechanism of formation of these eddies and their link to the bathymetry could not be confirmed. In the subsurface upwelling regions, regenerated Ba_d at intermediate depths when associated with the decomposed organic matter/carbon, upwells at the surface (Dymond *et al.*, 1992; Cardinal *et al.*, 2005).

The anomalously high DOC concentrations are also measured in the surface samples from this region. Thus upwelling of these intermediate waters brings Ba_d to the surface waters which eventually elevates the surface concentrations. The role of the organic matter as the carrier is still not well understood and needs to be investigated using various isotopic analyses of the dissolved, particulate, and ocean bottom sediments which would reveal the association of the dissolved and particulate Barium with organic aggregates and their role in the Barium biogeochemistry.

Role of biogeochemical processes

The Ba_d distribution in the water column of the global ocean depicts a similar variation as the silica profile (Jeandel *et al.*, 1996). Surface removal followed by enrichment at intermediate depths is responsible for their identical variation in the ocean water column (Jeandel *et al.*, 1996; Rubin *et al.*, 2003). The positive $Si(OH)_4 - Ba_d$ covariation has been reported for the water column below 200 meters (Jacquet *et al.*, 2005, 2007). In the surface waters, it shows potential deviation from the established linear correlation (Pyle *et al.*, 2018). Unlike $Si(OH)_4$, direct metabolic uptake of Ba_d is unknown (Sternberg *et al.*, 2005). In the surface waters of INSO, the $Si(OH)_4/Ba_d$ regression line shows an exponential relation (Figure 5.8) which supports the previously reported trend (Jeandel *et al.*, 1996). The possible reason for the deviation could be the difference in the dominant controlling factors of Ba_d and $Si(OH)_4$. The difference in the magnitude of the biological requirement of $Si(OH)_4$ and Ba_d could also result in the deviation from the ideal $Si(OH)_4/Ba_d$ regression.

Another important process that regulates the Ba_d variation is Barite ($BaSO_4$) precipitation which could be responsible for the observed deviation from the ideal $Si(OH)_4-Ba$ correlation. Barite forms in the seawaters upon supersaturation of the Ba and/or SO_4^{2-} which is further exported to deeper conditions when associated with the

decaying organic matter/ biogenic debris (Gonzalez-Muñoz *et al.*, 2012). It affects the overall Barium biogeochemistry of the ocean water column. Majorly the Barite formation and precipitation do not necessarily require the supersaturation state of the Ba_d and/or SO_4^{2-} and are often mediated through the bacterioplankton in the Ba_d rich microenvironments. However, the exact mechanism is still unknown. The potential of Barite formation in the surface waters is estimated through the saturation indices (SI) which depend on the ionic concentrations and physicochemical conditions (Jeandel *et al.*, 1996).

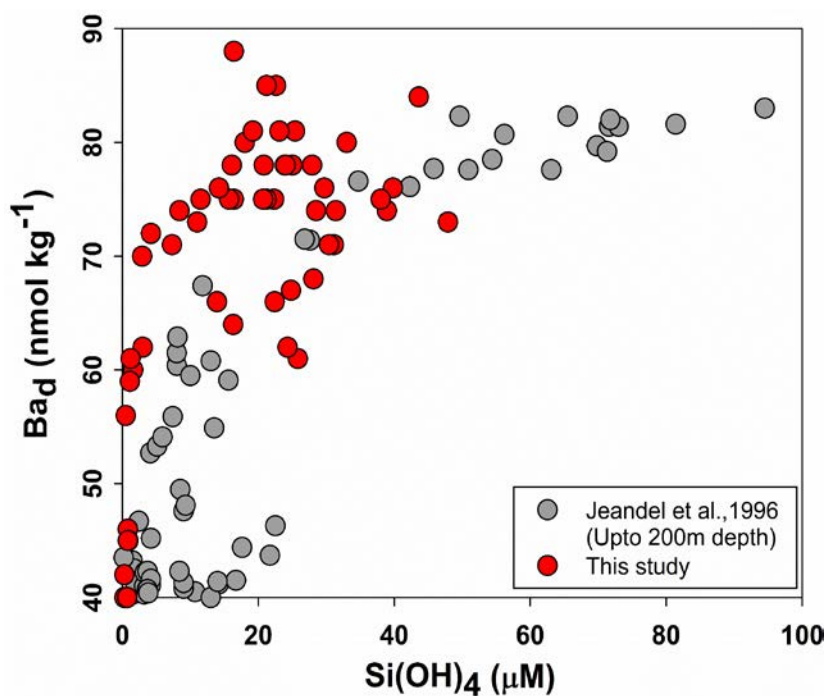


Figure 5.8. Correlation of the dissolved Barium with the dissolved silica showing the deviation from the linear regression (exponential correlation)

The estimated SI for Barite in surface waters of the INSO varies from 0.6-1.75 (Table 5.1; Figure 5.4) which suggests the control of widely varying biogeochemical processes. Most of the samples located in the STZ waters show undersaturated conditions whereas, in the SAZ, the SI reaches up to 1.50 i.e supersaturated state of Ba_d . This anomalous change in the Barite SI indicates the influence of a steep SST gradient located near frontal demarcations. In the PFZ and AASW, the SI varies between 1.1-1.25 i.e. the saturated conditions. Another anomalous zone of the undersaturated SI (<0.8) is found in the samples from transect T3 in the AASW (Figure

5.4). This could be due to the lower Barium supply or potential deep water formation in the region. However, the exact mechanism of the lower SI in coastal Antarctica is unknown.

Samples from coastal transect T2 also show slightly under saturated conditions suggesting the balance between the Ba_d supply and uptake/export. The lower supply of the Ba_d through the chemical weathering processes in a few selective regions around coastal Antarctica could be responsible for the low SI. Since, in the Antarctic continental regions, a significant portion of the dissolved barium which is generated through chemical weathering is precipitated in the Antarctic streams due to the high diurnal temperature fluctuations (Saelens *et al.*, 2018; Nuruzzama *et al.*, 2021). Thus a combination of differences in biological uptake ratio ($Si(OH)_4/Ba_d$), Barite precipitation, and continental supply/upwelling are responsible for the deviation from ideal $Si(OH)_4$ - Ba_d covariation.

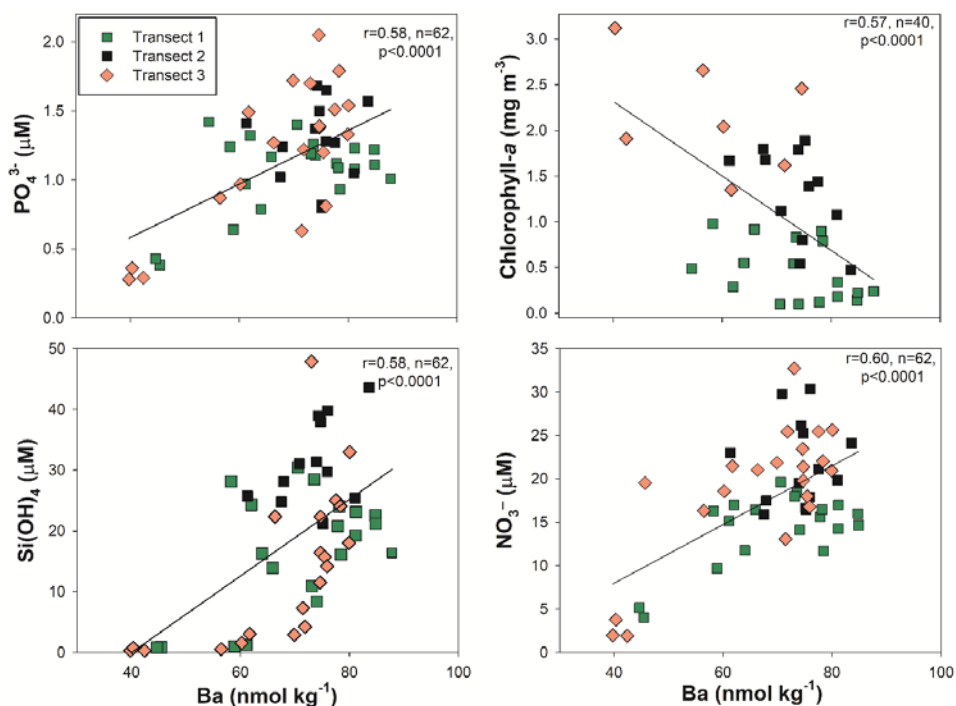


Figure 5.9. Co-variation of the seawater Barium with the physicochemical parameters in the Southern Ocean surface water samples.

The direct metabolic uptake of the Ba_d by photoautotrophs is not known (Sternberg *et al.*, 2005), however, association with the dissolved PO_4^{3-} is often

observed in the oceanic systems. The Ba_d binding to PO_4^{3-} groups on bacteria cells and Extracellular Polymeric Substances (EPS) locally increases Ba concentrations, followed by replacement of PO_4^{3-} by SO_4^{2-} from seawater and barite crystal nucleation and growth (Gonzalez-Muñoz *et al.*, 2012). Thus Ba_d association with the $Si(OH)_4$ and PO_4^{3-} could influence primary productivity indirectly. A significant positive linear correlation of Ba_d with PO_4^{3-} (Figure 5.9) and an inverse correlation with the chlorophyll-*a* concentration has been observed (Figure 5.9). This indicates the non-involvement of the Ba_d in the direct biological uptake processes. Thus the role of Ba_d in the primary productivity of surface waters of INSO is ruled out although bacterial-mediated bio-mineralization of the Barite controlling the Ba_d is active and play important role in the Barium biogeochemical cycling in the region.

5.3.3 Nutrient utilization, silica biogeochemical cycling, and Ba-Si(OH)₄ in the Antarctic surface waters (AASW)

The highest silica fractionation occur in the uppermost oceanic layer i.e. the euphotic zone where silica uptake processes occur by the siliceous organisms (Cao *et al.*, 2012; de Souza *et al.*, 2012b; Fripiat *et al.*, 2007). Two main types of high Si fractionation signature ($>3.0\%$) are characteristics of the surface ocean; the ultra-oligotrophic waters where the $Si(OH)_4$ are below 1 μM (Reynolds *et al.*, 2006) and the upwelling zones where $Si(OH)_4$ concentrations vary between 2-13 μM (Fripiat *et al.*, 2007; Varela *et al.*, 2004). The values observed in the samples measured in the surface waters of INSO show a variation between +1.74 to +3.2% indicating a variety of the processes operating to control the silica cycling in the region (Table 5.2). Samples show a signature of the highly fractionated characteristics which suggests the combination of the deep water upwelling and biological uptake.

Overall, the nutrient utilization dominantly controls the silica cycling in the AASW, as a clear correlation between the $Si(OH)_4$ and $\delta^{30}Si$ has been observed (Figure 5.10). The highly enriched seawater sample from the Prydz Bay region ($Si(OH)_4 = 6.7 \mu M$) suggests a combination of the deep water upwelling and biological uptake in the region.

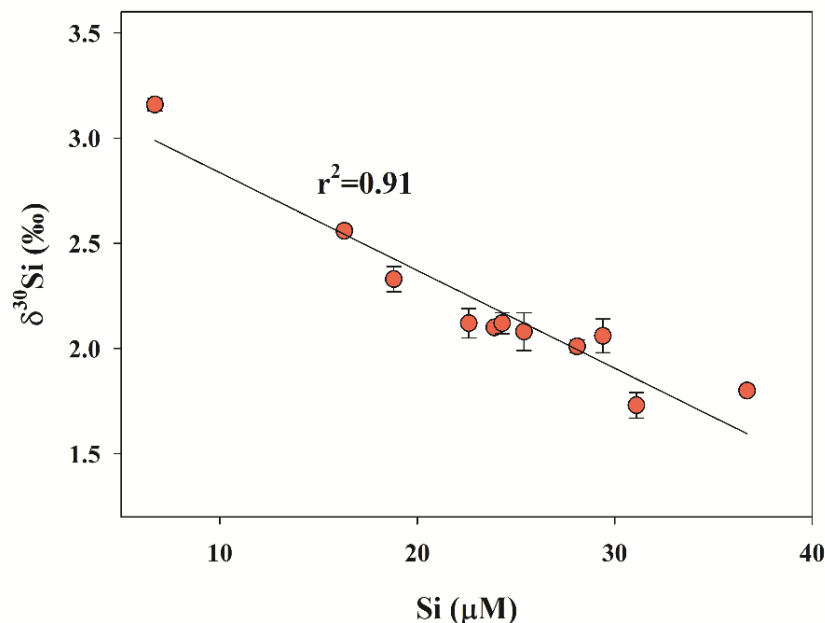


Figure 5.10. Covariation between Si and $\delta^{30}\text{Si}$ in the Antarctic surface waters (AASW) indicating nutrient utilization in the region.

However, further evidence such as anomalous dissolved Ba (Figure 5.4), and macronutrients (Figure 5.2) suggests the Prydz Bay region as the potential zone for deep water upwelling. Based on the $\delta^{30}\text{Si}$, Ba and anomalous nutrient characteristics shown by the Prydz Bay region confirms it as a potential deep water upwelling region. The elevated signature of $\delta^{30}\text{Si}$ (2.09 ± 43 ‰; $n=10$) with high $\text{Si}(\text{OH})_4$ throughout the AASW than the global surface seawaters (less than 2‰) (Cassarino et al., 2017; De La Rocha et al., 2011) lead to formation of relatively silica rich subsurface waters. The high fractionation of Si in the AASW results in the stripping of $\text{Si}(\text{OH})_4$ from surface waters and the formation of the Antarctic Intermediate waters (AAIW) and Sub Antarctic Mode waters (SAMW) with relatively high $\delta^{30}\text{Si}(\text{OH})_4$ characteristics (de Souza et al., 2012b; de Souza et al., 2015). The term “Southern Ocean Isotope distillation” explain this phenomenon for the formation of AAIW and SAMW and Silica depletion from the surface waters (Brzezinski and Jones, 2015). This phenomenon of high $\delta^{30}\text{Si}$ fractionation of AASW and transfer of these signatures to the AAIW and SAMW export to the surface seawaters via upwelling on a global scale specially to the silica poor low latitude regions, making this an important

biogeochemical process and contribute to the global silica and carbon budget. The influence of Southern Ocean surface waters signatures however does not reach the North Pacific Ocean where major silica inventory is derived from upwelling in the subarctic pacific (Beucher et al., 2007; Beucher et al., 2008; Reynolds, 2009). These findings support the earlier mechanisms proposed for the high fractionation in the silica-sufficient surface ocean systems and its contribution to the global silica pool (De La Rocha et al., 2011; de Souza et al., 2012b; Ehlert et al., 2012).

Biogeochemical cycling of Si(OH)_4 and Ba are coherent throughout the global ocean although the existing mechanism does not completely explain their co-varying behaviour (Jeandel et al., 1996, 2000). The Ba- Si(OH)_4 relation was observed throughout the Southern Ocean which indicates their possible close association with common controlling factors. The results obtained through the $\delta^{30}\text{Si(OH)}_4$ measurements in the AASW primarily indicate the dominance of nutrient utilization in the region. However, the variability of the Barium in the AASW and comparison with the $\delta^{30}\text{Si}$ datasets show insignificant participation to the biogeochemical cycling of silica in polar waters.

5.4 Summary and Conclusion

Based on obtained results and interpretations on Silica and Barium biogeochemistry and its covariation with the dissolved macronutrients and biological parameters in the surface waters of the INSO, the important findings and constraints are summarised below;

1. The surface latitudinal variation of Ba_d shows strong gradients along the major fronts in the INSO. The water mass changes along these fronts could be the dominant controlling factor for Ba_d variability. The strong $\text{Ba}_d\text{-PO}_4^{3-}$ correlation indicates the role of bio-mineralization in Barium cycling where the PO_4^{3-} is replaced with seawater SO_4^{2-} and induces the Barite precipitation

3. Two anomalously high Ba_d regions are observed in the AASW, one along 10°E and another in the Prydz Bay region. Subsurface water upwelling in which Ba_d transports with organic matters/biogenic debris are identified as a potential carrier to

surface waters. Thus the elevated Ba_d zones in the open ocean can be identified as upwelling regions. These findings will help to better interpret paleoclimate records of Barium in the Southern Ocean with region-specific processes.

4. The biological uptake of macronutrients ($Si(OH)_4$, NO_3^- , PO_4^{3-}) varies along the PF where the samples from the STZ and SAZ show an order lower concentrations than PFZ and AASW, suggesting the potential difference in the ecological niche between two zones. Intra-seasonal heterogeneities also affect the macronutrient cycling in the Southern Ocean.

5. Relative nutrient utilization in the sampling region of the INSO estimated using N^* . Optimum utilization of the macronutrients (N^* close to zero) is observed in the coastal Antarctic samples whereas unutilized conditions prevail during peak summer and macronutrient limiting conditions during late austral summer. The identified upwelling zones show elevated macronutrient concentrations except for NO_3 which could be due to the localized denitrification induced by the elevated DOC supply from the subsurface. However, the exact mechanism of the diminished nitrate in the upwelling region is unknown.

6. The $\delta^{30}Si$ values obtained from the AASW shows highly fractionated signatures. High nutrient utilization by the siliceous organisms pose dominant factor in these elevated $\delta^{30}Si$ samples from AASW. The findings support the 'Southern Ocean Silicon isotope distillation' which is supposed to be responsible for the supply of polar silica nutrients to the global surface waters. Another important factor that controlled the $\delta^{30}Si$ characteristics in the surface waters of Prydz Bay is the deep water upwelling which confirmed Prydz Bay as a potential upwelling zone. Additionally, the $\delta^{30}Si$ variation show insignificant relation with the Ba_d in the AASW and depict the absence of the role of Ba_d in the direct biological utilization along with $Si(OH)_4$.

Chapter-6

Conclusion and future perspectives

This thesis was designed aiming to fill the research gap about what type of factors control lake water chemistry in the coastal Antarctic region, and the behaviour of the silica and Barium in the Indian sector of the Southern Ocean which in turn make these regions as a potential CO₂ sink. Addressing these research questions, we have investigated the biogeochemical (major ions, nutrients, trace metals, Ba, Chlorophyll-*a*, DOC) and isotopic composition ($^{87}\text{Sr}/^{86}\text{Sr}$ and $\delta^{30}\text{Si}$) of these polar regimes during austral summer (January- April) of the year 2017. In addition to dissolved components, the sediments from lake catchments and lake bottom were also investigated as they pose sink to various trace metals and major nutrients. The geochemical characterization of sedimentary components along with dissolved solutes reveals the unique processes of barium attenuation and cycling in Antarctica. Utilizing these datasets, we were able to identify the major ongoing biogeochemical processes controlling lake water chemistry as chemical weathering, seasalt spray, biological consumption, inorganic attenuation, and bacterial mediated decomposition. Whereas, major processes controlling dissolved Barium and silica biogeochemistry in the surface waters of the Indian sector of Southern Ocean were identified as frontal migration, nutrient utilization, and deep water upwelling to surface waters.

6.1 Source identification, apportionment, estimation of silicate weathering and CO₂ consumption rates using Sr isotopic approach:

Dissolved major ions, Sr and $^{87}\text{Sr}/^{86}\text{Sr}$ in the freshwater lakes of Antarctica have been investigated to decipher solute sources, and estimate the rate of glacial-induced chemical weathering in their catchments. The $^{87}\text{Sr}/^{86}\text{Sr}$ of these lake waters is close to global seawater and Antarctica snows, indicating a dominant role of seawater and snow precipitation in regulating the solute chemistry. Results of inverse modelling show that the cations are dominantly supplied from oceanic sources ($80 \pm 5\%$), with less but significant contribution from weathering of carbonates and silicates (together contributing $20 \pm 10\%$). Computations of the results from the inverse model yielded SWR of 1.4 ± 0.1 mm/yr which is lower than the global average (2.08 mm/yr). Our estimate of SWR and corresponding CO₂ consumption rates are slightly lower (~ 0.6

times) that of the global average reported for the global river basins. Though chemical weathering is lower, considering vast regions of Antarctica that went through glacial waxing and waning in areal coverage; for example exposure of large ice-free regions during the last interglacial and mid-Pliocene warm periods. This could be a potential region for silicate weathering and atmospheric CO₂ consumptions, unaccounted so far in the global estimates and hence could be a source of uncertainty.

6.2 Trace metal biogeochemistry in the freshwater lakes of Antarctica:

Detailed spatial water column distributions of selected dissolved trace elements, nutrients, and biological parameters (Chlorophyll a and DOC) have been investigated to infer their behaviour and controlling factors in the freshwater lakes of the Larsemann Hills, East Antarctica. Sea-salt spray together with chemical weathering of the catchment rocks are the dominant sources of trace elements and nutrients to the LH lakes. Dissolved PO₄ and Mo play a significant role in biological productivity and act as limiting nutrients in most of the LH lakes. DOC in the LH lakes shows a significant positive correlation ($r=0.79$, $n=23$, $p<0.001$) with dissolved Cu and therefore indicates their close association of the processes occurring in the water column. Bacterial-mediated organic matter decomposition is evident in these lakes. Such bacterial activity is found to be controlled by dissolved Cu concentration in these lakes. Assessment of Ba in bulk sediments from the lakes and their catchments sediments show excess Ba up to 20-63%. This Ba excess could be either due to biologically induced precipitations of Ba hosting minerals or inorganic precipitations in the catchment sediments and later transported to these lakes. However, biological-induced barite precipitation in the lakes is still unclear and could be scope for future investigations. Geochemical data does not show any detectable evidence of anthropogenic influence. Therefore, these data sets could provide baseline information to investigate and assess anthropogenic stress in the global aquatic system.

6.3 Barium, dissolved silica and silicon isotope study in the surface waters of the Indian sector of the Southern Ocean:

Barium concentration and silicon isotope compositions of the surface waters of the Indian sector of the Southern Ocean (INSO) and its driving factors have been investigated for the austral summer of the year 2017. The surface latitudinal variation of Ba_d shows strong gradients along the major fronts throughout INSO which infer that the water mass changes along these fronts could act as a dominant controlling factor for Ba_d variability. The estimated Barite saturation indices for water samples indicate that Barite precipitation through biological and/or inorganic means also control the Barium cycling in the region however the exact role of the biological processes in the barite precipitation is not much revealed. Two anomalously high Ba_d regions are observed in the AASW, one along 10°E and another in the Prydz Bay region. Subsurface water upwelling in which Ba_d transports with organic matters/biogenic debris are identified as a potential carrier. Thus the elevated Ba_d zones in the open ocean can be identified as upwelling regions. The biological uptake of macronutrients ($Si(OH)_4$, NO_3^- , PO_4^{3-}) vary along the PF where the samples from the STZ and SAZ show an order lower concentrations than PFZ and AASW, suggesting the potential difference in the ecological niche between two zones. The values obtained for $\delta^{30}Si$ in the Antarctic surface waters (AASW) vary from +1.74 to +3.2 ‰ suggesting variable factors controlling nutrient utilization. The higher $\delta^{30}Si$ values observed for samples with lower $Si(OH)_4$ concentrations indicate higher nutrient utilization. The co-variation between Ba - $Si(OH)_4$ further rules out the direct involvement of the Ba_d in the nutrient utilization in the surface waters of the Southern Ocean, particularly the AASW. Intra-seasonal heterogeneities also affect the macronutrient cycling in the Southern Ocean. Relative nutrient utilization in the sampling region of the INSO is estimated using N^* and $\delta^{30}Si$. Optimum utilization of the macronutrients (N^* close to zero with low $\delta^{30}Si$) is observed in the AASW whereas unutilized conditions prevail during peak summer and macronutrient limiting conditions during late austral summer. The identified upwelling zones show elevated macronutrient concentrations except for NO_3 which

could be due to the localized denitrification induced by the elevated DOC supply from the subsurface.

6.4 Future directions

Detailed investigation of the selected trace elements, isotopes, and biological parameters analyzed in this study has led us to characterize and quantify the sources and their contribution to the dissolved solutes in the Antarctic lakes and the factor controlling Barium-Silica biogeochemistry in the surface water of Indian sector of Southern Ocean. In the course of conducting this thesis work, we realized that there exists future scope of research on the following few key aspects.

1. The estimation of sources and their apportionment using Sr isotope approach led us to quantify the rates of chemical weathering and corresponding CO₂ consumption in Antarctic environments. Following the estimated silicate weathering rates, the silica attenuation during transport poses an important factor in the silica deficient lacustrine environments, as ~95% of the total silica generated due to chemical weathering of rocks is removed during the transport. However, the mechanism of the silica removal in the lake catchments is still unknown and requires further investigation focusing on water-rock interaction in the catchments (surface and subglacial) to reveal these unique processes in Antarctica.
2. This thesis work reveals the role of dissolved Mo as nutrient limiting trace metal in freshwater lakes of Antarctica and inorganic attenuation of Barium in the lake catchments. These observations led us to propose that dissolved Mo actively participate in the biological cycling in the oligotrophic conditions and hence can be utilized for the paleo-productivity interpretations in addition to their redox-sensitive character. This nutrient-limiting characteristic of dissolved Mo in the ultra-oligotrophic environments should be investigated in different polar environments to assess its wider applications. The unique behavior observed for Barium should also be investigated using the Barium isotope approach to reveal the mechanism for their attenuation i.e., control of diurnal temperature fluctuation vs biological induced attenuation.
3. Frontal controlled Barium distribution in the top surface waters of the Southern Ocean has been observed in this and earlier studies. The Barium-Silica enigma still exists as

well. The attempt to understand this enigma through the $\delta^{30}\text{Si}$ datasets rules out their direct relation to the relative nutrient utilization and phytoplankton productivity. Although further attempts require using multi-tracer studies in the Southern Ocean to untangle this tangled Ba-Si(OH)₄ relationship.

7 Bibliography

- Anderson, S.P., Drever, J.I., Humphrey, N.F., 1997. Chemical weathering in glacial environments. *Geology* 25, 399-405.
- Angino, E.E., Armitage, K.B., 1963. A geochemical study of lakes Bonney and Vanda, Victoria land, Antarctica *The Journal of Geology* 71, 89-95.
- Arteaga, L.A., Pahlow, M., Bushinsky, S.M., Sarmiento, J.L., 2019. Nutrient Controls on Export Production in the Southern Ocean. *Global Biogeochemical Cycles* 33, 942-956.
- Baines, S.B., Twining, B.S., Brzezinski, M.A., Nelson, D.M., Fisher, N.S., 2010. Causes and biogeochemical implications of regional differences in silicification of marine diatoms. *Global Biogeochemical Cycles* 24, GB4031.
- Bajerski, F., Wagner, D., 2013. Bacterial succession in Antarctic soils of two glacier forefields on Larsemann Hills, East Antarctica. *FEMS Microbiology Ecology* 85, 128-142.
- Basu, S., Mackey, K.R.M., 2018. Phytoplankton as Key Mediators of the Biological Carbon Pump: Their Responses to a Changing Climate. *Sustainability* 10, 869.
- Bein, A., Arad, A., 1992. Formation of saline groundwaters in the Baltic region through freezing of seawater during glacial periods. *Journal of Hydrology* 140, 75-87.
- Beucher, C.P., Brzezinski, M.A., Crosta, X., 2007. Silicic acid dynamics in the glacial sub-Antarctic: Implications for the silicic acid leakage hypothesis. *Global Biogeochemical Cycles* 21, GB3015.
- Beucher, C.P., Brzezinski, M.A., Jones, J.L., 2008. Sources and biological fractionation of Silicon isotopes in the Eastern Equatorial Pacific. *Geochimica et Cosmochimica Acta* 72, 3063-3073.
- Bickle, M.J., Chapman, H.J., Bunbury, J., Harris, N.B.W., Fairchild, I.J., Ahmad, T., Pomiès, C., 2005. Relative contributions of silicate and carbonate rocks to

riverine Sr fluxes in the headwaters of the Ganges. *Geochimica et Cosmochimica Acta* 69, 2221-2240.

- Blain, S., Queguiner, B., Armand, L., Belviso, S., Bombled, B., Bopp, L., Bowie, A., Brunet, C., Brussaard, C., Carlotti, F., Christaki, U., Corbiere, A., Durand, I., Ebersbach, F., Fuda, J.L., Garcia, N., Gerringa, L., Griffiths, B., Guigue, C., Guillerm, C., Jacquet, S., Jeandel, C., Laan, P., Lefevre, D., Lo Monaco, C., Malits, A., Mosseri, J., Obernosterer, I., Park, Y.H., Picheral, M., Pondaven, P., Remenyi, T., Sandroni, V., Sarthou, G., Savoye, N., Scouarnec, L., Souhaut, M., Thuiller, D., Timmermans, K., Trull, T., Uitz, J., van Beek, P., Veldhuis, M., Vincent, D., Viollier, E., Vong, L., Wagener, T., 2007. Effect of natural iron fertilization on carbon sequestration in the Southern Ocean. *Nature* 446, 1070-1074.
- Bonnand, P., Parkinson, I.J., Anand, M., 2016. Mass dependent fractionation of stable chromium isotopes in mare basalts: Implications for the formation and the differentiation of the Moon. *Geochimica et Cosmochimica Acta* 175, 208-221.
- Brand, L.E., Sunda, W.G., Guillard, R.R., 1986. Reduction of marine phytoplankton reproduction rates by copper and cadmium. *J. Exp. Mar. Biol. Ecol.* 96, 225-250.
- Brand, L.E., Sunda, W.G., Guillard, R.R.L., 1983. Limitation of marine phytoplankton reproductive rates by zinc, manganese, and iron¹. *Limnology and Oceanography* 28, 1182-1198.
- Brennan, S.R., Fernandez, D.P., Mackey, G., Cerling, T.E., Bataille, C.P., Bowen, G.J., Wooller, M.J., 2014. Strontium isotope variation and carbonate versus silicate weathering in rivers from across Alaska: Implications for provenance studies. *Chemical Geology* 389, 167-181.
- Bruland, K.W., Franks, R.P., 1983. Mn, Ni, Cu, Zn and Cd in the Western North Atlantic. In: Wong C.S., Boyle E., Bruland K.W., Burton J.D., Goldberg E.D. (eds) *Trace Metals in Sea Water*. NATO Conference Series (IV Marine Sciences), vol 9. Springer, Boston, MA.

- Buesseler, K.O., 1998. The decoupling of production and particulate export in the surface ocean. *Global Biogeochemical Cycles* 12, 297-310.
- Burton, H.R., 1981. Chemistry, physics and evolution of Antarctic saline lakes. *Hydrobiologia* 82, 339-362.
- Campbell, A.L., Mangan, S., Ellis, R.P., Lewis, C., 2014. Ocean Acidification Increases Copper Toxicity to the Early Life History Stages of the Polychaete *Arenicola marina* in Artificial Seawater. *Environmental Science & Technology* 48, 9745-9753.
- Campbell, D.H., Clow, D.W., Ingersoll, G.P., Mast, M.A., Spahr, N.E., Turk, J.T., 1995. Processes controlling the chemistry of two snowmelt-dominated streams in the Rocky Mountains. *Water Resource Research* 31, 2811-2282.
- Cao, Z., Frank, M., Dai, M., Grasse, P., Ehlert, C., 2012. Silicon isotope constraints on sources and utilization of silicic acid in the northern South China Sea. *Geochimica et Cosmochimica Acta* 97, 88-104.
- Cardinal, D., Alleman, L.Y., de Jong, J., Ziegler, K., André, L., 2003. Isotopic composition of silicon measured by multicollector plasma source mass spectrometry in dry plasma mode. *Journal of Analytical Atomic Spectrometry* 18, 213-218.
- Cardinal, D., Alleman, L.Y., Dehairs, F., Savoye, N., Trull, T.W., André, L., 2005. Relevance of silicon isotopes to Si-nutrient utilization and Si-source assessment in Antarctic waters. *Global Biogeochemical Cycles* 19, n/a-n/a.
- Carpenter, J.H., Manella, M.E., 1973. Magnesium to chlorinity ratios in seawater. *Journal of Geophysical Research* 78, 3621-3626.
- Carson, C., Dirks, P.H.G.M., Hand, M.P., Sims, J.P., Wilson, C.J.L., 1995. Compressional and extensional tectonics in low-medium pressure granulites from the Larsemann Hills, East Antarctica. *Geological Magazine* 132, 151-170.
- Cassarino, L., Hendry, K.R., Meredith, M.P., Venables, H.J., De La Rocha, C.L., 2017. Silicon isotope and silicic acid uptake in surface waters of Marguerite Bay, West Antarctic Peninsula. *Deep Sea Research Part II: Topical Studies in Oceanography* 139, 143-150.

- Castrillejo, M., Statham, P.J., Fones, G.R., Planquette, H., Idrus, F., Roberts, K., 2013. Dissolved trace metals (Ni, Zn, Co, Cd, Pb, Al, and Mn) around the Crozet Islands, Southern Ocean. *Journal of Geophysical Research: Oceans* 118, 5188-5201.
- Chan, L.H., Edmond, J.M., Stallard, R.F., Broecker, W.S., Chung, Y.C., Weiss, R.F., Ku, T.L., 1976. Radium and barium at GEOSECS stations in the Atlantic and Pacific. *Earth and Planetary Science Letters* 32, 258-267.
- Chisholm, S.W., 2000. Stirring times in the Southern Ocean. *Nature* 407, 685-686.
- Cid, A.P., Urushihara, S., Minami, T., Norisuye, K., Sohrin, Y., 2011. Stoichiometry among bioactive trace metals in seawater on the Bering Sea shelf. *Journal of Oceanography* 67, 747-764.
- Conley, D.J., 2002. Terrestrial ecosystems and the global biogeochemical silica cycle. *Global Biogeochemical Cycles* 16, 68-61-68-68.
- Conley, D.J., Carey, J.C., 2015. Biogeochemistry: Silica cycling over geologic time. *Nature Geoscience* 8, 431-432.
- Culkin, F., Cox, R.A., 1966. Sodium, potassium, magnesium, calcium and strontium in sea water. *Deep-Sea Research* 13.
- Cuozzo, N., Sletten, R.S., Hu, Y., Liu, L., Teng, F.-Z., Hagedorn, B., 2020. Silicate weathering in antarctic ice-rich permafrost: Insights using magnesium isotopes. *Geochimica et Cosmochimica Acta* 278, 244-260.
- Cutter, G.A., Cutter, L.S., Featherstone, A.M., Lohrenz, S.E., 2001. Antimony and arsenic biogeochemistry in the western Atlantic Ocean. *Deep-Sea Research II* 48, 2895-2915.
- Dalai, T.K., Krishnaswami, S., Sarin, M.M., 2002. Major ion chemistry in the headwaters of the Yamuna river system: Chemical weathering, its temperature dependence and CO₂ consumption in the Himalaya. *Geochimica et Cosmochimica Acta* 66, 3397-3416.
- Danielsson, L.-G., Magnusson, B., Westerlund, S., 1985. Cadmium, copper, iron, nickel and zinc in the north-east Atlantic Ocean. *Marine Chemistry* 17, 23-41.

- De La Rocha, C.L., 2006. Opal-based isotopic proxies of paleoenvironmental conditions. *Global Biogeochemical Cycles* 20, GB4S09.
- De La Rocha, C.L., Bescont, P., Croguennoc, A., Ponzevera, E., 2011. The silicon isotopic composition of surface waters in the Atlantic and Indian sectors of the Southern Ocean. *Geochimica et Cosmochimica Acta* 75, 5283-5295.
- De La Rocha, C.L., Mark A. Brzezinski, Deniro, M.J., 2000. A first look at the distribution of the stable isotopes of silicon in natural waters. *Geochimica et Cosmochimica Acta* 64, 2467–2477.
- de Souza, G.F., Reynolds, B.C., Johnson, G.C., Bullister, J.L., Bourdon, B., 2012a. Silicon stable isotope distribution traces Southern Ocean export of Si to the eastern South Pacific thermocline. *Biogeosciences* 9, 4199-4213.
- de Souza, G.F., Reynolds, B.C., Rickli, J., Frank, M., Saito, M.A., Gerringa, L.J.A., Bourdon, B., 2012b. Southern Ocean control of silicon stable isotope distribution in the deep Atlantic Ocean. *Global Biogeochemical Cycles* 26, GB2035.
- de Souza, G.F., Slater, R.D., Dunne, J.P., Sarmiento, J.L., 2014. Deconvolving the controls on the deep ocean's silicon stable isotope distribution. *Earth and Planetary Science Letters* 398, 66-76.
- de Souza, G.F., Slater, R.D., Hain, M.P., Brzezinski, M.A., Sarmiento, J.L., 2015. Distal and proximal controls on the silicon stable isotope signature of North Atlantic Deep Water. *Earth and Planetary Science Letters* 432, 342-353.
- de Souza, G.F., Vance, D., Sieber, M., Conway, T.M., Little, S.H., 2022. Re-assessing the influence of particle-hosted sulphide precipitation on the marine cadmium cycle. *Geochimica et Cosmochimica Acta*, 322, 274-296.
- Dehairs, F., Chesselet, R., Jedwab, J., 1980. Discrete suspended particles of barite and the barium cycle in the open ocean. *Earth and Planetary Science Letters* 49, 528-550.
- Delmonte, B., Baroni, C., Andersson, P.S., Narcisi, B., Salvatore, M.C., Petit, J.R., Scarchilli, C., Frezzotti, M., Albani, S., Maggi, V., 2013. Modern and Holocene aeolian dust variability from Talos Dome (Northern Victoria

- Land) to the interior of the Antarctic ice sheet. *Quaternary Science Reviews* 64, 76-89.
- Derry, L.A., Kurtz, A.C., Ziegler, K., Chadwick, O.A., 2005. Biological control of terrestrial silica cycling and export fluxes to watersheds. *Nature* 433, 728-731.
- Diaz, M.A., Welch, S.A., Sheets, J.M., Welch, K.A., Khan, A.L., Adams, B.J., McKnight, D.M., Cary, S.C., Lyons, W.B., 2020. Geochemistry of aeolian material from the McMurdo Dry Valleys, Antarctica: Insights into Southern Hemisphere dust sources. *Earth and Planetary Science Letters* 547, 116460.
- Dickinson, W.W., Rosen, M.R., 2003. Antarctic permafrost: An analogue for water and diagenetic minerals on Mars. *Geology* 31, 199-202.
- Dickson, J.L., Head, J.W., Levy, J.S., Marchant, D.R., 2013. Don Juan Pond, Antarctica: near-surface CaCl₂-brine feeding Earth's most saline lake and implications for Mars. *Scientific reports* 3, 1166.
- Ding, T., Wan, D., Bai, R., Zhang, Z., Shen, Y., Meng, R., 2005. Silicon isotope abundance ratios and atomic weights of NBS-28 and other reference materials. *Geochimica et Cosmochimica Acta* 69, 5487-5494.
- Donat, J.R., Lao, K.A., Bruland, K.W., 1994. Speciation of dissolved copper and nickel in South San Francisco Bay: a multi-method approach. *Analytica chimica acta* 284, 547-571.
- Drever, J.I., 1997. *The Geochemistry of Natural waters*, 3rd edition. Prentice Hall New Jersey, 215-234.
- Dymond, J., Suess, E., Lyle, M., 1992. Barium in Deep-Sea Sediment: A Geochemical Proxy for Paleoproductivity. *Paleoceanography* 7, 163-181.
- Eagle, M., Paytan, A., Arrigo, K.R., van Dijken, G., Murray, R.W., 2003. A comparison between excess barium and barite as indicators of carbon export. *Paleoceanography* 18.
- Edmond, J.M., Spivack, A., Grant, B.C., Ming-Hui, H., Zexiam, C., Sung, C., Xiushau, Z., 1985. Chemical dynamics of the Changjiang estuary. *Continental Shelf Research* 4, 17-36.

- Ehlert, C., Grasse, P., Mollier-Vogel, E., Bösch, T., Franz, J., de Souza, G.F., Reynolds, B.C., Stramma, L., Frank, M., 2012. Factors controlling the silicon isotope distribution in waters and surface sediments of the Peruvian coastal upwelling. *Geochimica et Cosmochimica Acta* 99, 128-145.
- Emerson, S.R., Husted, S.S., 1991. Ocean anoxia and the concentrations of molybdenum and vanadium in seawater. *Marine Chemistry* 34, 177-196.
- Engström, E., Rodushkin, I., Baxter, D.C., Ohlander, B., 2006. Chromatographic purification for the determination of dissolved silicon isotopic compositions in natural waters by high-resolution multicollector inductively coupled plasma mass spectrometry. *Analytical chemistry* 78, 250-257.
- Fang, L., Lee, S., Lee, S.-A., Hahm, D., Kim, G., Druffel, E.R.M., Hwang, J., 2020. Removal of Refractory Dissolved Organic Carbon in the Amundsen Sea, Antarctica. *Scientific reports* 10, 1213.
- Fisher, N.S., Guillard, R.R.L., Bankston, D.C., 1991. The accumulation of barium by marine phytoplankton grown in culture. *Journal of Marine Research* 49, 339-354.
- Fontorbe, G., De La Rocha, C.L., Chapman, H.J., Bickle, M.J., 2013. The silicon isotopic composition of the Ganges and its tributaries. *Earth and Planetary Science Letters* 381, 21-30.
- Foster, G.L., Vance, D., 2006. Negligible glacial–interglacial variation in continental chemical weathering rates. *Nature* 444, 918-921.
- Fretwell, P., Pritchard, H.D., Vaughan, D.G., Bamber, J.L., Barrand, N.E., Bell, R., Bianchi, C., Bingham, R.G., Blankenship, D.D., Casassa, G., Catania, G., Callens, D., Conway, H., Cook, A.J., Corr, H.F.J., Damaske, D., Damm, V., Ferraccioli, F., Forsberg, R., Fujita, S., Gim, Y., Gogineni, P., Griggs, J.A., Hindmarsh, R.C.A., Holmlund, P., Holt, J.W., Jacobel, R.W., Jenkins, A., Jokat, W., Jordan, T., King, E.C., Kohler, J., Krabill, W., Riger-Kusk, M., Langley, K.A., Leitchenkov, G., Leuschen, C., Luyendyk, B.P., Matsuoka, K., Mouginot, J., Nitsche, F.O., Nogi, Y., Nost, O.A., Popov, S.V., Rignot, E., Rippin, D.M., Rivera, A., Roberts, J., Ross, N.,

Siegert, M.J., Smith, A.M., Steinhage, D., Studinger, M., Sun, B., Tinto, B.K., Welch, B.C., Wilson, D., Young, D.A., Xiangbin, C., Zirizzotti, A., 2013. Bedmap2: improved ice bed, surface and thickness datasets for Antarctica. *The Cryosphere* 7, 375-393.

- Friedlingstein, P., Jones, M.W., O'Sullivan, M., Andrew, R.M., Hauck, J., Peters, G.P., Peters, W., Pongratz, J., Sitch, S., Le Quéré, C., Bakker, D.C.E., Canadell, J.G., Ciais, P., Jackson, R.B., Anthoni, P., Barbero, L., Bastos, A., Bastrikov, V., Becker, M., Bopp, L., Buitenhuis, E., Chandra, N., Chevallier, F., Chini, L.P., Currie, K.I., Feely, R.A., Gehlen, M., Gilfillan, D., Gkritzalis, T., Goll, D.S., Gruber, N., Gutekunst, S., Harris, I., Haverd, V., Houghton, R.A., Hurtt, G., Ilyina, T., Jain, A.K., Joetzjer, E., Kaplan, J.O., Kato, E., Klein Goldewijk, K., Korsbakken, J.I., Landschützer, P., Lauvset, S.K., Lefèvre, N., Lenton, A., Lienert, S., Lombardozzi, D., Marland, G., McGuire, P.C., Melton, J.R., Metzl, N., Munro, D.R., Nabel, J.E.M.S., Nakaoka, S.I., Neill, C., Omar, A.M., Ono, T., Peregón, A., Pierrot, D., Poulter, B., Rehder, G., Resplandy, L., Robertson, E., Rödenbeck, C., Séférian, R., Schwinger, J., Smith, N., Tans, P.P., Tian, H., Tilbrook, B., Tubiello, F.N., van der Werf, G.R., Wiltshire, A.J., Zaehle, S., 2019. Global Carbon Budget 2019. *Earth Syst. Sci. Data* 11, 1783-1838.
- Fripiat, F., Cardinal, D., Tison, J.-L., Worby, A., André, L., 2007. Diatom-induced silicon isotopic fractionation in Antarctic sea ice. *Journal of Geophysical Research* 112.
- Gaillardet, J., Dupre, B., Louvat, P., Alle`gre, C.J., 1999. Global silicate weathering and CO₂ consumption rates deduced from the chemistry of large rivers. *Chemical Geology* 159, 3–30.
- Gaillardet, J., Viers, J., Dupré, B., 2003. Trace elements in River Waters A2-Holland heinrich D. In : Turekian KK (ed) *Treatise on Geochemistry*, 2nd edn. Elsevier, Oxford, 195-235.
- Galy, A., France-Lanord, C., 1999. Weathering processes in the Ganges–Brahmaputra basin and the riverine alkalinity budget. *Chemical Geology* 159, 31-60.

- Ganeshram, R.S., François, R., Commeau, J., Brown-Leger, S.L., 2003. An experimental investigation of barite formation in seawater. *Geochimica et Cosmochimica Acta* 67, 2599-2605.
- Gao, S., Wolf-Gladrow, D.A., Völker, C., 2016. Simulating the modern $\delta^{30}\text{Si}$ distribution in the oceans and in marine sediments. *Global Biogeochemical Cycles* 30, 120-133.
- Gasparon, M., Lanyon, R., Burgess, J.S., Sigurdsson, I.A., 2002. The freshwater lakes of the Larsemann Hills, East Antarctica: Chemical characteristics of the water column ANARE Reports and ANARE Research Notes 147.
- Gasparon, M., Matschullat, J., 2006a. Geogenic sources and sinks of trace metals in the Larsemann Hills, East Antarctica: Natural processes and human impact. *Applied Geochemistry* 21, 318-334.
- Gasparon, M., Matschullat, J., 2006b. Trace metals in Antarctic ecosystems: Results from the Larsemann Hills, East Antarctica. *Applied Geochemistry* 21, 1593-1612.
- Georg, R.B., Reynolds, B.C., Frank, M., Halliday, A.N., 2006. New sample preparation techniques for the determination of Si isotopic compositions using MC-ICPMS. *Chemical Geology* 235, 95-104.
- George, J.V., Nuncio, M., Chacko, R., Anilkumar, N., Noronha, S.B., Patil, S.M., Pavithran, S., Alappattu, D.P., Krishnan, K.P., Achuthankutty, C.T., 2013. Role of physical processes in chlorophyll distribution in the western tropical Indian Ocean. *Journal of Marine Systems* 113–114, 1-12.
- Giacomino, A., Abollino, O., Malandrino, M., Mentasti, E., 2011. The role of chemometrics in single and sequential extraction assays: A Review. Part II. Cluster analysis, multiple linear regression, mixture resolution, experimental design and other techniques. *Analytica Chimica Acta* 688, 122-139
- Gibbs, M.T., Kump, L.R., 1994. Global chemical erosion during the Last Glacial Maximum and the present: Sensitivity to changes in lithology and hydrology. *Paleoceanography* 9, 529-543.

- Gibson, E.K., Wentworth, S.J., McKay, D.S., 1983. Chemical weathering and diagenesis of a cold desert soil from Wright Valley, Antarctica: An analog of Martian weathering processes. *Journal of Geophysical Research: Solid Earth* 88, A912-A928.
- Gillieson, D., Burgess, J.S., Spate, A., Cochrane, A., 1990. An atlas of the lakes of the Larsemann Hills, Princess Elizabeth Land, Antarctica. ANARE Research Notes No. 74, 173 pp.
- Glass, J.B., Axler, R.P., Chandra, S., Goldman, C.R., 2012. Molybdenum limitation of microbial nitrogen assimilation in aquatic ecosystems and pure cultures. *Frontiers in microbiology* 3, 331.
- Gonneea, M.E., Paytan, A., 2006. Phase associations of barium in marine sediments. *Marine Chemistry* 100, 124-135.
- Gooseff, M.N., McKnight, D.M., Lyons, W.B., Blum, A.E., 2002. Weathering reactions and hyporheic exchange controls on stream water chemistry in a glacial meltwater stream in the McMurdo Dry Valleys. *Water Resources Research* 38, 15-11-15-17.
- Gough, H.L., Stahl, D.A., 2011. Microbial community structures in anoxic freshwater lake sediment along a metal contamination gradient. *The ISME Journal* 5, 543-558.
- Grasse, P., Brzezinski, M.A., Cardinal, D., de Souza, G.F., Andersson, P., Closset, I., Cao, Z., Dai, M., Ehlert, C., Estrade, N., François, R., Frank, M., Jiang, G., Jones, J.L., Kooijman, E., Liu, Q., Lu, D., Pahnke, K., Ponzevera, E., Schmitt, M., Sun, X., Sutton, J.N., Thil, F., Weis, D., Wetzel, F., Zhang, A., Zhang, J., Zhang, Z., 2017. GEOTRACES inter-calibration of the stable silicon isotope composition of dissolved silicic acid in seawater. *J. Anal. At. Spectrom.* 32, 562-578.
- Grasse, P., Ehlert, C., Frank, M., 2013. The influence of water mass mixing on the dissolved Si isotope composition in the Eastern Equatorial Pacific. *Earth and Planetary Science Letters* 380, 60-71.
- Green, W.J., Stage, B.R., Preston, A., Wagers, S., Shacat, J., Newell, S., 2005. Geochemical processes in the Onyx River, Wright Valley, Antarctica:

- Major ions, nutrients, trace metals. *Geochimica et Cosmochimica Acta* 69, 839-850.
- Grew, E.S., Carson, C.J., Christy, A.G., Boger, S.D., 2013. Boron- and phosphate-rich rocks in the Larsemann Hills, Prydz Bay, East Antarctica: tectonic implications. *Geological Society, London, Special Publications* 383, 73-94.
- Griffith, E.M., Paytan, A., 2012. Barite in the ocean – occurrence, geochemistry and palaeoceanographic applications. *Sedimentology* 59, 1817-1835.
- Grotti, M., Soggia, F., Ardini, F., Magi, E., Becagli, S., Traversi, R., Udisti, R., 2015. Year-round record of dissolved and particulate metals in surface snow at Dome Concordia (East Antarctica). *Chemosphere* 138, 916-923.
- Group, S.W., 2007. GEOTRACES – An international study of the global marine biogeochemical cycles of trace elements and their isotopes. *Geochemistry* 67, 85-131.
- Hansel, C.M., 2017. Manganese in Marine Microbiology. *Advances in microbial physiology* 70, 37-83.
- Hauck, J., Völker, C., Wolf-Gladrow, D.A., Laufkötter, C., Vogt, M., Aumont, O., Bopp, L., Buitenhuis, E.T., Doney, S.C., Dunne, J., Gruber, N., Hashioka, T., John, J., Quéré, C.L., Lima, I.D., Nakano, H., Séférian, R., Totterdell, I., 2015. On the Southern Ocean CO₂ uptake and the role of the biological carbon pump in the 21st century. *Global Biogeochemical Cycles* 29, 1451-1470.
- Hawkings, J.R., Wadham, J.L., Benning, L.G., Hendry, K.R., Tranter, M., Tedstone, A., Nienow, P., Raiswell, R., 2017. Ice sheets as a missing source of silica to the polar oceans. *Nature communications* 8, 14198.
- Heldmann, J.L., Pollard, W., McKay, C.P., Marinova, M.M., Davila, A., Williams, K.E., Lacelle, D., Andersen, D.T., 2013. The high elevation Dry Valleys in Antarctica as analog sites for subsurface ice on Mars. *Planetary and Space Science* 85, 53-58.

- Hendry, K.R., Brzezinski, M.A., 2014. Using silicon isotopes to understand the role of the Southern Ocean in modern and ancient biogeochemistry and climate. *Quaternary Science Reviews* 89, 13-26.
- Hendry, K.R., Pyle, K.M., Butler, G.B., Cooper, A., Fransson, A., Chierici, M., Leng, M.J., Meyer, A., Dodd, P.A., 2018. Spatiotemporal Variability of Barium in Arctic Sea-Ice and Seawater. *Journal of Geophysical Research:Oceans* 123, 3507–3522.
- Hendry, K.R., Robinson, L.F., McManus, J.F., Hays, J.D., 2014. Silicon isotopes indicate enhanced carbon export efficiency in the North Atlantic during deglaciation. *Nature communications* 5, 3107.
- Herman, F., Seward, D., Valla, P.G., Carter, A., Kohn, B., Willett, S.D., Ehlers, T.A., 2013. Worldwide acceleration of mountain erosion under a cooling climate. *Nature* 504, 423-426.
- Herut, B., Starinski, A., Katz, A., Bein, A., 1990. The role of seawater freezing in the formation of subsurface brines. *Geochimica et Cosmochimica Acta* 54, 13-21.
- Ho, T.Y., Chien, C.T., Wang, B.N., Siriraks, A., 2010. Determination of trace metals in seawater by an automated flow injection ion chromatograph pretreatment system with ICPMS. *Talanta* 82, 1478-1484.
- Hodgson D A., Verleyen Elie, Sabbe Koen, Squier Angela H., Keely Brendan J., Leng Melanie J., Saunders Krystyna M., Vyverman, W., 2005. Late Quaternary climate-driven environmental change in the Larsemann Hills, East Antarctica, multi-proxy evidence from a lake sediment core. *Quaternary Research* 64, 83-99.
- Hodgson, D.A., Noon, P., Vyverman, W., W., B., Bryant, C., Gore, D., Appleby, P., Gilmour, M., Verleyen, E., Sabbe, K., Johnes, V.J., Ellis-Evans, Wood, P., 2012. Were the Larsemann Hills ice-free through the Last Glacial Maximum? . *Antarctic Science* 13, 440-454.
- Hodgson, D.A., Whitehouse, P.L., Gijss De Cort, Berg, S., Verleyen, E., Tavernier, I., Roberts, S.J., Vyverman, W., Sabbe, K., Brien, P.O., 2016. Rapid early

- Holocene sea-level rise in Prydz Bay, East Antarctica. *Global and Planetary Change* 139, 128-140.
- Honjo, S., T.I. Eglinton, C.D. Taylor, K.M. Ulmer, S.M. Sievert, A. Bracher, C.R. German, V. Edgcomb, R. Francois, M.D. Iglesias-Rodriguez, B. van Mooy, Repeta., D.J., 2014. Understanding the role of the biological pump in the global carbon cycle: An imperative for ocean science. *Oceanography* 27, 10-16.
- Horner, T.J., Lee, R.B., Henderson, G.M., Rickaby, R.E., 2013. Nonspecific uptake and homeostasis drive the oceanic cadmium cycle. *Proc. Natl. Acad. Sci. USA* 110, 2500-2505.
- Hsieh, Y.-T., Henderson, G.M., 2017. Barium stable isotopes in the global ocean: Tracer of Ba inputs and utilization. *Earth and Planetary Science Letters* 473, 269-278.
- Jacobson, A.D., Blum, J.D., 2000. Ca/Sr and $^{87}\text{Sr}/^{86}\text{Sr}$ geochemistry of disseminated calcite in Himalayan silicate rocks from Nanga Parbat: Influence on river-water chemistry. *Geology* 28, 463.
- Jacobson, A.D., Blum Joel D., Lynn, W.M., 2002. Reconciling the elemental and Sr isotope composition of Himalayan weathering fluxes: Insights from the carbonate geochemistry of stream waters. *Geochimica et Cosmochimica Acta* 66, 3417-3429.
- Jacquet, S.H.M., Dehairs, F., Cardinal, D., Navez, J., Delille, B., 2005. Barium distribution across the Southern Ocean frontal system in the Crozet–Kerguelen Basin. *Marine Chemistry* 95, 149-162.
- Jacquet, S.H.M., Henjes, J., Dehairs, F., Worobiec, A., Savoye, N., Cardinal, D., 2007. Particulate Ba-barite and acantharians in the Southern Ocean during the European Iron Fertilization Experiment (EIFEX). *Journal of Geophysical Research: Biogeosciences* 112.
- Jean-Baptiste, P., Petit, J.-R., Lipenkov, V.Y., Raynaud, D., Barkov, N.I., 2001. Constraints on hydrothermal processes and water exchange in Lake Vostok from helium isotopes. *Nature* 411, 460-462.

- Jeandel, C., Caisso, M., Minster, J.F., 1987. Vanadium behaviour in the global ocean and in the Mediterranean sea. *Marine Chemistry* 21, 51-74.
- Kapitsa, A.P., Ridley, J.K., de Q. Robin, G., Siegert, M.J., Zotikov, I.A., 1996. A large deep freshwater lake beneath the ice of central East Antarctica. *Nature* 381, 684-686.
- Karl, D.M., Tien, G., 1992. MAGIC A sensitive and precise method for measuring dissolved phosphorus in aquatic environments. *Limnol. Oceanogr.*, 37, 105-116.
- Kaup, E.N.N., Burgess, J.S., 2002. Surface and subsurface flows of nutrients in natural and human impacted lake catchments on Broknes, Larsemann Hills, Antarctica. *Antarctic Science* 14, 343-352.
- Klump, J., Hebbeln, D., Wefer, G., 2000. The impact of sediment provenance on barium-based productivity estimates. *Marine Geology* 169, 259-271.
- Krishnaswami, S., Singh, S.K., 2005. Chemical weathering in the river basins of the Himalaya, India. *CURRENT SCIENCE* 89, 10.
- Krishnaswami, S., Trivedi, J.R., Sarin, M.M., Ramesh, R., Sharma, K.K., 1992. Strontium isotopes and rubidium in the Ganga-Brahmaputra river system: Weathering in the Himalaya, fluxes to the Bay of Bengal and contributions to the evolution of oceanic $^{87}\text{Sr}/^{86}\text{Sr}$. *Earth and Planetary Science Letters* 109, 243-253.
- Laluraj, C.M., Rahaman, W., Thamban, M., Srivastava, R., 2020. Enhanced Dust Influx to South Atlantic Sector of Antarctica During the Late-20th Century: Causes and Contribution to Radiative Forcing. *Journal of Geophysical Research: Atmospheres* 125, e2019JD030675.
- Lane, T.W., Saito, M.A., George, G.N., Pickering, I.J., Prince, R.C., Morel, F.M., 2005. Biochemistry: a cadmium enzyme from a marine diatom. *Nature* 435, 42-42.
- Lea, D., Boyle, E., 1989. Barium content of benthic foraminifera controlled by bottom-water composition. *Nature* 338, 751-753.

- Lea, D.W., 1993. Constraints on the alkalinity and circulation of glacial circumpolar deep water from benthic foraminiferal barium. *Global Biogeochemical Cycles* 7, 695-710.
- Lecomte, K.L., Vignoni, P.A., Córdoba, F.E., Chaparro, M.A.E., Chaparro, M.A.E., Kopalová, K., Gargiulo, J.D., Lirio, J.M., Irurzun, M.A., Böhnell, H.N., 2016. Hydrological systems from the Antarctic Peninsula under climate change: James Ross archipelago as study case. *Environmental Earth Sciences* 75.
- Lecomte, K.L., Vignoni, P.A., Echegoyen, C.V., Santolaya, P., Kopalova, K., Kohler, T.J., Roman, M., Coria, S.H., Lirio, J.M., 2020. Dissolved major and trace geochemical dynamics in Antarctic lacustrine systems. *Chemosphere* 240, 124938.
- Leng, M.J., Swann, G.E.A., Hodson, M.J., Tyler, J.J., Patwardhan, S.V., Sloane, H.J., 2009. The Potential use of Silicon Isotope Composition of Biogenic Silica as a Proxy for Environmental Change. *Silicon* 1, 65-77.
- Li, X., Wang, N., Ding, Y., Hawkings, J.R., Yde, J.C., Raiswell, R., Liu, J., Zhang, S., Kang, S., Wang, R., Liu, Q., Liu, S., Bol, R., You, X., Li, G., 2022. Globally elevated chemical weathering rates beneath glaciers. *Nature communications* 13, 407.
- Liu, X., Sun, L., Xie, Z., Yin, X., Zhu, R., Wang, Y., 2007. A preliminary record of the historical seabird population in the Larsemann Hills, East Antarctica, from geochemical analyses of Mochou Lake sediments. *Boreas* 36, 182-197.
- Livingstone, D.A., 1963. Chapter G. Chemical Composition of Rivers and Lakes. *Geological Survey Professional Paper* 440-G
- Lutjeharms, J.R.E., 2006. The southern Agulhas Current, in: Lutjeharms, J.R.E. (Ed.), *The Agulhas Current*. Springer Berlin Heidelberg, Berlin, Heidelberg, pp. 121-150.
- Lyons, W.B., Bullen, T.D., Welch, K.A., 2017. Ca isotopic geochemistry of an Antarctic aquatic system. *Geophys. Res. Lett.* 44, 882-891.

- Lyons, W.B., Dailey, K.R., Welch, K.A., Deuerling, K.M., Welch, S.A., McKnight, D.M., 2015. Antarctic streams as a potential source of iron for the Southern Ocean. *Geology* 43, 1003-1006.
- Lyons, W.B., Dowling, C., A.Welch, K., Synder, G., J.Poreda, R., T.Doran, P., Fountain, A., 2005. Dating water and solute additions to ice-covered Antarctic lakes, Goldschmidt Conference Abstracts 2005, A720.
- Lyons, W.B., Leslie, D.L., Gooseff, M.N., 2021. Chemical Weathering in the McMurdo Dry Valleys, Antarctica, *Hydrogeology, Chemical Weathering, and Soil Formation*, pp. 205-216.
- Lyons, W.B., Nezat, C.A., V.Benson, L., Thomas D. Bullen, Y.Graham, E., Kidd, J., A., K., M.Thomas, J., 2002. Strontium Isotopic Signatures of the Streams and Lakes of Taylor Valley, Southern Victoria Land, Antarctica *Chemical Weathering in a Polar Climate. Aquatic Geochemistry* 8, 75-95.
- Lyons, W.B., Welch, K.A., Fountain, A.G., Dana, G.L., Vaughn, B.H., McKnight, D.M., 2003. Surface glaciochemistry of Taylor Valley, southern Victoria Land, Antarctica and its relationship to stream chemistry. *Hydrological Processes* 17, 115-130.
- Maas, R., Grew, E.S., Carson, C.J., 2015. Isotopic constrain (Pb, Rb-Sr, Sm-Nd) on the sources of Early Cambrian pegmatites with Boron and Beryllium minerals in the Larsemann Hills, Prydz Bay, Antarctica. *The Canadian Mineralogist* 53, 249-272.
- Maceda-Veiga, A., Monroy, M., Navarro, E., Viscor, G., de Sostoa, A., 2013. Metal concentrations and pathological responses of wild native fish exposed to sewage discharge in a Mediterranean river. *Sci. Total Environ* 449.
- Magesh, N.S., Botsa, S.M., Dessai, S., Mestry, M., Leitao, T.D.L., Tiwari, A., 2020. Hydrogeochemistry of the deglaciated lacustrine systems in Antarctica: Potential impact of marine aerosols and rock-water interactions. *The Science of the total environment* 706, 135822.
- Maldonado, M., Navarro, L., Grasa, A., Gonzalez, A., Vaquerizo, I., 2011. Silicon uptake by sponges: a twist to understanding nutrient cycling on continental margins. *Scientific reports* 1, 30.

- Maldonado, M.T., Allen, A.E., Chong, J.S., Lin, K., Leus, D., Karpenko, N., Harris, S.L., 2006. Copper-dependent iron transport in coastal and oceanic diatoms. *Limnology and Oceanography* 51, 1729-1743.
- Martinez-Ruiz, F., Jroundi, F., Paytan, A., Guerra-Tschuschke, I., Abad, M.d.M., González-Muñoz, M.T., 2018. Barium bioaccumulation by bacterial biofilms and implications for Ba cycling and use of Ba proxies. *Nature communications* 9, 1619.
- Meybeck, M., 2005. Looking for water quality. *Hydrological Processes* 19, 331-338.
- Milligan, A.J., Varela, D.E., Brzezinski, M.A., More, F.M.M., 2004. Dynamics of silicon metabolism and silicon isotopic discrimination in a marine diatom. *Limnol. Oceanogr.*, 49.
- Millot, R., Gaillardet, J.é., Dupré, B., Allègre, C.J., 2003. Northern latitude chemical weathering rates: clues from the Mackenzie River Basin, Canada. *Geochimica et Cosmochimica Acta* 67, 1305-1329.
- Mitchell, A.C., Brown, G.H., 2007. Diurnal hydrological – physicochemical controls and sampling methods for minor and trace elements in an Alpine glacial hydrological system. *Journal of Hydrology* 332, 123-143.
- Moon, S., Chamberlain, C.P., Hilley, G.E., 2014. New estimates of silicate weathering rates and their uncertainties in global rivers. *Geochimica et Cosmochimica Acta* 134, 257-274.
- Moon, S., Huh, Y., Qin, J., van Pho, N., 2007. Chemical weathering in the Hong (Red) River basin: Rates of silicate weathering and their controlling factors. *Geochimica et Cosmochimica Acta* 71, 1411-1430.
- Morlighem, M., Rignot, E., Binder, T., Blankenship, D., Drews, R., Eagles, G., Eisen, O., Ferraccioli, F., Forsberg, R., Fretwell, P., Goel, V., Greenbaum, J.S., Gudmundsson, H., Guo, J., Helm, V., Hofstede, C., Howat, I., Humbert, A., Jokat, W., Karlsson, N.B., Lee, W.S., Matsuoka, K., Millan, R., Mouginit, J., Paden, J., Pattyn, F., Roberts, J., Rosier, S., Ruppel, A., Seroussi, H., Smith, E.C., Steinhage, D., Sun, B., Broeke, M.R.v.d., Ommen, T.D.v., Wessem, M.v., Young, D.A., 2019. Deep glacial troughs

and stabilizing ridges unveiled beneath the margins of the Antarctic ice sheet. *Nature Geoscience*.

- Morris, A.W., 1975. Dissolved molybdenum and vanadium in the northeast Atlantic Ocean. *Deep-Sea Res.* 22, 49-54.
- Murphy, E.J., Johnston, N.M., Hofmann, E.E., Phillips, R.A., Jackson, J.A., Constable, A.J., Henley, S.F., Melbourne-Thomas, J., Trebilco, R., Cavanagh, R.D., Tarling, G.A., Saunders, R.A., Barnes, D.K.A., Costa, D.P., Corney, S.P., Fraser, C.I., Höfer, J., Hughes, K.A., Sands, C.J., Thorpe, S.E., Trathan, P.N., Xavier, J.C., 2021. Global Connectivity of Southern Ocean Ecosystems. *Frontiers in Ecology and Evolution* 9.
- Murray, A.E., Kenig, F., Fritsen, C.H., McKay, C.P., Cawley, K.M., Edwards, R., Kuhn, E., McKnight, D.M., Ostrom, N.E., Peng, V., Ponce, A., Priscu, J.C., Samarkin, V., Townsend, A.T., Wagh, P., Young, S.A., Yung, P.T., Doran, P.T., 2012. Microbial life at $-13\text{ }^{\circ}\text{C}$ in the brine of an ice-sealed Antarctic lake. *Proceedings of the National Academy of Sciences*, 201208607.
- Murray, J.W., 1987. Mechanisms Controlling the Distribution of Trace Elements in Oceans and Lakes, Sources and Fates of Aquatic Pollutants. American Chemical Society, pp. 153-184.
- Negrel, P., Allegre, C.J., Dupr, B., Lewin, E., 1993. Erosion sources determined by inversion of major and trace element ratios and strontium isotopic ratios in river water: The Congo Basin case. *Earth and Planetary Science Letters* 120, 59-76.
- Nezat, C.A., Lyons, W.B., Welch, K.A., 2001 Chemical weathering in streams of a polar desert (Taylor Valley, Antarctica). *GSA Bulletin* 113, 1401-1408.
- Nuruzzama, M., Rahaman, W., Tripathy, G.R., Mohan, R., Patil, S., 2020. Dissolved major ions, Sr and $^{87}\text{Sr}/^{86}\text{Sr}$ of coastal lakes from Larsemann hills, East Antarctica: Solute sources and chemical weathering in a polar environment. *Hydrological Processes*.
- Obryk, M.K., Doran, P.T., Priscu, J.C., 2014. The permanent ice cover of Lake Bonney, Antarctica: The influence of thickness and sediment distribution on

- photosynthetically available radiation and chlorophyll-a distribution in the underlying water column. *Journal of Geophysical Research: Biogeosciences* 119, 1879-1891.
- Oelze, M., Schuessler, J.A., von Blanckenburg, F., 2016. Mass bias stabilization by Mg doping for Si stable isotope analysis by MC-ICP-MS. *Journal of Analytical Atomic Spectrometry* 31, 2094-2100.
- Oliva, P., Viers, J., Dupré, B., 2003. Chemical weathering in granitic environments. *Chemical Geology* 202, 225-256.
- Orsi, A.H., Whitworth, T., Nowlin, W.D., 1995. On the meridional extent and fronts of the Antarctic Circumpolar Current. *Deep Sea Research Part I: Oceanographic Research Papers* 42, 641-673.
- Palmer, M.R., Edmond, J.M., 1992. Controls over the strontium isotope composition of river water. *Geochimica et Cosmochimica Acta* 56, 2099-2111.
- Parkhurst, D.L., 1995. User's guide to PHREEQE—a computer program for speciation, reaction-path, advective transport, and inverse geochemical calculations. US Geological Survey Water Resources graphical user interface for the geochemical computer program Investigations Report.
- Paytan, A., Kastner, M., Chavez, F.P., 1996. Glacial to Interglacial Fluctuations in Productivity in the Equatorial Pacific as Indicated by Marine Barite. *Science* 274, 1355-1357.
- Peers, G., Price, N.M., 2006. Copper-containing plastocyanin used for electron transport by an oceanic diatom. *Nature* 441, 341-344.
- Peucker-Ehrenbrink, B., Miller, M.W., Arsouze, T., Jeandel, C., 2010. Continental bedrock and riverine fluxes of strontium and neodymium isotopes to the oceans. *Geochemistry, Geophysics, Geosystems* 11, Q03016.
- Pyle, K.M., Hendry, K.R., Sherrell, R.M., Legge, O., Hind, A.J., Bakker, D., Venables, H., Meredith, M.P., 2018. Oceanic fronts control the distribution of dissolved barium in the Southern Ocean. *Marine Chemistry* 204, 95-106.
- Quinby-Hunt, M.S., Turehian, K.K., 1983. Distribution of elements in sea water. *Eos, Transactions American Geophysical Union* 64, 130-130.

- Ragueneau, O., Tréguer, P., Leynaert, A., Anderson, R.F., Brzezinski, M.A., DeMaster, D.J., Dugdale, R.C., Dymond, J., Fischer, G., François, R., Heinze, C., Maier-Reimer, E., Martin-Jézéquel, V., Nelson, D.M., Quéguiner, B., 2000. A review of the Si cycle in the modern ocean: recent progress and missing gaps in the application of biogenic opal as a paleoproductivity proxy. *Global and Planetary Change* 26, 317-365.
- Rahaman, W., Goswami, V., Singh, S.K., Rai, V.K., 2014. Molybdenum isotopes in two Indian estuaries: Mixing characteristics and input to oceans. *Geochimica et Cosmochimica Acta* 141, 407-422.
- Rahaman, W., Singh, S.K., 2012. Sr and $^{87}\text{Sr}/^{86}\text{Sr}$ in estuaries of western India: Impact of submarine groundwater discharge. *Geochimica et Cosmochimica Acta* 85, 275-288.
- Rahaman, W., Singh, S.K., Raghav, S., 2010. Dissolved Mo and U in rivers and estuaries of India: Implication to geochemistry of redox sensitive elements and their marine budgets. *Chemical Geology* 278, 160-172.
- Rahaman, W., Thamban, M., Laluraj, C.M., 2016. Twentieth-century sea ice variability in the Weddell Sea and its effect on moisture transport: Evidence from a coastal East Antarctic ice core record. *The Holocene* 26, 338-349.
- Rai, S.K., Singh, S.K., Krishnaswami, S., 2010. Chemical weathering in the plain and peninsular sub-basins of the Ganga: Impact on major ion chemistry and elemental fluxes. *Geochimica et Cosmochimica Acta* 74, 2340-2355.
- Revelrolland, M., Dedeccker, P., Delmonte, B., Hesse, P., Magee, J., Basile-Doelsch, I., Grousset, F., Bosch, D., 2006. Eastern Australia: A possible source of dust in East Antarctica interglacial ice. *Earth and Planetary Science Letters* 249, 1-13.
- Reynolds, B., Frank, M., Halliday, A., 2006. Silicon isotope fractionation during nutrient utilization in the North Pacific. *Earth and Planetary Science Letters* 244, 431-443.
- Reynolds, B.C., 2009. Modeling the modern marine $\delta^{30}\text{Si}$ distribution. *Global Biogeochemical Cycles* 23, GB2015.

- Richter, F.M., Rowley, D.B., DePaolo, D.J., 1992. Sr isotope evolution of seawater: the role of tectonics. *Earth and Planetary Science Letters* 109, 11-23.
- Rickli, J., Janssen, D.J., Hassler, C., Ellwood, M.J., Jaccard, S.L., 2019. Chromium biogeochemistry and stable isotope distribution in the Southern Ocean. *Geochimica et Cosmochimica Acta* 262, 188-206.
- Robert, C., Kennett, J.P., 1997. Antarctic continental weathering changes during Eocene-Oligocene cryosphere expansion: Clay mineral and oxygen isotope evidence. *Geology* 25, 587-590.
- Rubin, S.I., King, S.L., Jahnke, R.A., Froelich, P.N., 2003. Benthic barium and alkalinity fluxes: Is Ba an oceanic paleo-alkalinity proxy for glacial atmospheric CO₂? *Geophysical Research Letters* 30.
- Rudnick, R.L., Gao, S., 2003. 3.01 - Composition of the Continental Crust, in: Holland, H.D., Turekian, K.K. (Eds.), *Treatise on Geochemistry*. Pergamon, Oxford, pp. 1-64.
- Sabbe, K., Hodgson, D.A., Verleyen, E., Taton, A., Wilmotte, A., Vanhoutte, K., Vyverman, W., 2004. Salinity, depth and the structure and composition of microbial mats in continental Antarctic lakes. *Freshwater Biology* 49, 296-319.
- Sabbe, K., Verleyen, E., Hodgson, D.A., Vanhoutte, K., Vyverman, W., 2003. Benthic diatom flora of freshwater and saline lakes in the Larsemann Hills and Rauer Islands, East Antarctica. *Antarctic Science* 15, 227-248.
- Saelens, E., Gardner, C.B., Welch, K.A., Welch, S.A., Lyons, W.B., 2018. Barium and barite dynamics in Antarctic streams. *Geology* 46, 811-814.
- Sanyal, A., Antony, R., Ganesan, P., Thamban, M., 2020. Metabolic activity and bioweathering properties of yeasts isolated from different supraglacial environments of Antarctica and Himalaya, *Antonie van Leeuwenhoek* 113, 2243–2258
- Scherer, N.M., Gibbons, H.L., Stoops, K.B., Muller, M., 1995. Phosphorus Loading of an Urban Lake by Bird Droppings. *Lake and Reservoir Management* 11, 317-327.

- Shand, P., Darbyshire, D.P.F., Love, A.J., Edmunds, W.M., 2009. Sr isotopes in natural waters: Applications to source characterisation and water–rock interaction in contrasting landscapes. *Applied Geochemistry* 24, 574-586.
- Sheraton, J.W., Black, L.P., McCulloch, M.T., 1984. Regional geochemical and isotopic characteristics of high-grade metamorphics of the Prydz bay area: The extent of proterozoic reworking of Qrchaean continental crust in East Antarctica. *Precambrian Research* 26, 169-198.
- Shevnina, E., Kourzeneva, E., 2017. Thermal regime and components of water balance of lakes in Antarctica at the Fildes peninsula and the Larsemann Hills. *Tellus A: Dynamic Meteorology and Oceanography* 69, 1317202.
- Shi, G., Teng, J., Ma, H., Wang, D., Li, Y., 2018. Metals in topsoil in Larsemann Hills, an ice-free area in East Antarctica: Lithological and anthropogenic inputs. *Catena* 160, 41-49.
- Sholkovitz, E.R., 1978. The flocculation of dissolved Fe, Mn, Al, Cu, Ni, Co and Cd during estuarine mixing. *Earth and Planetary Science Letters* 41, 77-86.
- Siegert, M., Atkinson, A., Banwell, A., Brandon, M., Convey, P., Davies, B., Downie, R., Edwards, T., Hubbard, B., Marshall, G., Rogelj, J., Rumble, J., Stroeve, J., Vaughan, D., 2019. The Antarctic Peninsula Under a 1.5°C Global Warming Scenario. *Front. Environ. Sci.* 7, 102.
- Sigman, D.M., Boyle, E.A., 2000. Glacial/interglacial variations in atmospheric carbon dioxide. *Nature* 407, 859-869.
- Singh, S.P., Singh, S.K., Bhushan, R., 2013. Internal cycling of dissolved barium in water column of the Bay of Bengal, *Marine Chemistry* 154, 12-23.
- Singh, S.P., Singh, S.K., Bhushan, R., Rai, V.K., 2015. Dissolved silicon and its isotopes in the water column of the Bay of Bengal: Internal cycling versus lateral transport. *Geochimica et Cosmochimica Acta* 151, 172-191.
- Sinha, A.K., Parli Venkateswaran, B., Tripathy, S.C., Sarkar, A., Prabhakaran, S., 2019. Effects of growth conditions on siderophore producing bacteria and siderophore production from Indian Ocean sector of Southern Ocean. *Journal of basic microbiology* 59, 412-424.

- Smedley, P.L., Kinniburgh, D.G., 2017. Molybdenum in natural waters: A review of occurrence, distributions and controls. *Applied Geochemistry* 84, 387-432.
- Smetacek, V., Klaas, C., Strass, V.H., Assmy, P., Montresor, M., Cisewski, B., Savoye, N., Webb, A., d'Ovidio, F., Arrieta, J.M., Bathmann, U., Bellerby, R., Berg, G.M., Croot, P., Gonzalez, S., Henjes, J., Herndl, G.J., Hoffmann, L.J., Leach, H., Losch, M., Mills, M.M., Neill, C., Peeken, I., Röttgers, R., Sachs, O., Sauter, E., Schmidt, M.M., Schwarz, J., Terbrüggen, A., Wolf-Gladrow, D., 2012. Deep carbon export from a Southern Ocean iron-fertilized diatom bloom. *Nature* 487, 313-319.
- Sobek, S., Tranvik, L.J., Prairie, Y.T., Kortelainen, P., Cole, J.J., 2007. Patterns and regulation of dissolved organic carbon: An analysis of 7,500 widely distributed lakes. *Limnology and Oceanography* 52, 1208-1219.
- Sohrin, Y., Fujishima, Y., Ueda, K., Akiyama, S., Mori, K., Hasegawa, H., Matsui, M., 1998. Dissolved niobium and tantalum in the North Pacific. *Geophys. Res. Lett.* 25, 999-1002.
- Sokolov, S., Rintoul, S.R., 2007. On the relationship between fronts of the Antarctic Circumpolar Current and surface chlorophyll concentrations in the Southern Ocean. *Journal of Geophysical Research: Oceans* 112.
- Spate, A.P., Burgess, J.S., Shevlin, J., 1995. Rates of rock surface lowering, Princess Elizabeth Land, Eastern Antarctica. *Earth Surface Processes and Landform* 20, 567-573.
- Spurr, B., 1975. Limnology of Bird Pond, Ross Island, Antarctica. *New Zealand Journal of Marine and Freshwater Research* 9, 547-562.
- Sternberg, E., Tang, D., Ho, T.-Y., Jeandel, C., Morel, F.M.M., 2005. Barium uptake and adsorption in diatoms. *Geochimica et Cosmochimica Acta* 69, 2745-2752.
- Stokes, C.R., Sanderson, J.E., Miles, B.W.J., Jamieson, S.S.R., Leeson, A.A., 2019. Widespread distribution of supraglacial lakes around the margin of the East Antarctic Ice Sheet. *Scientific reports* 9.
- Strickland, J.D.H., Parsons, T.R., 1972. *A Practical Handbook of seawater Analysis Fisheries Research Board of Canada, Bulletin 167, Second edition*

- Stüwe, K., Braun, H.M., Peer, H., 1989. Geology and structure of the Larsemann Hills area, Prydz Bay, East Antarctica. *Australian Journal of Earth Sciences* 36, 219-241.
- Sunda, W.G., Huntsman, S.A., 1998. Processes regulating cellular metal accumulation and physiological effects: Phytoplankton as model systems. *Science of The Total Environment* 219, 165-181.
- Sutton, J.N., André, L., Cardinal, D., Conley, D.J., de Souza, G.F., Dean, J., Dodd, J., Ehlert, C., Ellwood, M.J., Frings, P.J., Grasse, P., Hendry, K., Leng, M.J., Michalopoulos, P., Panizzo, V.N., Swann, G.E.A., 2018. A Review of the Stable Isotope Bio-geochemistry of the Global Silicon Cycle and Its Associated Trace Elements. *Frontiers in Earth Science* 5.
- Sutton, J.N., Varela, D.E., Brzezinski, M.A., Beucher, C.P., 2013. Species-dependent silicon isotope fractionation by marine diatoms. *Geochimica et Cosmochimica Acta* 104, 300-309.
- Takacs, C.D., Priscu, J.C., McKnight, D.M., 2001. Bacterial dissolved organic carbon demand in McMurdo Dry Valley lakes, Antarctica. *Limnology and Oceanography* 46, 1189-1194.
- Takano, S., Tanimizu, M., Hirata, T., Sohrin, Y., 2014. Isotopic constraints on biogeochemical cycling of copper in the ocean. *Nature communications* 5.
- Tarantola, A., 2005. The least square criterion, in *Inverse Problem theory and Methods for model parameter estimation* Soc. for Ind. and Appl. Math., Philadelphia, Pa, 68-72.
- Taylor, S.R., McLennan, S.M., 1995. The geochemical evolution of the continental crust. *Reviews of Geophysics* 33, 241-265.
- Toner, J.D., Sletten, R.S., 2013. The formation of Ca-Cl-rich groundwaters in the Dry Valleys of Antarctica: Field measurements and modeling of reactive transport. *Geochimica et Cosmochimica Acta* 110, 84-105.
- Torres, M.A., Moosdorf, N., Hartmann, J., Adkins, J.F., West, A.J., 2017. Glacial weathering, sulfide oxidation, and global carbon cycle feedbacks. *Proceedings of the National Academy of Sciences of the United States of America* 114, 8716-8721.

- Treguer, P.J., De La Rocha, C.L., 2013. The world ocean silica cycle. *Annual review of marine science* 5, 477-501.
- Tripathy, G.R., Das, A., 2014. Modeling geochemical datasets for source apportionment: Comparison of least square regression and inversion approaches. *Journal of Geochemical Exploration* 144, 144-153.
- Tripathy, G.R., Mishra, S., Danish, M., Ram, K., 2019. Elevated Barium concentrations in rain water from east-coast of India: role of regional lithology. *Journal of Atmospheric Chemistry* 76, 59-72.
- Tripathy, G.R., Singh, S.K., 2010. Chemical erosion rates of river basins of the Ganga system in the Himalaya: Reanalysis based on inversion of dissolved major ions, Sr, and $^{87}\text{Sr}/^{86}\text{Sr}$. *Geochemistry, Geophysics, Geosystems* 11.
- Tripathy, G.R., Singh, S.K., Krishnaswami, S., 2012. Sr and Nd Isotopes as Tracers of Chemical and Physical Erosion. M. Baskaran (ed.), *Handbook of Environmental Isotope Geochemistry, Advances in Isotope Geochemistry*.
- Turner, D.R., Whitfield, M., Dickson, A.G., 1981. The equilibrium speciation of dissolved components in freshwater and sea water at 25°C and 1 atm pressure. *Geochimica et Cosmochimica Acta* 45, 855-881.
- van den Berg, C.M., Merks, A.G., Duursma, E.K., 1987. Organic complexation and its control of the dissolved concentrations of copper and zinc in the Scheldt estuary. *Estuar. Coast. Shelf Sci.* 24, 785-797.
- van Horsten, N.R., Planquette, H., Sarthou, G., Ryan-Keogh, T.J., Lemaitre, N., Mtshali, T.N., Roychoudhury, A., Bucciarelli, E., 2022. Early winter barium excess in the southern Indian Ocean as an annual remineralisation proxy (GEOTRACES GIPr07 cruise). *Biogeosciences* 19, 3209-3224.
- van Hulst, M., Middag, R., Dutay, J.C., de Baar, H., Roy-Barman, M., Gehlen, M., Tagliabue, A., Sterl, A., 2017. Manganese in the west Atlantic Ocean in the context of the first global ocean circulation model of manganese. *Biogeosciences* 14, 1123-1152.
- Vanhaecke, F., Moens, L., 2004. Overcoming spectral overlap in isotopic analysis via single- and multi-collector ICP-mass spectrometry. *Analytical and bioanalytical chemistry* 378, 232-240.

- Varela, D.E., Pride, C.J., Brzezinski, M.A., 2004. Biological fractionation of silicon isotopes in Southern Ocean surface waters. *Global Biogeochemical Cycles* 18, n/a-n/a.
- Veizer, J., 1989. Strontium Isotopes in Sea Water Through Time. *Ann. Rev. Earth Planet. Sci.*, 141-167.
- Verleyen, E., Hodgson, D.A., Gibson, J., Imura, S., Kaup, E., Kudoh, S., De Wever, A., Hoshino, T., McMinn, A., Obbels, D., Roberts, D., Roberts, S., Sabbe, K., Souffreau, C., Tavernier, I., van Nieuwenhuyze, W., van Ranst, E., Vindeogel, N., Vyverman, W., 2011a. Chemical limnology in coastal East Antarctic lakes: monitoring future climate change in centres of endemism and biodiversity. *Antarctic Science* 24, 23-33.
- Verleyen, E., Hodgson, D.A., Sabbe, K., Cremer, H., Emslie, S.D., Gibson, J., Hall, B., Imura, S., Kudoh, S., Marshall, G.J., McMinn, A., Melles, M., Newman, L., Roberts, D., Roberts, S.J., Singh, S.M., Sterken, M., Tavernier, I., Verkulich, S., de Vyver, E.V., Van Nieuwenhuyze, W., Wagner, B., Vyverman, W., 2011b. Post-glacial regional climate variability along the East Antarctic coastal margin—Evidence from shallow marine and coastal terrestrial records. *Earth-Science Reviews* 104, 199-212.
- Wadham, J.L., Tranter, M., Skidmore, M., Hodson, A.J., Prisco, J., Lyons, W.B., Sharp, M., Wynn, P., Jackson, M., 2010. Biogeochemical weathering under ice: Size matters. *Global Biogeochemical Cycles* 24, GB3025.
- Walker, J.C.G., Hays, P.B., Kasting, J.F., 1981. A negative feedback mechanism for the long-term stabilization of Earth's surface temperature. *Journal of Geophysical Research* 86, 9776.
- Wang, L., Wang, Y., Xu, C., An, Z., Wang, S., 2011. Analysis and evaluation of the source of heavy metals in water of the River Changjiang. *Environ. Monit. Assess.* 173, 201-313.
- Weis, D., Kieffer, B., Maerschalk, C., Barling, J., de Jong, J., Williams, G.A., Hanano, D., Pretorius, W., Mattielli, N., Scoates, J.S., Goolaerts, A., Friedman, R.M., Mahoney, J.B., 2006. High-precision isotopic characterization of

- USGS reference materials by TIMS and MC-ICP-MS. *Geochemistry, Geophysics, Geosystems* 7, Q08006.
- Weyer, S., Schwieters, J.B., 2003. High precision Fe isotope measurements with high mass resolution MC-ICPMS. *International Journal of Mass Spectrometry* 226, 355-368.
- Whitworth III, T., Nowlin Jr., W.D., 1987. Water masses and currents of the Southern Ocean at the Greenwich Meridian. *Journal of Geophysical Research: Oceans* 92, 6462-6476.
- WHO, 2017. *Guidelines for Drinking Water Quality: Fourth edition Incorporating the First addendum*, World Health Organization, Geneva.
- Wieser, M.E., Schwieters, J.B., 2005. The development of multiple collector mass spectrometry for isotope ratio measurements. *International Journal of Mass Spectrometry* 242, 97-115.
- Wilson, A.T., 1979. Geochemical problems of Antarctic dry areas *Nature* 280.
- Wu, J., Roshan, S., Chen, G., 2014. The distribution of dissolved manganese in the tropical–subtropical North Atlantic during US GEOTRACES 2010 and 2011 cruises. *Mar. Chem.* 166, 9-24.
- Wu, L., Huh, Y., Qin, J., Du, G., van Der Lee, S., 2005. Chemical weathering in the Upper Huang He (Yellow River) draining the eastern Qinghai-Tibet Plateau. *Geochimica et Cosmochimica Acta* 69, 5279-5294.
- Zachos, J.C., Opdyke, B.N., Quinn, T.M., Jones, C.E., Halliday, A.N., 1999. Early cenozoic glaciation, antarctic weathering, and seawater $87\text{Sr}/86\text{Sr}$: is there a link? *Chemical Geology* 161, 165-180.
- Zambardi, T., Poitrasson, F., 2011. Precise Determination of Silicon Isotopes in Silicate Rock Reference Materials by MC-ICP-MS. *Geostandards and Geoanalytical Research* 35, 89-99.
- Zelano, I., Malandrino, M., Giacomino, A., Buoso, S., Conca, E., Sivry, Y., Benedetti, M., Abollino, O., 2017. Element variability in lacustrine systems of Terra Nova Bay (Antarctica) and concentration evolution in surface waters. *Chemosphere* 180, 343-355.

Zhang, A., Zhang, J., Zhang, R., Xue, Y., 2014. Modified enrichment and purification protocol for dissolved silicon-isotope determination in natural waters. *J. Anal. At. Spectrom.* 29, 2414-2418.